sherritt

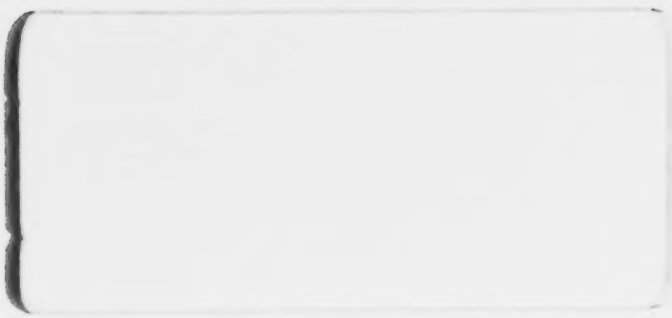

Sherritt Gordon Mines Limited
Fort Saskatchewan, Alberta, Canada T8L 2P2 / Telephone (403) 998-8911 / Telex 037-2290

Sherritt Research Centre

EVALUATION OF STRESS-RUPTURE PROPERTIES OF STAINLESS ALLOYS IN FLUIDIZED BED COMBUSTION ENVIRONMENTS
FINAL REPORT

For the Period
October 1982 to February 1986

K.G. Reid
M.J.H. Ruscoe

Evaluation of Stress-Rupture Properties of Stainless Alloys in Fluidized Bed Combustion Environments

Final Report

by

Sherritt Research Centre
Sherritt Gordon Mines Limited
Fort Saskatchewan, Alberta
K.G. Reid, M.J.H. Ruscoe

Work on this project was conducted under the auspices of the Canada Centre for Mineral and Energy Technology, Energy, Mines and Resources, Canada

DSS FILE NUMBER	:	03SQ.23440-2-9053
DSS CONTRACT SERIAL NUMBER	:	OSQ82-00148
CANMET PROJECT NUMBER	:	430902
CANMET SCIENTIFIC AUTHORITY	:	Dr. D.C. Briggs

51 pp

DATE: October 1982 to February 1986

This report should be cited as Contract Report No: OSQ82-00148

AUG 15 1988

MICROMEDIA

This work was performed for the Physical Metallurgy Research Laboratories of CANMET, Energy, Mines and Resources, Canada on Supply and Services Contract OSQ82-00148. The authors acknowledge the support received from Dr. David Briggs of PMRL in the scientific administration of the contract.

Any data presented, opinions, findings, conclusions or recommendations expressed in this report are those of the contractor and do not necessarily reflect the views of CANMET.

TABLE OF CONTENTS

		Page No
	SUMMARY	1
1.0	INTRODUCTION	2
2.0	EXPERIMENTAL	3
2.1	Materials	3
	2.1.1 Alloys	3
	2.1.2 Stress-Rupture Specimen Preparation	4
	2.1.3 Synthetic Combustion Gas	4
2.2	Apparatus and Procedure	5
	2.2.1 Apparatus	5
	2.2.2 Procedure	6
	2.2.2.1 Stress-Rupture Testing	6
	2.2.2.2 Technique for the Application of a Simulated Deposit to the Test Specimens	8
	2.2.2.3 Perparation of the Actual Bed Material from the Nova Scotia Pilot Plant	8
3.0	RESULTS AND DISCUSSION	9
4.0	CONCLUSIONS	14

LIST OF TABLES

		Page No
Table 1	Chemical Analyses of Test Alloys	15
Table 2	Physical Properties of Test Alloys	16
Table 3	Analyses of the Actual Bed Material from the Nova Scotia Fluidized Bed Coal Combustor Pilot Plant	20
Table 4	Phase 1 Stress-Rupture Data for the Program Alloys Tested at 800°C in 2000 ppm SO_2 Synthetic Combustion Gas	21
Table 5	Phase 1 Stress-Rupture Data for the Program Alloys Tested at 900°C in 2000 ppm SO_2 Synthetic Combustion Gas	22
Table 6	Phase 2 Stress-Rupture Data for the Program Alloys Tested at 800°C in 2000 ppm SO_2 Synthetic Combustion Gas and Simulated Fluidized Bed Deposit	23
Table 7	Phase 2 Stress-Rupture Data for the Program Alloys Tested at 900°C in 2.0% SO_2 Synthetic Combustion Gas	24
Table 8	Phase 3, Part 1 Stress-Rupture Data for the Program Alloys Tested at 900°C in 2.0% SO_2 Synthetic Combustion Gas and Simulated Fluidized Bed Deposit	25
Table 9	Phase 3, Part 3 Stress-Rupture Data for the Program Alloys Tested at 800°C in 2000 ppm SO_2 Synthetic Combustion Gas and Actual Bed Material	26
Table 10	Phase 3, Part 3 Stress-Rupture Data for the Program Alloys Tested at 900°C in 2.0% SO_2 Synthetic Combustion Gas and Actual Bed Material	27

LIST OF FIGURES

		Page No
Figure 1	Schematic of Stress-Rupture Testing Apparatus	17
Figure 2	Larson-Miller Parameter Versus Stress for Stainless Alloy 310	18
Figure 3	Predicted Rupture Life in Air for Stainless Alloy 310	19
Figure 4	Stress-Rupture Tests for Stainless Alloy 310 at 800°C in Synthetic Combustion Gas	28
Figure 5	Stress-Rupture Tests for Cast Alloy HK40 at 800°C in Synthetic Combustion Gas	29
Figure 6	Stress-Rupture Tests for Incoloy 800H at 800°C in Synthetic Combustion Gas	30
Figure 7	Stress-Rupture Tests for Stainless Alloy 347H at 800°C in Synthetic Combustion Gas	31
Figure 8	Stress-Rupture Tests for Stainless Alloy 310 at 900°C in Synthetic Combustion Gas	32
Figure 9	Stress-Rupture Tests for Cast Alloy HK40 at 900°C in Synthetic Combustion Gas	33
Figure 10	Stress-Rupture Tests for Incoloy 800H at 900°C in Synthetic Combustion Gas	34
Figure 11	Stress-Rupture Tests for Stainless Alloy 347H at 900°C in Synthetic Combustion Gas	35
Figure 12	Appearance of Ruptured Stainless Alloy 310 and Cast Alloy HK40 Specimens After 800°C Tests in 2000 ppm SO_2 Synthetic Combustion Gas and Actual Bed Material	36
Figure 13	Appearance of Ruptured Incoloy 800H and Stainless Alloy 347H Specimens After 800°C Tests in 2000 ppm SO_2 Synthetic Combustion Gas and Actual Bed Material	37
Figure 14	Appearance of Ruptured Stainless Alloy 310 and Cast Alloy HK40 Specimens After 900°C Tests in 2.0% SO_2 Synthetic Combustion Gas and Actual Bed Material	38
Figure 15	Appearance of Ruptured Incoloy 800H and Stainless Alloy 347H Specimens After 900°C Tests in 2.0% SO_2 Synthetic Combustion Gas and Actual Bed Material	39

Page No

Figure 16 Sulphidation Observed in Stainless Alloy 347H Specimens After Rupture Lives of 9.9 and 1123 h at 800°C in 2000 ppm SO_2 Combustion Gas and Actual Bed Material 40

Figure 17 Effect of Hot Corrosion on Incoloy 800H, Stainless Alloy 310 and Cast Alloy HK40 After Stress-Rupture Tests Using High Stress at 800°C in 2000 ppm SO_2 Combustion Gas and Actual Bed Material 41

Figure 18 Effect of Hot Corrosion on Incoloy 800H, Stainless Alloy 310 and Cast Alloy HK40 After Stress-Rupture Tests Using Low Stress at 800°C in 2000 ppm SO_2 Combustion Gas and Actual Bed Material 42

Figure 19 Effect of Hot Corrosion on the Program Test Alloys After Stress-Rupture Tests Using High Stress at 900°C in 2.0% SO_2 Combustion Gas and Actual Bed Material 43

Figure 20 Effect of Hot Corrosion on the Program Test Alloys After Stress-Rupture Tests Using Low Stress at 900°C in 2.0% SO_2 Combustion Gas and Actual Bed Material 44

Figure 21 Microprobe Analyses of Stainless Alloy 347H After 4.3 h Rupture Life at 900°C in 2.0% SO_2 Combustion Gas and Actual Bed Material 45

Figure 22 Microprobe Analyses of Incoloy 800H After 333.7 h Rupture Life at 900°C in 2.0% SO_2 Combustion Gas and Actual Bed Material 46

Figure 23 Microprobe Analyses of Cast Alloy HK40 After 90 h Rupture Life at 800°C in 2000 ppm SO_2 Combustion Gas and Actual Bed Material 47

Figure 24 Simulated Creep Curve for Incoloy 800H as Determined During Stress-Rupture Test at 800°C in 2000 ppm SO_2 Combustion Gas and Actual Bed Material 48

Figure 25 Simulated Creep Curve for Stainless Alloy 347H as Determined During Stress-Rupture Test at 800°C in 2000 ppm SO_2 Combustion Gas and Actual Bed Material 49

Figure 26 Appearance of Cast Alloy HK40 Ruptured Specimen After Being Thermally Cycled During a 900°C Stress-Rupture Test in 2.0% SO_2 Combustion Gas 50

SUMMARY

Stress-rupture tests as defined for Phase 1, 2 and 3 of the contract were successfully completed according to the Statement of Work.

The tests were conducted at 800 and 900°C and had targeted rupture lives of 10 to 1000 h. Alloys tested were stainless alloys 310 and 347H, cast alloy HK40 and Incoloy 800H. Phase 1 800 and 900°C tests were conducted in a synthetic coal combustion atmosphere that contained 2000 ppm sulphur dioxide (SO_2). For the 800°C tests of Phase 2 the alloys were tested with a simulated fluidized bed combustor deposit enveloping the specimen in addition to the synthetic combustion gas of Phase 1. The simulated deposit consisted of six parts by weight calcium sulphate and one part calcium oxide. The 900°C tests of Phase 2 were carried out without the simulated deposit but the SO_2 content of the synthetic combustion gas was increased from 0.2 to 2.0%. In Part 1 of Phase 3, 900°C stress-rupture tests were conducted using the 2.0% SO_2 combustion gas and the simulated deposit enveloped the test specimen. Part 2 of Phase 3 consisted of 800°C stress-rupture tests for two alloys. Each of these tests used the simulated combustor deposit and the 0.2% SO_2 simulated combustion gas. In Part 3 of Phase 3 actual bed material from the fluidized bed combustor test facility of EMR/NSPC (Nova Scotia Power Corporation) enveloped the alloy specimens during 800 and 900°C tests. The synthetic combustion gas for the 800°C tests contained 0.2% SO_2 while the 2.0% SO_2 content combustion gas was used for the 900°C tests.

Results showed that the 800°C rupture lives of the coated specimens were similar to rupture lives of the uncoated test samples. Rupture lives at 900°C did not appear to be affected by the SO_2 content of the combustion gas nor by the coatings employed during the tests. In general rupture lives were similar to those expected from tests in air as reported in the literature.

Metallographic and microprobe evaluation showed that hot corrosion of the ruptured test alloys had occurred during stress-rupture testing and was generally associated with highly stressed areas of the samples.

Tests conducted outside the scope of the Statement of Work indicated that thermal stress, i.e. temperature cycling, promoted hot corrosion during stress-rupture testing and decreased the expected rupture life of the test specimens. Additional work conducted under the experimental conditions of the program suggested that conventional

creep behavior might be responsible for the lack of accelerated degradation of the specimens during the stress-rupture tests.

1.0 INTRODUCTION

When coal is burned in a fluidized bed combustor, a large proportion of the sulphur in the fuel is trapped in the calcined limestone which, along with the resulting $CaSO_4$ makes up 95% of the bed. This capture of sulphur is most efficient in the temperature range 850 to 900°C but even in this temperature range, the concentration of SO_2 in the flue gas can reach 0.5%. Conditions vary from oxidizing (concentration of oxygen up to 5%) generally to reducing locally in the combustor. In addition, complex layers of compounds of oxygen, sulphur, calcium, iron, aluminum and silicon build up on the surfaces of metal components.

Boiler tubes in fluidized bed combustors operate at temperatures below the bed temperature but superheater tubes and hangers operate near bed temperature and are subjected to operating stresses and aggressive environments. The creep and stress-rupture properties of the stainless alloys which may be required in these high temperature applications are well known in air environments. However, in the aggressive environment of the fluidized bed combustor where progressive metal degradation is expected, data on mechanical properties are lacking. Consequently, an evaluation of the stress-rupture properties of these alloys in fluidized bed combustion atmospheres is required.

To fulfill this need Sherritt Gordon Mines Limited was engaged by the Department of Supply and Services (DSS) to conduct stress-rupture tests. The effective commencement date was October 21, 1982. The contractual guidance for the project was provided by the Science Procurement Manager at DSS whilst the technical guidance came from the Scientific Authority at CANMET (Canada Centre for Materials and Energy Technology). A three phase Statement of Work was provided with the contract and the revised date for conclusion of the third phase was set at February 28, 1986.

As outlined in the Statement of Work, the task of evaluating the stress-rupture properties of stainless alloys types 310 and 347H, cast alloy HK40 and Incoloy 800H was divided into three phases. The objective of Phase 1 was to evaluate stress-rupture properties of the specified alloys in synthetic combustion gas using test temperatures of 800 and 900°C. The synthetic combustion gas for Phase 1 contained

200 ppm carbon monoxide (CO), 2000 ppm sulphur dioxide (SO_2), 20% carbon dioxide (CO_2) and balance nitrogen (N_2).

In the original statement of work for the stress-rupture test program, Phase 2 had as its objective to essentially repeat Phase 1 except that the program alloys were to be tested with a simulated fluidized bed deposit enveloping the gauge length of the stress-rupture test specimen. However, during discussion of the Phase I results with the project Scientific Authority, it was concluded that the sulphidizing potential of the test gas at 900°C was too low, and thus it was decided to redesign the gas composition for tests at that temperature. Accordingly, Phase 2 was revised to accommodate the change in scope. Part 1 of revised Phase 2 consisted of 800°C stress-rupture tests conducted using the Phase 1 synthetic combustion gas certified to contain $\leq$10 ppm oxygen (O_2) and with each alloy having the simulated fluidized bed deposit enveloping the specimen gauge length. In Part 2 of Phase 2, 900°C stress-rupture tests were conducted using uncoated test specimens in a synthetic combustion gas that contained 540 ppm CO, 2.0% SO_2, 18% CO_2, $\leq$30 ppm O_2 and balance N_2.

Phase 3 of the test program was revised to reflect the change in scope of Phase 2 and to incorporate additional tests using the four alloys. The objective for Phase 3, Part 1 was to determine the effect of the new Phase 2 combustion gas, together with the simulated deposit, on the stress-rupture lives of the alloys when tested at 900°C. Part 2 of Phase 3 was undertaken to augment the data for the 800°C tests of Phase 2. In Part 3 of Phase 3, 800°C stress-rupture tests were carried out using the synthetic combustion gas of Phase 1 and the actual bed material from the Nova Scotia pilot plant enveloped the specimen gauge length. The 900°C tests of Part 3 used the redefined combustion gas and the actual bed material enveloped the specimen during testing.

Comprehensive interim progress reports were issued at the conclusion of Phase 1, Phase 2 and Part 2 of Phase 3. This present report tabulates the unreported data of Phase 3 and also serves as a final report for the program.

2.0 EXPERIMENTAL

2.1 Materials

2.1.1 Alloys

The required stainless steel alloys types 310 and 347 H, cast alloy HK40 and Incoloy 800H were obtained from commercial suppliers. Incoloy

800H and stainless alloys types 310 and 347H were purchased in the form of round bar of nominally 12.7 mm diameter. In the case of cast alloy HK40, centrifugally cast pipe having a wall thickness of 12.7 mm was obtained. The alloys were purchased under the ASTM and UNS designations as shown below.

Alloy	Designation	
	ASTM	UNS
Stainless Steel Type 310	A249-80	S31000
Stainless Steel Type 347H	A479-80a	S34709
Alloy HK40	A608-79	J94224
Incoloy 800H	B408-77	N08810

Tables 1 and 2 show the chemical composition and room temperature physical properties of each alloy, together with comparative reference data. As indicated by the comparative data all alloys had chemical analyses and physical properties within the specified limits.

2.1.2 Stress-Rupture Specimen Preparation

Machined specimens were prepared for stress-rupture testing according to ASTM designation E8-81 sections 6.1 and 6.4. Finished specimens conformed to the dimensional tolerances specified for small size specimens having nominal diameters of 6.25 mm and 25 mm gauge lengths, as shown in ASTM E8-81 Figure 8.

2.1.3 Synthetic Combustion Gas

The synthetic combustion gas for the program was purchased from Matheson of Canada. For the 800 and 900°C tests of Phase 1 the nominal gas composition was 200 ppm CO, 2000 ppm SO_2, 20% CO_2 and balance N_2. The oxygen and sulphur potentials of this gas have been calculated to be $\log_{10} Po_2 = -13.1$, $\log_{10} Ps_2 = -7.6$ at 800°C, and $\log_{10} Po_2 = -10.8$, $\log_{10} Ps_2 = -9.2$ at 900°C (where P = atmosphere). This gas was also used for the 800°C tests of Phases 2 and 3 but the composition was also certified to contain $\leq$10 ppm O_2. Synthetic combustion gas for the 900°C tests of Phases 2 and 3 had a nominal composition of 540 ppm CO, 2.0% SO_2, 18% CO_2, $\leq$30 ppm O_2 and balance N_2. The oxygen and sulphur potentials calculated for this gas at 900°C are $\log_{10} Po_2 = -11.7$ and $\log_{10} Ps_2 = -5.4$. Both the carbon monoxide and sulphur dioxide concentrations were guaranteed to be within ±10% of the nominal composition while the preparation tolerance for carbon dioxide and nitrogen was ±5% of nominal. The actual composition of the gas contained in each type 1R cylinder was certified by Matheson. The accuracy of the certification analyses was ±2% of the nominal composition.

2.2 Apparatus and Procedure

2.2.1 Apparatus

The stress-rupture evaluations for each phase were conducted using stress-rupture machines and furnaces manufactured by Satec Inc. The equipment was designed so that stress-rupture testing could be conducted in accordance with ASTM designation E139-79.

The apparatus was described in detail in the Phase 1 interim report but because it was necessary to modify the equipment, a description of the revised apparatus follows. With reference to Figure 1, each resistance heated furnace consisted of a sealed cylindrical retort equipped with a removable top and bottom. Viton O-rings and cup seals provided the required gas seal for the top, bottom and also around the specimen pull rods. Cooling water which flowed through the removable top and bottom of each furnace protected the Viton seals. Synthetic combustion gas was supplied to each furnace through a common mild steel manifold to which four gas cylinders were connected. Gas from one or two of the cylinders connected to the manifold passed through a single pressure regulator which was used to maintain the gauge pressure at 140 kPa in the line which directed the gas to the bottom of each furnace via calibrated flowmeters. For the tests which employed 2000 ppm SO_2 gas, the flowmeters were used to control gas flowrates such that the gas velocity over the specimen surface was 100 mm/min. Flowrates of 75 mm/min were used for the 2.0% SO_2 synthetic combustion gas. Each furnace gas inlet line was equipped with a valved gas sample point which could be used as a separate purge line when required. Exhaust gas exiting from the top of each furnace through Tygon tubing was scrubbed using a caustic solution to remove sulphur dioxide and then vented to atmosphere.

Furnace temperatures were maintained using automatic temperature controllers in conjunction with calibrated type R platinum-rhodium thermocouples positioned in the middle of each furnace near the resistance wire. Specimen temperature was continuously monitored using a strip chart recorder connected to a calibrated type R thermocouple located close to the centre of the specimen gauge length. This thermocouple was not attached to the specimen gauge length because during Phase 2 and 3 stress-rupture testing, the oxide/sulphate deposit and actual bed material precluded thermocouple attachment to the gauge length.

Initially, Inconel 713 (a nickel base alloy) was the alloy material used for the retort liners, pull rods and clevises. As pointed out in the interim reports, the Inconel 713 equipment was changed to stainless alloy 310. The change was necessitated because extensive hot corrosion of the Inconel 713 alloy was encountered. The replacement stainless 310 alloy for the liner was purchased in the form of schedule 80 seamless pipe and it was necessary to completely dismantle and then rebuild the furnace each time the liner was replaced. In the case of the pull rods and clevises, attempts were made to protect these against hot corrosion through the use of diffusion coatings. Pack diffusion coatings of chromium were found to be more effective than those of aluminum although considerable corrosive attack was still encountered. The attack correlated with the number of times used rather than total time in contact with the aggressive environment, i.e. repetitive usage for short term tests resulted in greater attack than that encountered during a single long test. As a consequence of the hot corrosion, the useful life of the furnace retorts, pull rods and clevises was shortened.

2.2.2 Procedure

2.2.2.1 Stress-Rupture Testing

The same procedure was followed throughout the program. Briefly, prior to each stress-rupture test the uniformity of the hot zone, which would contain the 25 mm gauge length of the specimen, was verified. If required, the profile was adjusted so that the temperature was uniform within ±3°C over a 76 mm span. These profiles were determined using a furnace atmosphere of pure nitrogen (99.998% N_2) and gas flow rates similar to those which would be employed for actual stress-rupture testing.

After a test specimen was positioned in the furnace, pure nitrogen was used to purge the furnace and the purge was continued until the specimen reached the desired test temperature.

The required load was then added to the load pan of the stress-rupture machine and synthetic combustion gas replaced the nitrogen in the furnace retort. During the tests, gas flows and specimen test temperature were routinely checked. In the case of specimen temperature, a calibrated digital potentiometer was used to verify the strip chart temperature record. It was observed that specimen temperature remained constant within ±3°C of the test temperature for the duration

of each test. Analyses of gas samples, taken from the furnace inlet and exit gas flows, were conducted at various times during the testing program. In all cases the composition of both gases was found to be the same. Additionally, in two tests the gas flow was reduced by 50% to each retort and during this period both the inlet and exit gas flows were sampled then analyzed. No significant difference in gas composition was found. The specimen temperature monitoring thermocouple was checked after various long term tests and in each instance no change in calibration was apparent.

As indicated in the Phase 1 report, the initial stress levels for each alloy were predicted from graphs which were based on Larson-Miller Parameters (LMP)* computed with reference to stress-rupture test data in the literature. Because data for stainless alloy 347H were not available, reference data for alloy 347 were used. Although these graphs were based on stress-rupture tests conducted in air, they provided a logical starting point and also served as comparisons for the subsequent test results. Figure 2 shows the relationship of LMP to stress for stainless alloy 310 while Figure 3 shows the corresponding predicted rupture life in air for the alloy. Similar graphs were constructed for the other three alloys. In Figure 3, the two pairs of parallel lines bracket the minimum and maximum results expected for the test temperatures of 800 and 900°C and were based on data from Figure 2. It should be pointed out that the parallel lines indicate only in a general way the slope of data contained within them.

For Phase 3, Part 3 stress-rupture tests, the initial stress levels were chosen with reference to data obtained previously in the program together with a least squares analysis of actual test results.

After rupture of the test specimen, electric power to the furnace was automatically switched off but synthetic combustion gas continued to flow through the retort during the furnace cooling period. Synthetic combustion gas flow was halted after the cooling period and the specimen was then removed from the retort. One of the two pieces of the ruptured specimen was set aside for subsequent transmittal to the Scientific Authority while the other piece was examined metallographically.

---

* $LMP = T\,(20 + \log_{10} t)/556$ where T = Temperature (K) and t = time (h)

2.2.2.2 Technique for the Application of a Simulated Deposit to the Test Specimens

Development of the technique for application of the simulated bed deposit to test specimens was conducted concurrently with Phase 1 testing. The application technique was required for Phase 2 stress-rupture tests. The simulated deposit consisted of CaO and $CaSO_4$ mixed in the ratio of 1:6 by weight. Initial trials involved mixing the two components with water to produce a slurry which was then applied to metal rods to build up the 3 mm thick deposit as specified by the Scientific Authority. After air drying the deposit, the slurry coated rods were heated for ~30 min at 900°C in pure N_2.

Inspection of the coated rods after heating showed that severe cracking of the dried slurry deposit had occurred and in some instances the simulated deposit had flaked off the rod.

Addition of the deposit to an aqueous 3% gelatin solution could be used to prepare a slurry which produced a deposit that remained intact and adhered to test rods after heat treatment. However, it was found that the deposit failed to remain in intimate contact with test specimens during stress-rupture testing. Elongation of the test specimen during stress-rupture testing caused a reduction in cross sectional area and resulted in the specimen breaking away from the inelastic mortar-like deposit.

Since it was necessary that the deposit remain in contact with the specimen over the gauge length during stress-rupture testing it was decided to use a loose granular mixture of the simulated deposit packed in a bag which surrounded the test specimen. The bag was fabricated using commercially available refrasil cloth (an amorphous refractory SiO_2 product). Platinum-rhodium wire secured the bag to the test specimen. The technique was used in a stress-rupture test in which stainless alloy type 310 was subjected to a stress of 34.5 MPa in synthetic combustion gas at 900°C. The test was terminated after 60 h. After cooling and removing the sample from the retort it was found that the deposit containment bag was intact. From these tests it was concluded, after consultation with the Project Scientific Authority, that the latter procedure would be employed for subsequent Phase 2 and 3 stress-rupture tests.

2.2.2.3 Preparation of the Actual Bed Material from the Nova Scotia Pilot Plant

Approximately 20 kg of the bed material were received from the EMR/NSPC atmospheric fluidized bed combustor facility at Point Tupper,

Nova Scotia. The bed material had been collected over a two week period. At Sherritt, the bed material was crushed under an argon atmosphere using a hammer mill. The crushed material was blended, sampled then stored under argon. Screen and chemical analyses are shown in Table 3. For the Phase 3 stress-rupture tests, the application of the bed material to the test specimen was done using the procedure employed for the simulated bed deposit. The technique as described in Section 2.2.2.2 involved loosely packing the bed material into a refrasil bag which surrounded the specimen gauge length. Platinum-rhodium wire secured the bag to the specimen. At the conclusion of each Phase 3 test the containment bag was found to be intact.

3.0 RESULTS AND DISCUSSION

Stress-rupture data for the 800 and 900°C tests of the program are tabulated in Tables 4 to 10 and are compared in Figures 4 to 11. In the Figures the dashed lines indicate the minimum and maximum expected results for comparable tests conducted in air without any deposit contacting the specimen.

The stress-rupture results for the 800°C tests of Phase 1 in which the alloys were tested in the 0.2% SO_2 synthetic combustion gas showed that two of the alloys, cast alloy HK40 and Incoloy 800H, when tested using low stress had rupture lives which were somewhat shorter than the expected rupture lives when tested in air. Data for stainless alloys 310 and 347H compared well with the reference data from the literature. Results from the Phase 2 and 3 800°C tests which incorporated the simulated deposit and the actual bed material respectively, in addition to the 0.2% SO_2 combustion gas indicated that the rupture lives of both 310 and 347H were unaffected by the coatings. The apparent trend of Phase 1 for shorter rupture life at lower stress levels for both HK40 and Incoloy 800H was reflected by the Phase 2 and 3 test results.

Testing the alloys under Phase 1 conditions of 900°C and 2000 ppm SO_2 combustion gas resulted in rupture lives which showed little deviation from the expected rupture lives of the alloys when tested in air. The rupture lives of the alloys when tested in the 2.0% SO_2 content combustion gas of Phase 2 were similar to the results of Phase 1. Combining the 2.0% SO_2 gas with the simulated deposit in Phase 3, Part 1 tests or using the 2.0% SO_2 gas and the actual bed material in Part 3 of Phase 3 had little comparative effect on the rupture lives of the alloys. Note that the data for the HK40 and

and Incoloy 800H 900°C tests in Figures 9 and 10 had the same general fit to the reference data that was apparent for the 800°C tests as shown in Figures 5 and 6. This suggested that the deviation from the literature values at low stress reflected an alloy heat variation rather than an effect imposed by the experimental conditions of the program. In Figures 4 to 11, the solid line represents the curve of best fit for all the data. Indices of determination, r^2, for these curves were ≥ 0.93 and suggested that the data could be treated as if from one population.

The appearances of the Phase 3, Part 3 800°C ruptured test specimens are shown in Figures 12 and 13. The photographs show that 347H appeared to be least affected by the test conditions and Incoloy 800H was affected the most. This was the same trend observed in previous work for Phase 1 and 2 and was also similar to the 900°C test specimens of Phase 3 as shown in Figures 14 and 15.

Metallographic examination of the Phase 3, Part 3 ruptured specimens showed that sulphidation had occurred in all test pieces. For each suite of test samples, the degree of attack appeared to correlate with areas of the specimens which had undergone high deformation, and with time of exposure in the test environment. For example Figure 16 shows the sulphidation observed near the fracture and fillet areas in stainless alloy 347H specimens which had rupture lives of 9.9 and 1123 h at 800°C. Effects of hot corrosion observed in Incoloy 800H, stainless alloy 310 and cast alloy HK40 which were tested at 800°C under conditions of high and low stress are shown in Figures 17 and 18. Similar results were observed in the 900°C test specimens as shown in Figures 19 and 20.

Electron microprobe analysis was done of an area exhibiting hot corrosion in a Phase 3 stainless alloy 347H test specimen which had failed after 4.3 h at 900°C and the results are shown in Figure 21. As illustrated by the white dots in the X-ray maps and with reference to the absorbed electron image it was apparent that inward penetration of sulphur had occurred. In some areas of the corrosion deposit, nickel, chromium and to a lesser extent iron appeared to be associated with the sulphur. In other regions the iron and chromium were not associated with sulphur and were probably present as oxides.

In Figure 22 the results from the microprobe analysis of an area in Incoloy 800H are shown. This specimen was tested at 900°C using 31.7 MPa and had a rupture life of 333.7 h. The area of the test piece

which was analyzed was located just above the unattacked matrix as shown in the photomicrograph of the Figure. The absorbed electron image (negative polarity) indicates the precise area over which the electron beam was scanned. The X-ray map for chromium illustrates that the element has diffused from the grains to the grain boundaries and then along the boundaries to the alloy surface. Evidence of the inward penetration of sulphur along the boundaries can be seen in the X-ray map for sulphur.

Evidence of the outward diffusion of chromium was also observed in cast alloy HK40 which had a rupture life of 90 h at 800°C. In Figure 23 the sulphidation associated with a stress crack in this alloy can be seen. In this instance, the microprobe analysis indicates a primary association of sulphur with nickel and to a lesser extent with chromium and iron. Note the high chromium concentration in the outside surface suggesting an association with oxygen as an oxide.

These microprobe analyses together with the analysis of ruptured specimens from previous work of Phases 1 and 2 have illustrated the effects that sulphidation had on the distribution of chemical elements. Collectively, the analyses have shown that chromium diffusion was generally in the direction of the alloy surface and was greater than the diffusion of iron or nickel. Inward penetration of sulphur was also found and the diffusion occurred generally along grain boundaries and stress cracks.

Hot corrosion however did not appear to have an effect on the rupture life of the alloys, as indicated by the data of Figures 4 to 11. However the stress-rupture experimental conditions had a very marked affect on the clevises and pull rods which were employed as specimen supports, and on the furnace retort liner. Hot corrosion of these pieces of equipment was very apparent. The hot corrosion of the clevises and the retort liners has been discussed in previous reports. Briefly, in attempts to reduce the effect of hot corrosion, a chromium pack diffusion treatment was applied to the pull rods and clevises and the resulting coating appeared to offer protection against the aggressive environment; particularly for the long term tests. It was found that the diffusion coatings were not as effective for repetitive short term tests because of a breakdown of the protective coating. As a consequence, hot corrosion advanced rapidly under these conditions. Similar results, i.e. shorter life when used repetitively for short term tests, were apparent for the stainless alloy 310 retort liners, although

the liners were not chromium diffusion coated. Thus, throughout the program, the useful lives of the pull rods, clevises and retort liners were markedly reduced because of hot corrosion.

The normal model for hot corrosion (sulphidation) involves the diffusion of chromium from the matrix of the alloy to the surface which is exposed to sulphur attack. At the surface an oxide of chromium is formed which provides protection for the alloy, provided that the integrity of the oxide remains intact. If a break in the oxide should occur then additional chromium diffuses to the area and again a protective oxide is formed. Repetitive sustained damage to the oxide will result in a severe depletion of chromium from the alloy matrix (i.e. Figure 22) which leads to severe degradation of the alloy.

From the data obtained in the present studies, it is quite clear that hot corrosion of the test alloys was not severe enough to affect the behavior of the alloys during stress-rupture testing.

From the above simple outline of hot corrosion, it could be argued that one should expect more hot corrosion to occur under conditions of repetitive short duration high stress because of the increased probability of fracturing the protective oxide coating. But that suggests that alloys which exhibit different amounts of deformation during stress-rupture testing ought to be affected differently when tested under conditions in which hot corrosion could occur. Specifically, it should be expected that the protective oxide coating should sustain more damage if the alloy was characterized by high elongation during testing than if the alloy exhibited a low elongation. For example cast alloy HK40 at ~5 to 10% and stainless alloy 347H at ~70 to 90% are alloys that exhibited different elongation during testing. A possible reason for the apparent lack of aggressive attack of stainless alloy 347H was presented in a previous interim report. In the report it was suggested that most of the elongation, and hence subsequent damage to the oxide coating, occurred during tertiary creep in a relatively short time period prior to rupture of the specimen. At the conclusion of this project a number of special experiments were conducted in an attempt to confirm this model for the experimental findings of the program.

One series of experiments was undertaken to define a simulated creep curve for two of the test alloys. The simulated creep curve was constructed by monitoring the take up motor of the Satec stress-rupture

testing machine. Under this arrangement, the testing machine provides a balancing take up on the loading beam in order to maintain the specimen gauge length within the hot zone of the furnace. A system of sensing microswitches on the beam provides the necessary start and stop signals to the take up motor. The "creep" monitoring system involved a relatively simple parallel intercept of the signal sent to the take up motor. Output from the intercept was directed to a strip chart and a series of on-off events was recorded over time. Each event measured an approximately constant amount of specimen elongation. These on-off events were summed for the test and a normalized measure of deformation was obtained.

A plot of the normalized deformation against the normalized elapsed time of the Phase 3 800°C test for 800H is shown in Figure 24. The data indicate that about 60% of the elongation deformation occurred during the last ten percent of the elapsed time for the test. A similar result was obtained for stainless alloy 347H as illustrated in Figure 25. Since most of the elongation deformation occurred during a relatively short period of time, it should be expected that only limited hot corrosion would occur. Furthermore, it is possible that the early deformation sustained during the stress-rupture test may have been beneficial under the program conditions of hot corrosion, in that the rate of chromium diffusion along the strained grain boundaries would be accelerated. Any subsequent fracture of the protective oxide would then be repaired comparatively faster than during a test in which stress was negligible, and a consequence of this may be added protection against hot corrosion.

An additional 900°C stress-rupture test was conducted to determine the effect of significant temperature variations on the stress-rupture behavior of one of the program alloys. This test was conducted to superimpose onto the program stress-rupture test conditions, the temperature fluctuations that were encountered in service by the stainless alloy 310 retort. These conditions were believed to be responsible for the massive hot corrosion that occurred in the liners. For this test, uncoated cast alloy HK40 was used and a stress level of 30.8 MPa was chosen. This stress would normally cause rupture in ~1000 h. After 16 h at 900°C, the electric power to the furnace was shut off and the specimen was allowed to cool to ~200°C. Approximately 5.5 h was required to cool the specimen from 900 to 200°C. During the cooling period the stress on the specimen was maintained and the 2.0% SO_2 combustion gas continued to flow through the retort. After cooling to 200°C the furnace power was turned on and the specimen was reheated

to the 900°C test temperature and held at temperature for an additional 16 h. Approximately 2.5 h were required to regain the 900°C set point. Three thermal cycles were applied to the loaded test specimen and after the third cycle the specimen was maintained at 900°C until rupture occurred. Rupture occurred after only 201.6 h which was a significant reduction from the expected 1000 h life. The appearance of the ruptured thermally cycled specimen is shown in Figure 26 and it is quite clear that massive hot corrosion occurred. This result is completely different from the minimal amount of attack exhibited by the specimens during the stress-rupture tests conducted within the scope of the program.

4.0 CONCLUSIONS

The stress-rupture tests for the program were successfully completed according to the Statement of Work.

The experimental data showed that the stress-rupture properties of the program alloys were unaffected by the 2000 ppm SO_2 combustion gas at 800°C or by the 2.0% SO_2 combustion gas at 900°C.

Use of the simulated deposit or the actual bed material during 800 or 900°C tests in synthetic combustion gas had little effect on the rupture lives of the alloys.

Hot corrosion of the program alloys during the 800 or 900°C stress-rupture tests occurred but the degradation did not affect the rupture lives.

At 800 and 900°C, the extent of hot corrosion observed in stainless alloy 347H was less than for the other alloys whilst Incoloy 800H showed the most corrosion.

Temperature cycling during a 900°C stress-rupture test in 2.0% SO_2 combustion gas promoted hot corrosion and reduced the expected rupture life of the alloy. However, more work would be required to quantify the observed affect and determine the sensitivity of different alloys.

Table 1 Chemical Analyses of Test Alloys

	Analyses (%)											
	Incoloy 800H			310			HK40			347H		
	Min	Max	Actual	Min	Max	Actual	Min	Max	Actual	Min	Max	Actual
Al	0.15	0.6	0.31	n.s.	n.s.	-	n.s.	n.s.	-	n.s.	n.s.	-
C	0.05	0.10	0.08	-	0.15	0.12	0.35	0.45	0.45	0.04	0.10	0.07
Cb+Ta	n.s.	n.s.	-	n.s.	n.s.	-	n.s.	n.s.	-	8xC	1.0	0.90
Cr	19.0	23.0	20.17	24.0	26.0	24.37	23.0	27.0	24.81	17.0	19.0	18.2
Cu		0.75	0.61	n.s.	n.s.	-	n.s.	n.s.	-	n.s.	n.s.	-
Mn		1.50	0.94	-	2.00	1.69	-	1.50	0.73	-	2.00	1.83
Mo	n.s.	n.s.	-	n.s.	n.s.	-	-	0.50	0.052	n.s.	n.s.	-
Ni	30.0	35.0	32.9	19.0	22.0	19.01	19.0	22.0	20.69	9.0	13.0	10.77
P	n.s.	n.s.	-	-	0.040	0.031	-	0.040	0.019	-	0.040	0.030
S		0.015	0.001	-	0.030	0.006	-	0.040	0.012	-	0.030	0.007
Si		1.0	0.60	-	0.75	0.66	0.50	2.00	1.11	-	1.00	0.48
Fe	39.5	n.s.	43.95	n.s.	n.s.	-	n.s.	n.s.	-	n.s.	n.s.	-
Ti	0.15	0.60	0.45	n.s.	n.s.	-	n.s.	n.s.	-	n.s.	n.s.	-
ASTM: UNS:	B-408-77 N08810			A249-80 S31000			A608-79 J94224			A479-80a S34709		
Supplier	Inco Alloys Canada Ltd			Specialty Steels			Fahramet			Atlas Alloys		
Heat No:	HH0898A M1989			40477			75016			A11330		

n.s. Not specified

Table 2 Physical Properties of Test Alloys*

Alloy	Supplier	Heat No	Reference ASTM	Short Term Tensile			Hardness R_B	Grain Size ASTM
				YS(MPa)	UTS(MPa)	Elongation(%)		
310 Stainless	Specialty Steels	40477	A249-80	282(205)	642(515)	44(35)	80(90max)	8-9
347H	Atlas Alloys	A11330**	A479-80a	482(205)	662(515)	46(35)	99(n.s.)	9-10
HK40	Fahramet	75016	A608-79	n.s***	n.s.			
800H	Inco Alloys Canada Ltd	HH0898A M1989	B408-77	179(170)	568(450)	56(30)	78(n.s.)	4.5

* Bracketed numbers represent minimum values, except as noted, from reference data

** Alloy heated to 1066°C min for sufficient time to dissolve carbides then quenched in water

*** As outlined in ASTM A608 Section 8, "tensile tests at room temperature are not recommended as acceptance criteria"

n.s. Not specified

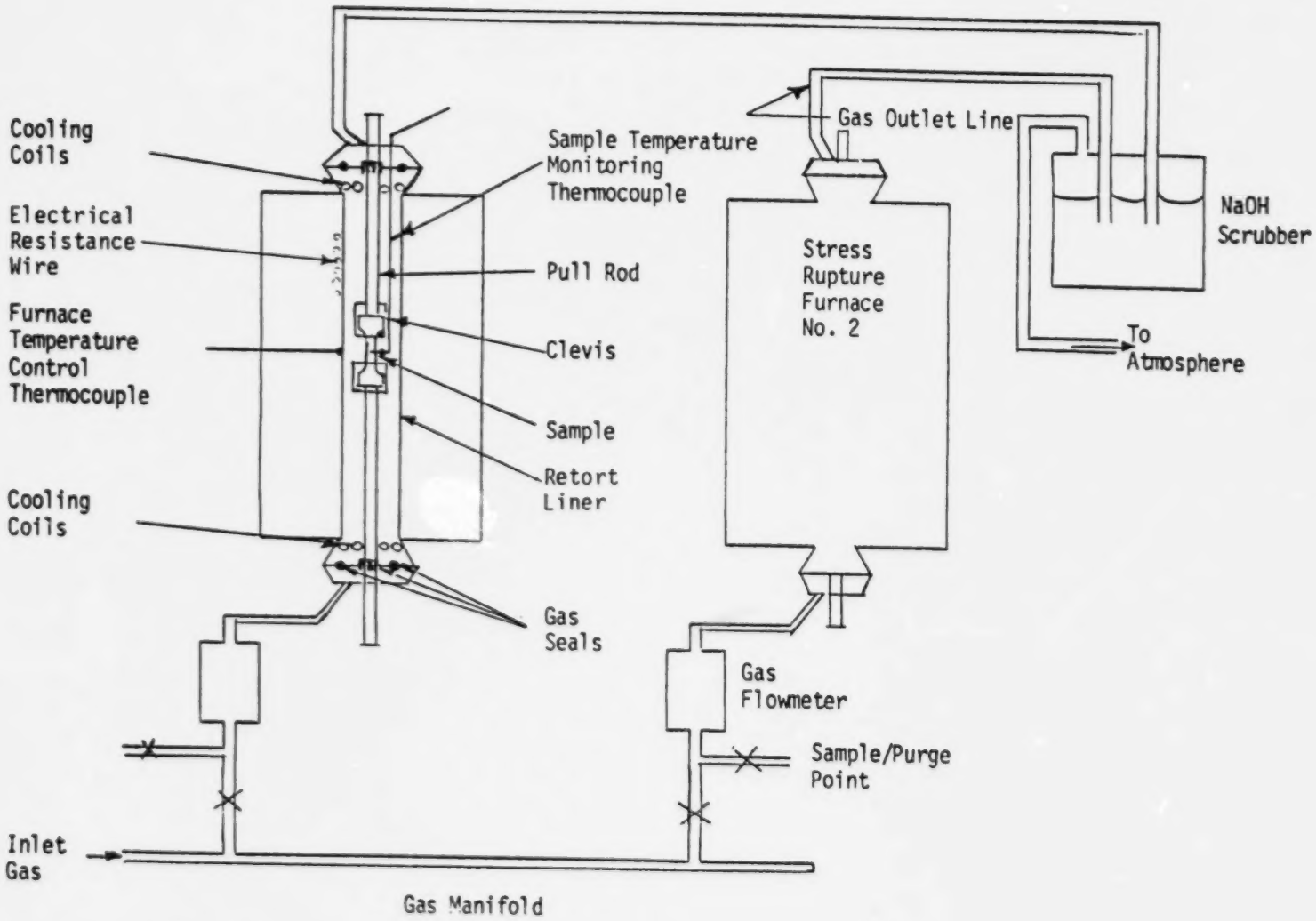

Figure 1 Schematic of Stress-Rupture Testing Apparatus

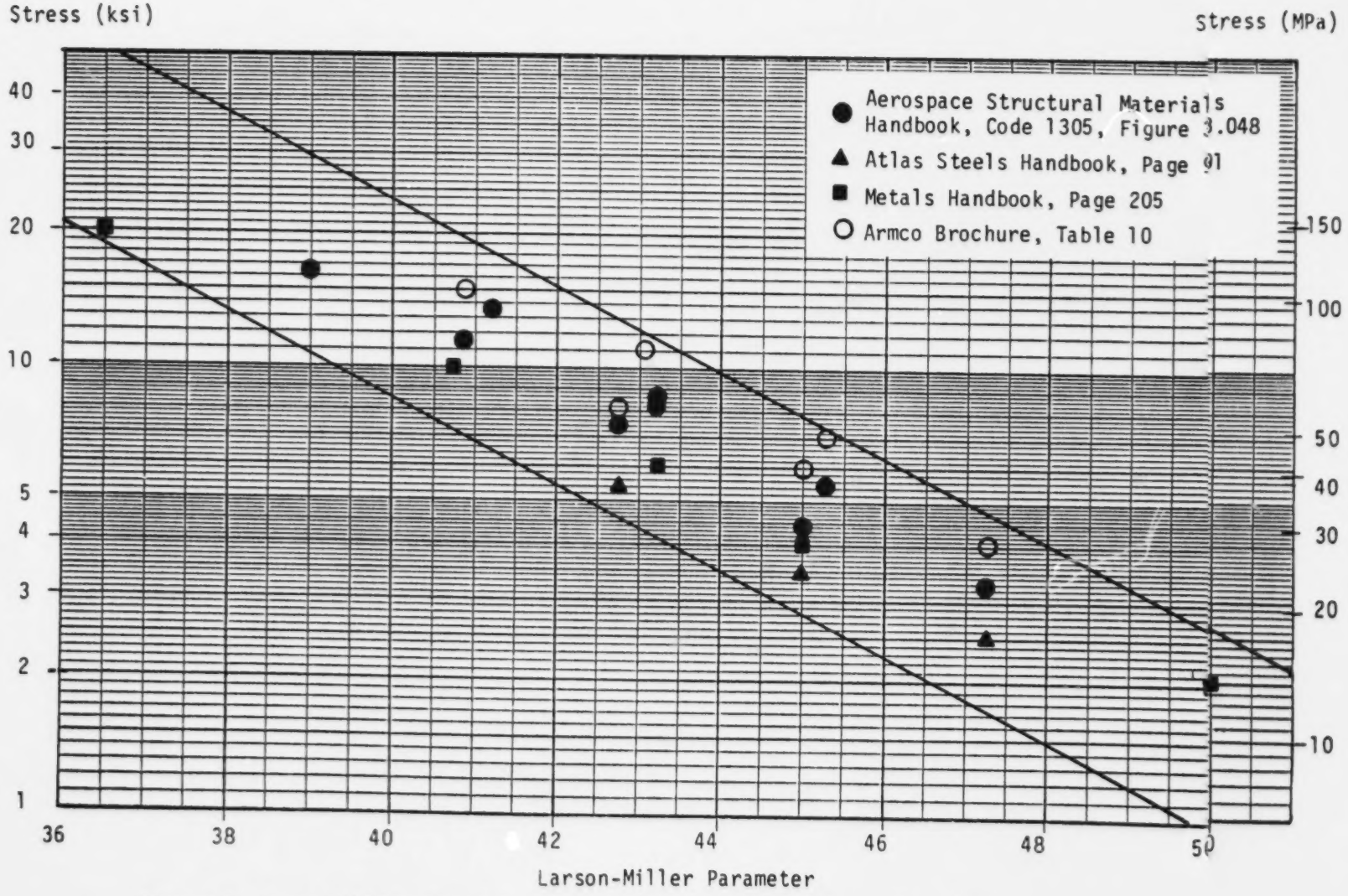

Figure 2 Larson-Miller Parameter Versus Stress for Stainless Alloy 310

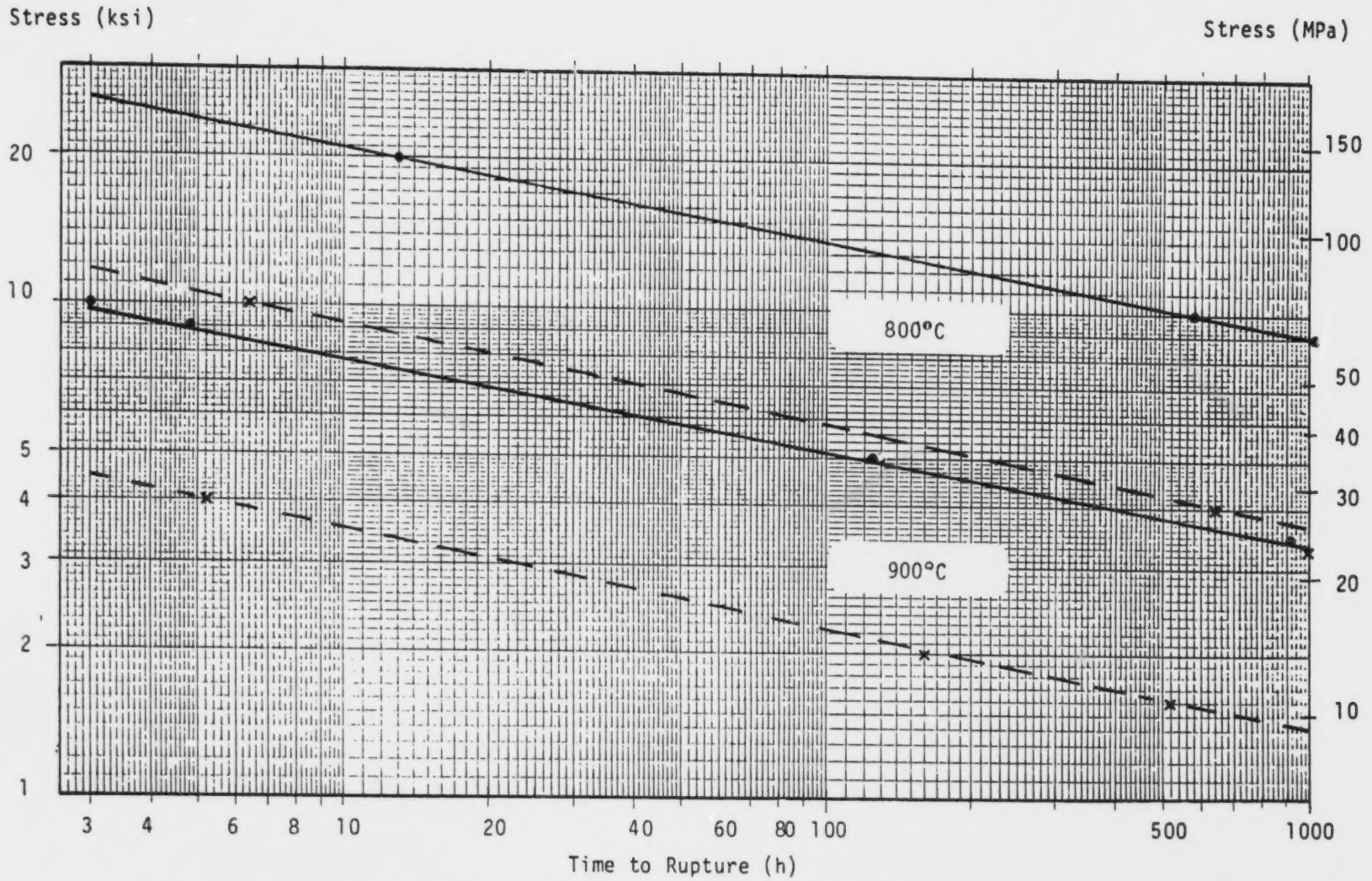

Figure 3 Predicted Rupture Life in Air for Stainless Alloy 310

Table 3 Analyses of the Actual Bed Material from the Nova Scotia Pilot Plant

(A) Chemical Analyses of As Received Material*

Analyses (% by Weight)										
Na	S	C	Cl	Fe	CaO	K_2O	SiO_2	Al_2O_3	MgO	LOI
0.34	3.10	0.31	<0.01	3.17	19.0	2.93	43.1	18.3	2.35	8.2

* Analysis by Canada Centre for Mineral and Energy Technology

(B) Screen Analyses of Milled Bed Material

Tyler Screen (mesh)	+48	-48 +100	-100 +150	-150 +200	-200 +250	-250 +325	-325
Analyses (%)	tr	tr	1.1	7.5	7.8	26.0	57.6

Table 4 Phase 1 Stress-Rupture Data for the Program Alloys Tested at 800°C in 2000 ppm SO_2 Synthetic Combustion Gas

Alloy	Test Stress (MPa)	Time to Rupture (h)	Elongation (%)
Stainless Alloy 310	110.4	3.2	66
	88.3	12.4	40
	74.5	24.7	33
	58.7	77.7	28
	38.0	511.2	21
Cast Alloy HK40	151.8	4.5	20
	131.1	13.1	12
	98.7	68.5	5
	86.3	73.5	n.d.
	86.3	91.1	6
	55.2	492.3(1)	n.d.
Incoloy 800H	124.2	2.6	58
	103.5	11.1	(2)
	82.8	25.1	(2)
	70.4	68.7	(2)
	44.5	573.7	(2)
Stainless Alloy 347H	189.8	0.3	40
	158.7	7.0	34
	131.1	16.7	43
	100.0	40.0	60
	75.9	76.5	60
	35.9	1352.7(3)	95

(1) Power failure, sample broke on cooling

(2) Heavy corrosion

(3) Gas was at half flow (i.e. 50 mm/min over the gauge length) for 168 h because of a shortage in gas supply

n.d. Not determined

Table 5 Phase 1 Stress-Rupture Data for the Program Alloys Tested at 900°C in 2000 ppm SO_2 Synthetic Combustion Gas

Alloy	Test Stress (MPa)	Time to Rupture (h)	Elongation (%)
Stainless Alloy 310	60.7	3.4	n.d.
	48.3	11.9	40
	34.5	50.2	37
	27.6	173.1	33
	20.7	833.7	32
Cast Alloy HK40	89.7	5.9	14
	75.9	15.7	(1)
	56.6	59.5	4
	44.9	95.3	2
	31.7	957.3(2)	5
Incoloy 800H	58.7	4.5	39
	48.3	13.8	25
	36.6	65.8	22
	30.4	291.0(3)	(1)
	26.2	240.8	n.d.
	22.4	1004.9	32
Stainless Alloy 347H	65.6	2.6	72
	44.2	14.5	80
	32.4	44.4	113
	24.8	107.0	88
	14.5	640.9	70

(1) Gauge marks obscured

(2) Gas was at half flow (i.e. 50 mm/min over the gauge length) for 168 h because of a shortage in gas supply

(3) Synthetic combustion gas ran out after 265 h; N_2 used for balance of test

n.d. Not determined

Table 6 Phase 2 Stress-Rupture Data for the Program Alloys Tested at 800°C in 2000 ppm SO_2 Synthetic Combustion Gas and Simulated Fluidized Bed Deposit

Alloy	Test Stress (MPa)	Time to Rupture (h)	Elongation (%)
Stainless Alloy 310	89.6	15.6	40
	71.0	55.2	25
	62.1	106.6	18
	50.3	109.2	29
	50.3(1)	148.4	29
	32.8	787.7	26
Cast Alloy HK40	133.8	19.0	13
	108.3	51.8	6
	96.5	78.1	6
	70.3	367.3	3
	56.9	423.8	4
	51.5(2)	1192.7	4
Incoloy 800H	103.4	12.4	63
	89.6	17.7	59
	76.6	96.3	n.d.
	56.5	83	40
	51.5(2)	788.8	25
	37.2	1445.1	n.d.
Stainless Alloy 347H	145.5	11.9	37
	106.2	40.7	50
	84.1	78.4	67
	54.5	320.0	67
	39.7	1031.4	100

(1) Retest

(2) Test conducted during Part 2 of Phase 3

n.d. Not determined because heavy corrosion obliterated the gauge marks

Table 7 Phase 2 Stress-Rupture Data for the Program Alloys Tested at 900°C in 2.0% SO_2 Synthetic Combustion Gas

Alloy	Test Stress (MPa)	Time to Rupture (h)	Elongation (%)
Stainless Alloy 310	54.0	11.6	37
	39.3	50.7	28
	34.3	69.4	28
	27.8	293.2	25
	21.0	264.6	30
	20.9	901.0	23
Cast Alloy HK40	82.7	13.5	6
	63.6	57.7	6
	54.0	95.9	3
	44.0	259.5	5
	(44.0)	(120.3)	(1)
	33.5	482.5	3
	30.5	835.6	6
Incoloy 800H	52.0	14.2	43
	40.0	31.3	14
	35.9	93.3	13
	27.6	575.0	19
	23.0	1219.5	20
Stainless Alloy 347H	48.0	10.8	21
	35.2	34.5	95
	26.2	89.2	73
	18.6	260.0	82
	12.6	1181.1	98

(1) Apparent reaction of SO_2 with an Inconel 713C clevis caused premature rupture

Table 8 Phase 3, Part 1 Stress-Rupture Data for the Program Alloys Tested at 900°C in 2.0 SO_2 Synthetic Combustion Gas and Simulated Fluidized Bed Deposit

Alloy	Test Stress (MPa)	Time to Rupture (h)	Elongation (%)
Stainless Alloy 310	55.0	5.6	52
	34.3	121.1	27
	27.6	247.0	28
	22.7	244.8	25
	18.8	822.4	36
Cast Alloy HK40	92.0	10.7	6
	62.9	45.2	4
	54.0	139.7	4
	44.0	170.4	3
	30.8	984.5	7
	30.0	n.d.	(1)
Incoloy 800H	52.0	12.9	32
	40.5	51.2	25
	36.0	93.8	13
	30.0	403.7	10
	24.8	650.2	20
Stainless Alloy 347H	50.0	16.7	78
	34.5	52.4	80
	28.3	92.2	90
	18.6	420.1	105
	14.3	680.3	92
	14.0	n.d.	(2)

(1) Not determined, test discontinued after 1432.0 h because specimen supports and interior wall of furnace retort were bonded together by corrosion products

(2) Not determined, test discontinued after 1596.5 h because specimen supports and interior wall of furnace retort were bonded together by corrosion products

Table 9 Phase 3, Part 3 Stress-Rupture Data for the Program Alloys Tested at 800°C in 2000 ppm SO_2 Synthetic Combustion Gas and Actual Bed Material

Alloy	Test Stress (MPa)	Time to Rupture (h)	Elongation (%)
Stainless Alloy 310	96.5	6.1	38
	67.6	47.5	25
	47.4	165.3	33
	34.1	407.6	28
Cast Alloy HK40	137.9	19.5	9
	120.6	37.2	6
	90.3	89.6	5
	70.3	258.6	3
	49.0	1036.8	5
Incoloy 800H	103.4	9.7	63
	89.6	32.0	40
	68.9	190.9	39
	55.2	293.5	20
	45.5	745.5	n.d.(1)
Stainless Alloy 347H	144.8	9.9	40
	100.0	36.8	46
	55.1	360.9	78
	40.7	1123.9	98

(1) Not determined because heavy corrosion obliterated the gauge marks

Table 10 Phase 3 Part 3 Stress-Rupture Data for the Program Alloys Tested at 900°C in 2.0% SO_2 Synthetic Combustion Gas and Actual Bed Material

Alloy	Test Stress (MPa)	Time to Rupture (h)	Elongation (%)
Stainless Alloy 310	50.1	14.4	25
	36.3	42.4	40
	26.3	133.1	40
	18.8	1756.5	25
Cast Alloy HK40	91.7	5.8	8
	71.0	26.4	6
	51.0	90.4	7
	37.2	280.7	13
	29.0	1070.3	6(1)
Incoloy 800H	53.1	10.0	35
	44.1	34.0	37
	36.0	153.8	36
	31.7	333.7	n.d.(2)
	22.0	1320.9	n.d.
Stainless Alloy 347H	59.0	4.3	70
	34.5	36.7	88
	20.3	366.2	95
	13.1	1502.9	80

(1) Sample broke outside gauge marks

(2) Not determined because heavy corrosion obliterated the gauge marks

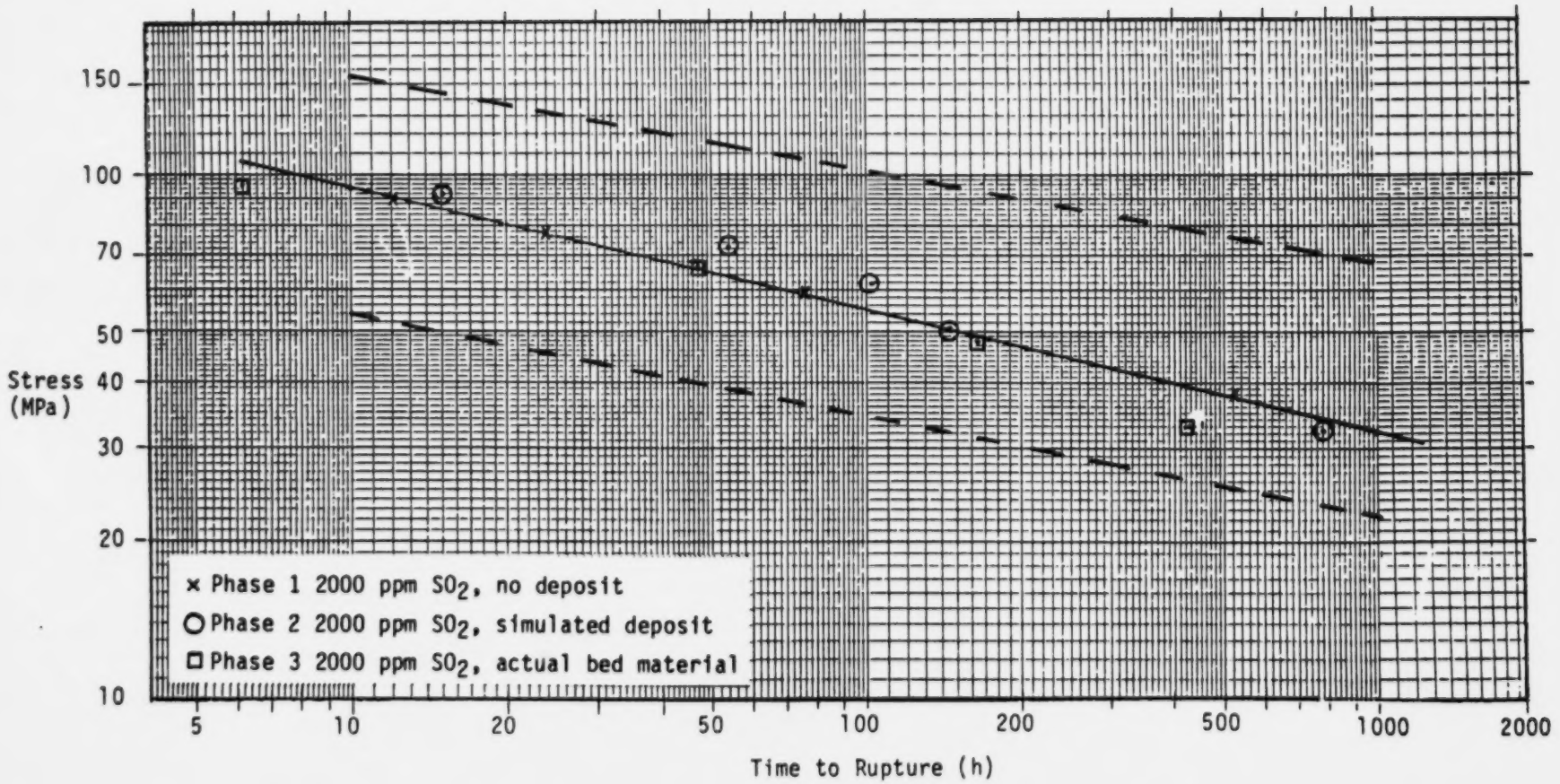

Figure 4 Stress-Rupture Tests for Stainless Alloy 310 at 800°C in Synthetic Combustion Gas

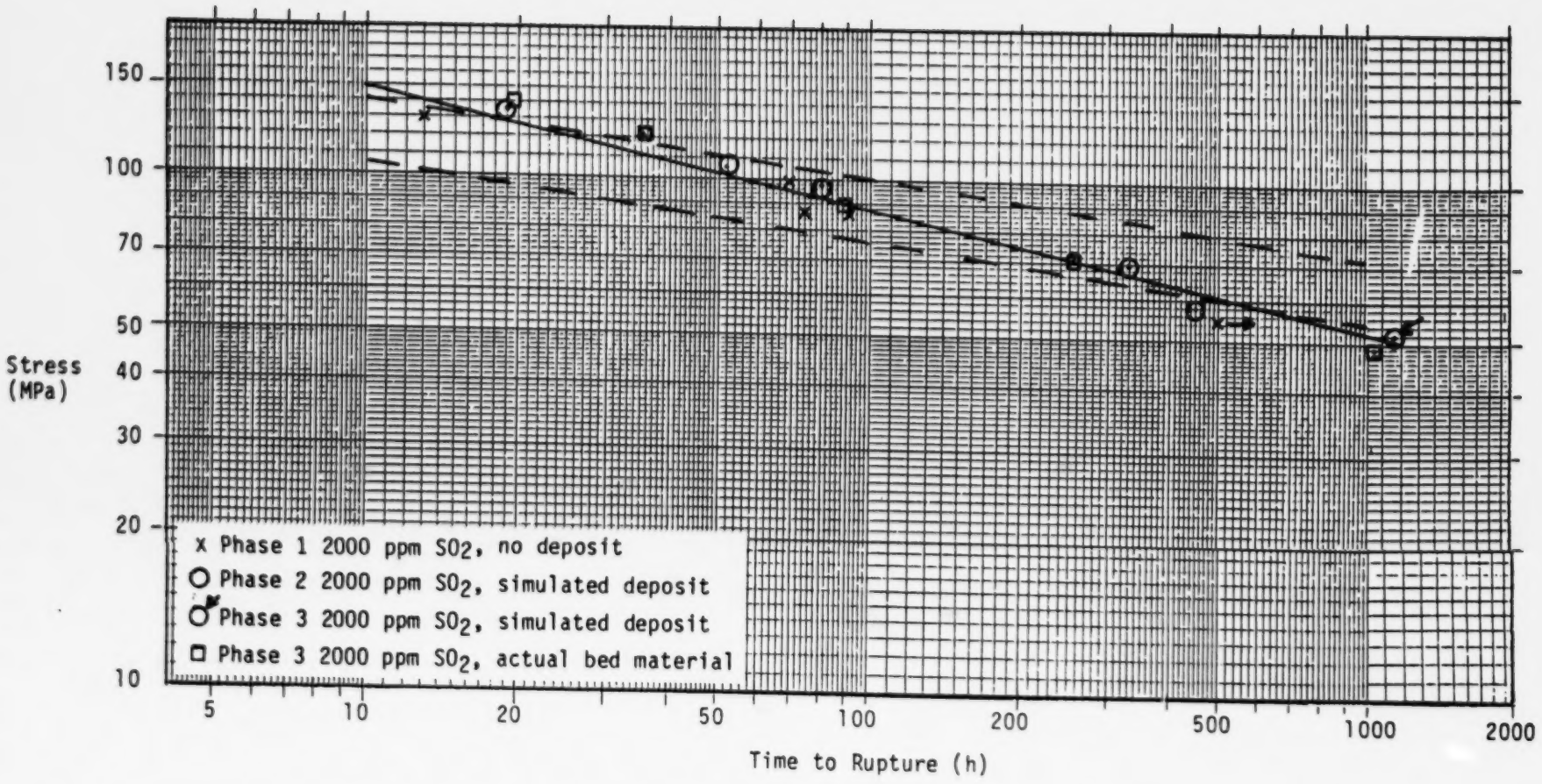

Figure 5 Stress-Rupture Tests for Cast Alloy HK40 at 800°C in Synthetic Combustion Gas

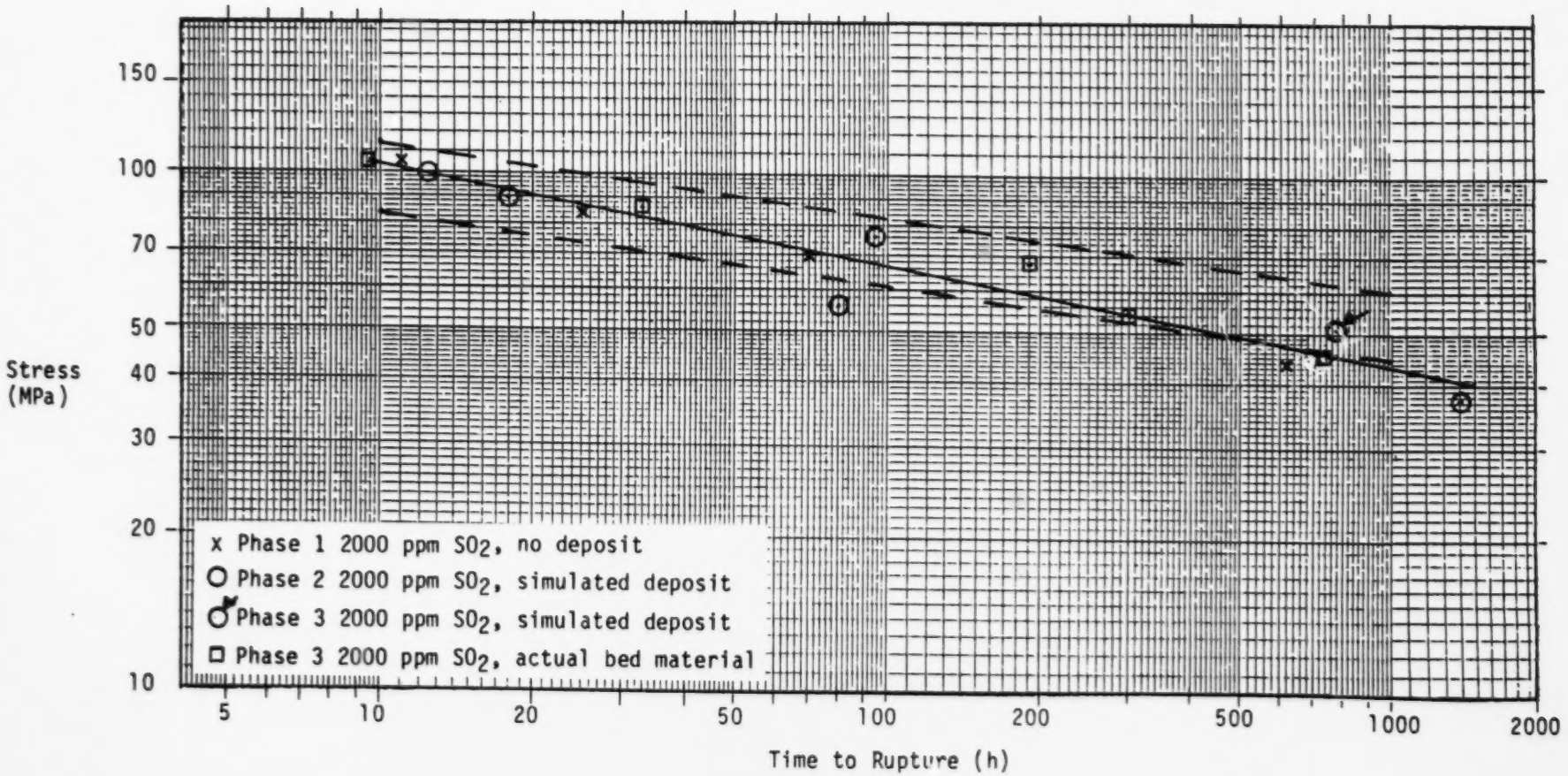

Figure 6 Stress-Rupture Tests for Incoloy 800H at 800°C in Synthetic Combustion Gas

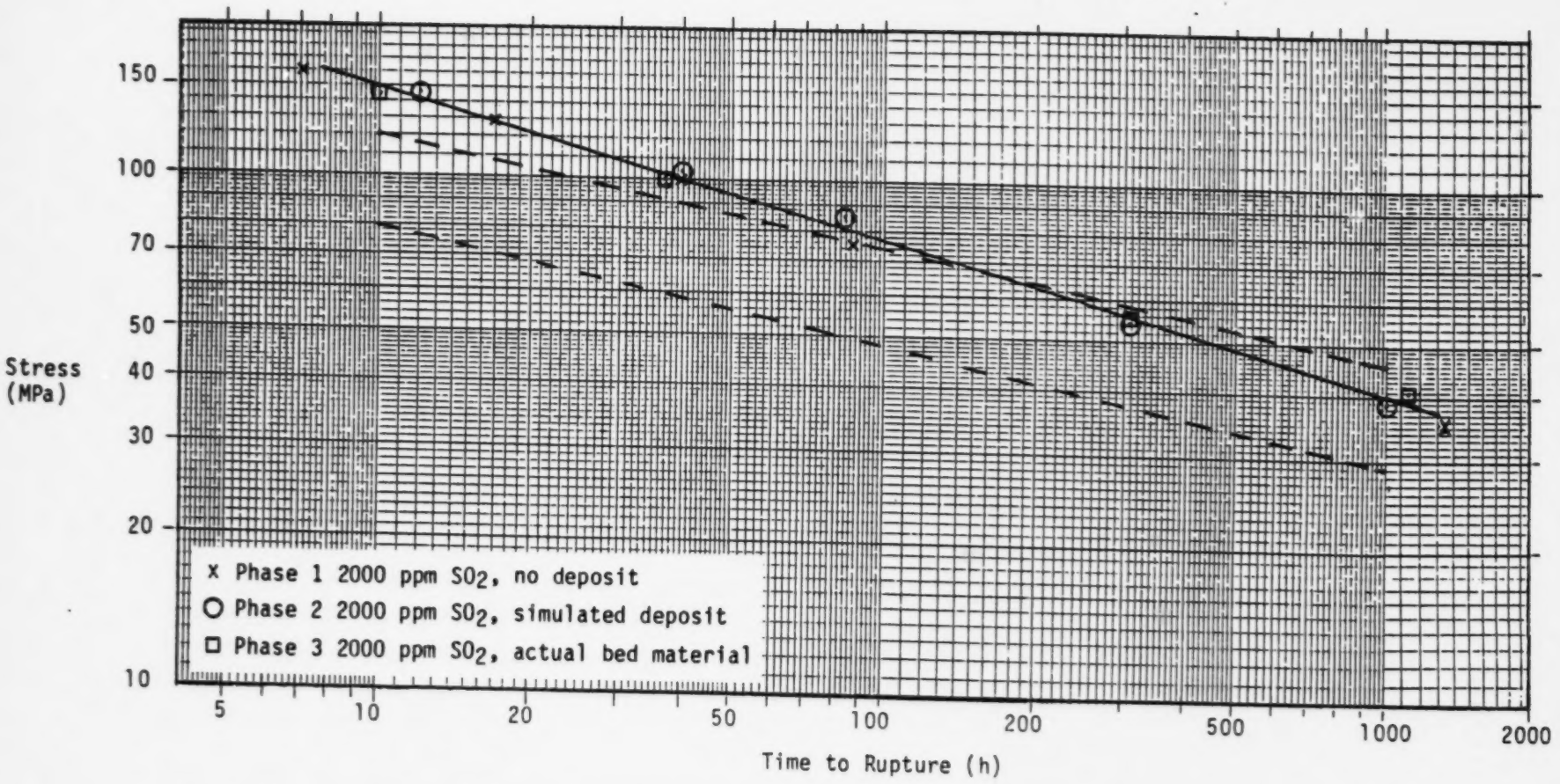

Figure 7 Stress-Rupture Tests for Stainless Alloy 347H at 800°C in Synthetic Combustion Gas

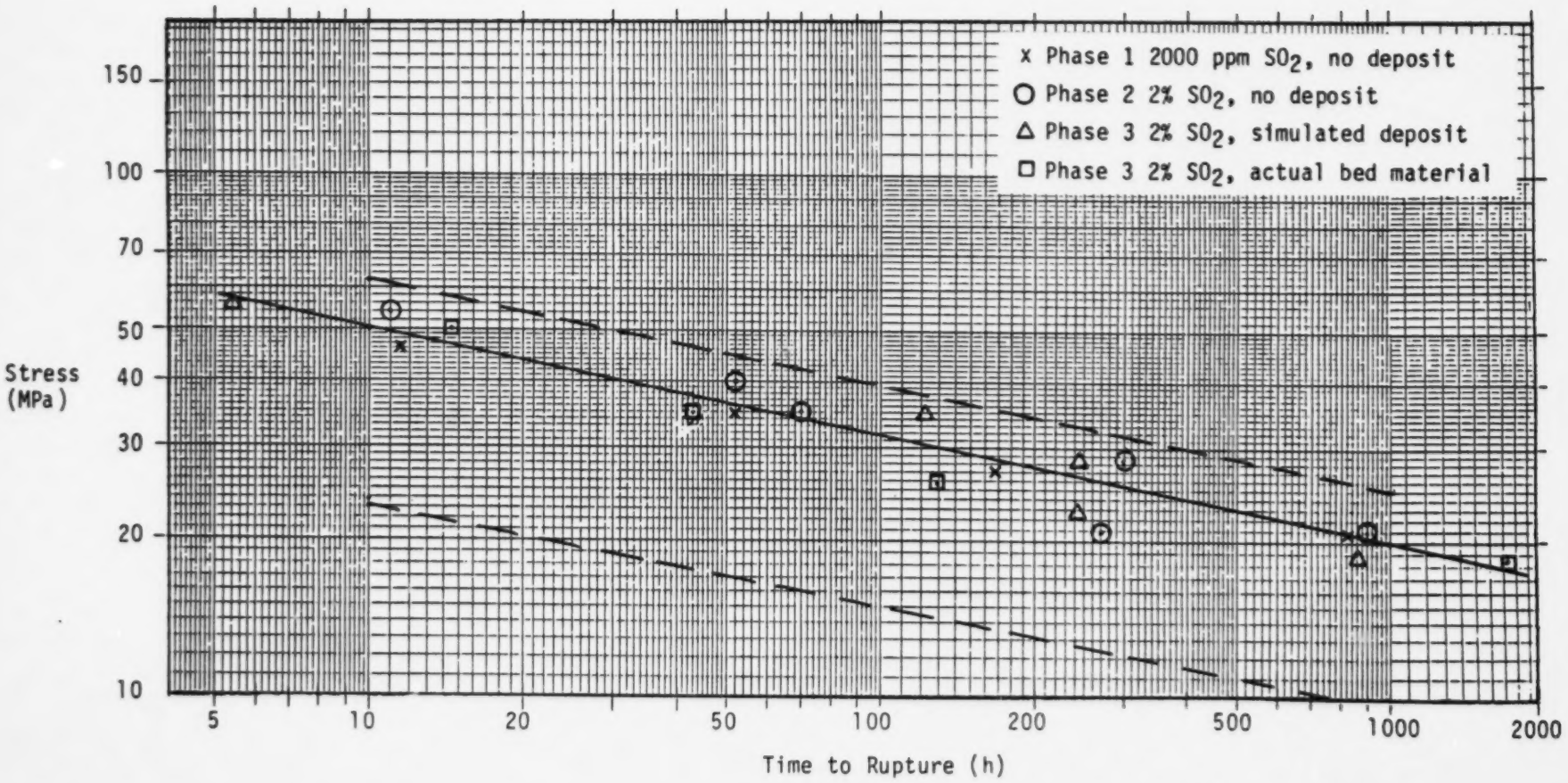

Figure 8 Stress-Rupture Tests for Stainless Alloy 310 at 900°C in Synthetic Combustion Gas

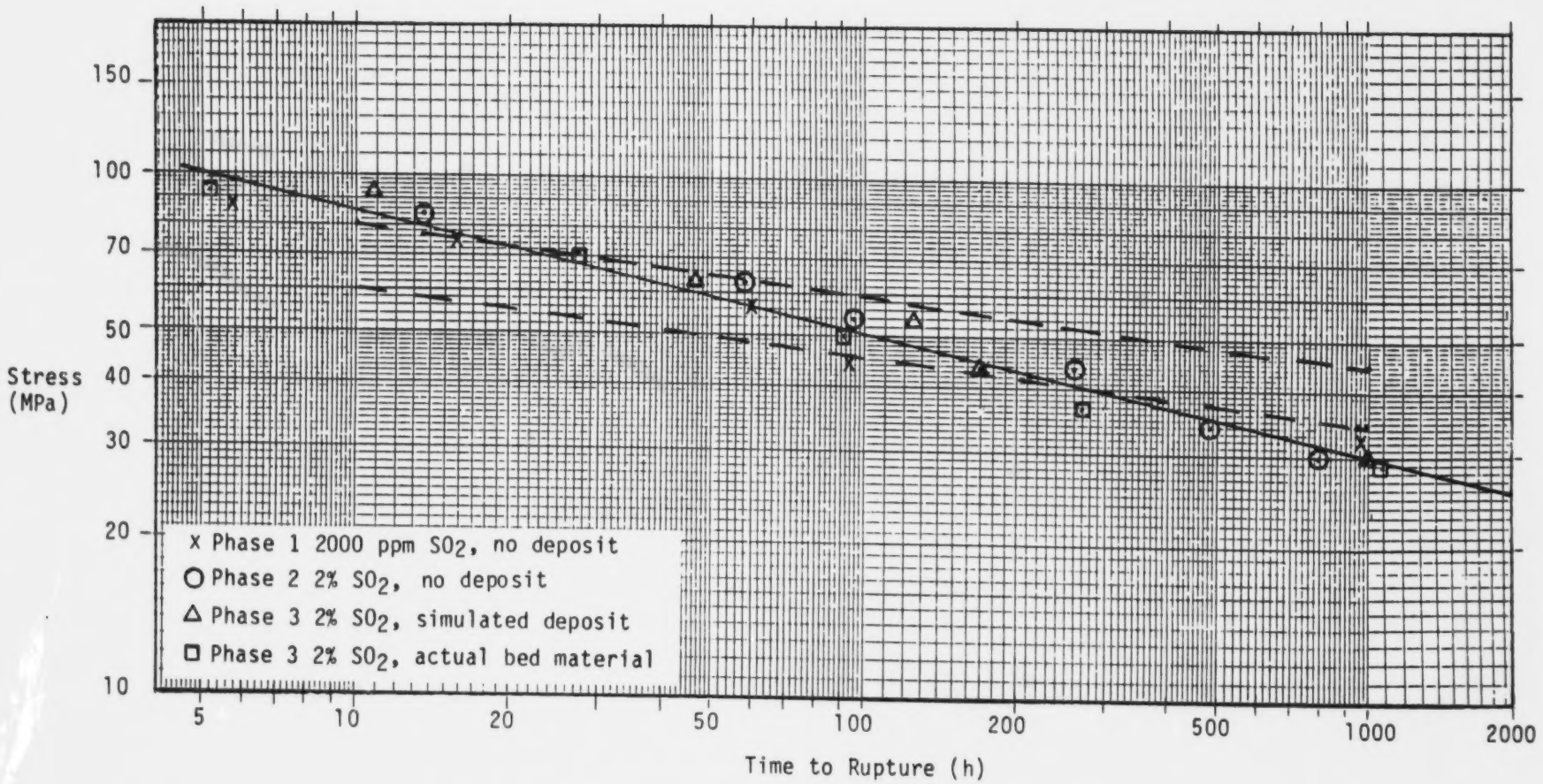

Figure 9 Stress-Rupture Tests for Cast Alloy HK40 at 900°C in Synthetic Combustion Gas

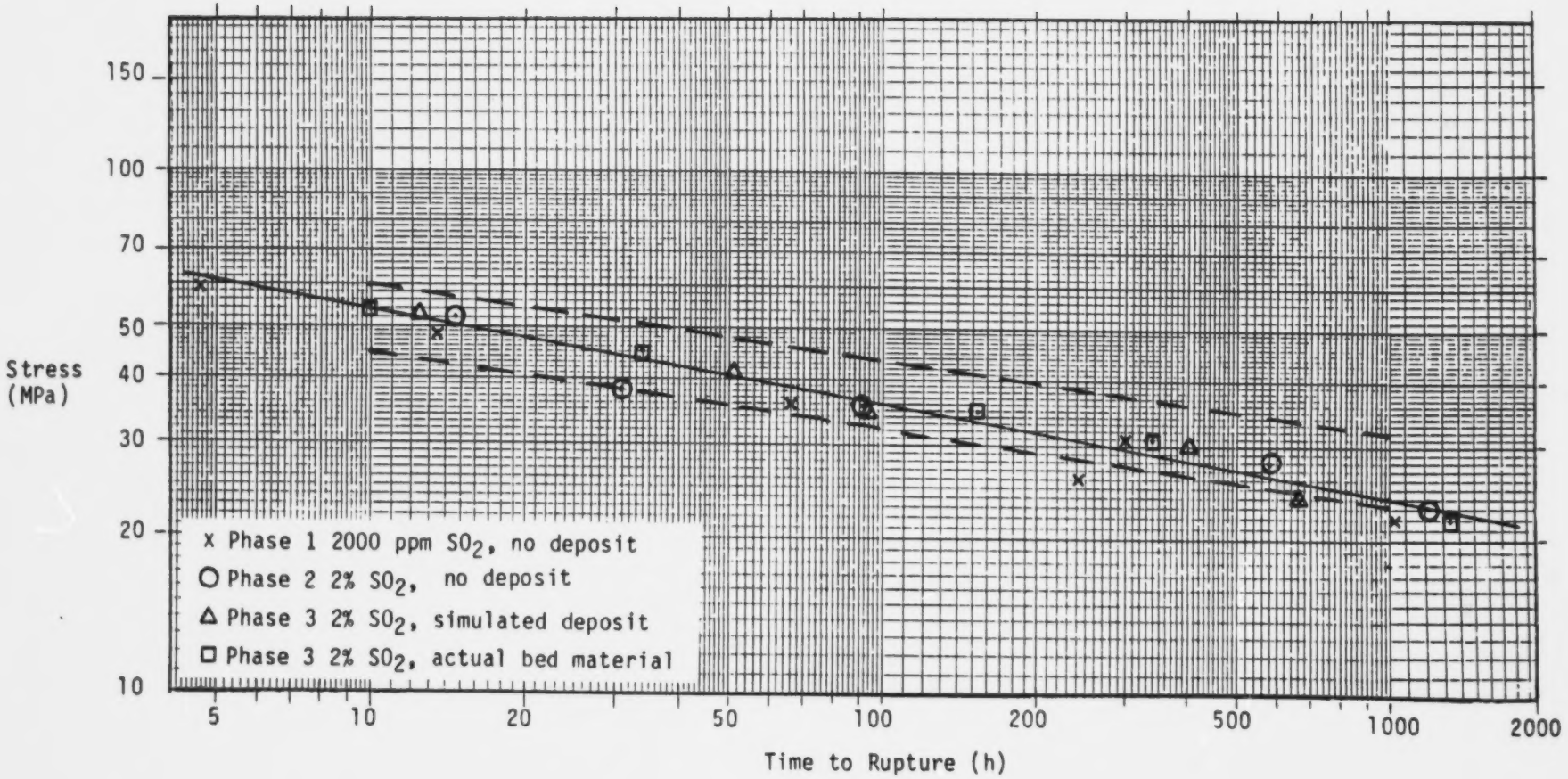

Figure 10 Stress-Rupture Tests for Incoloy 800H at 900°C in Synthetic Combustion Gas

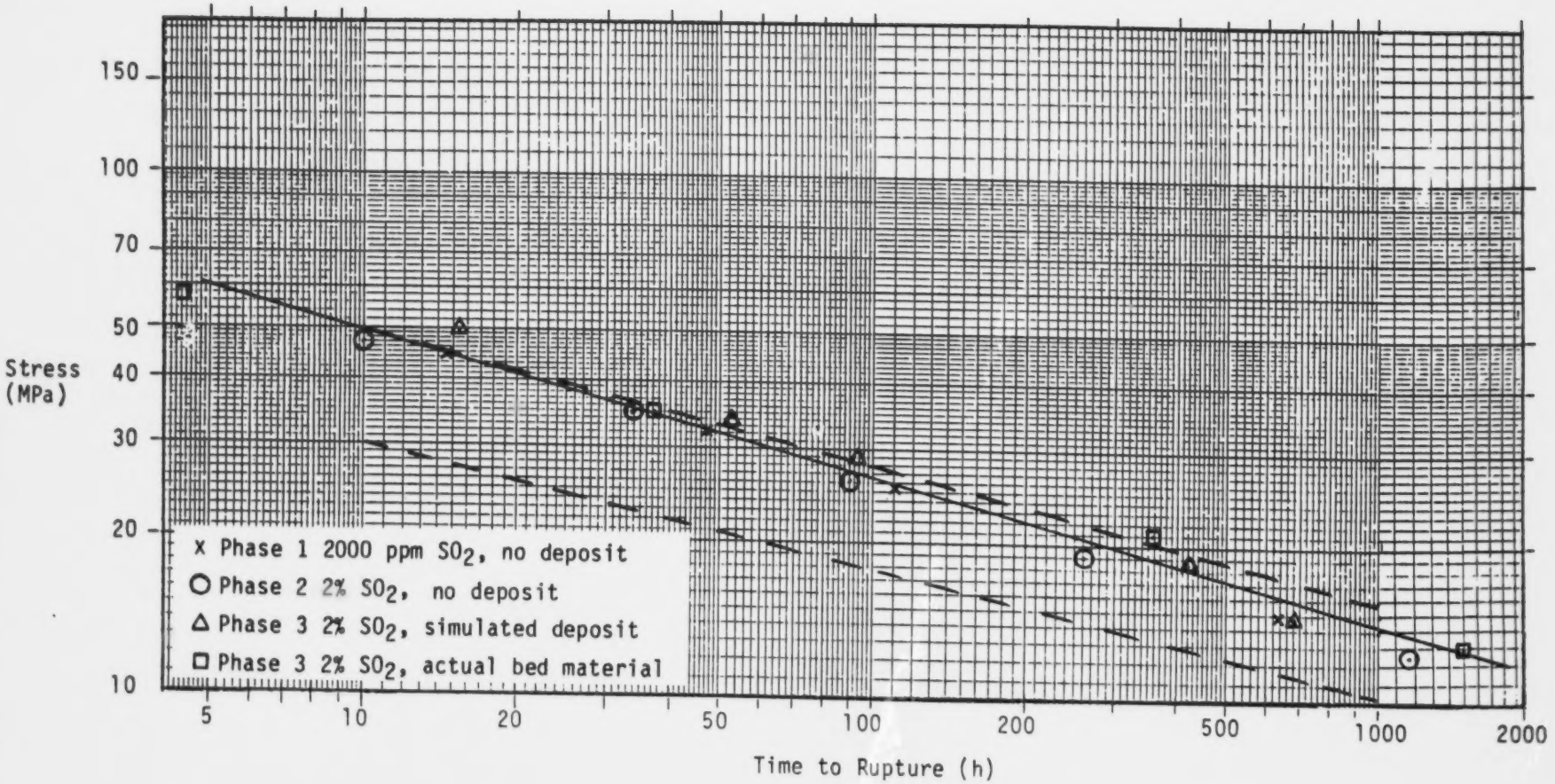

Figure 11 Stress-Rupture Tests for Stainless Alloy 347H at 900°C in Synthetic Combustion Gas

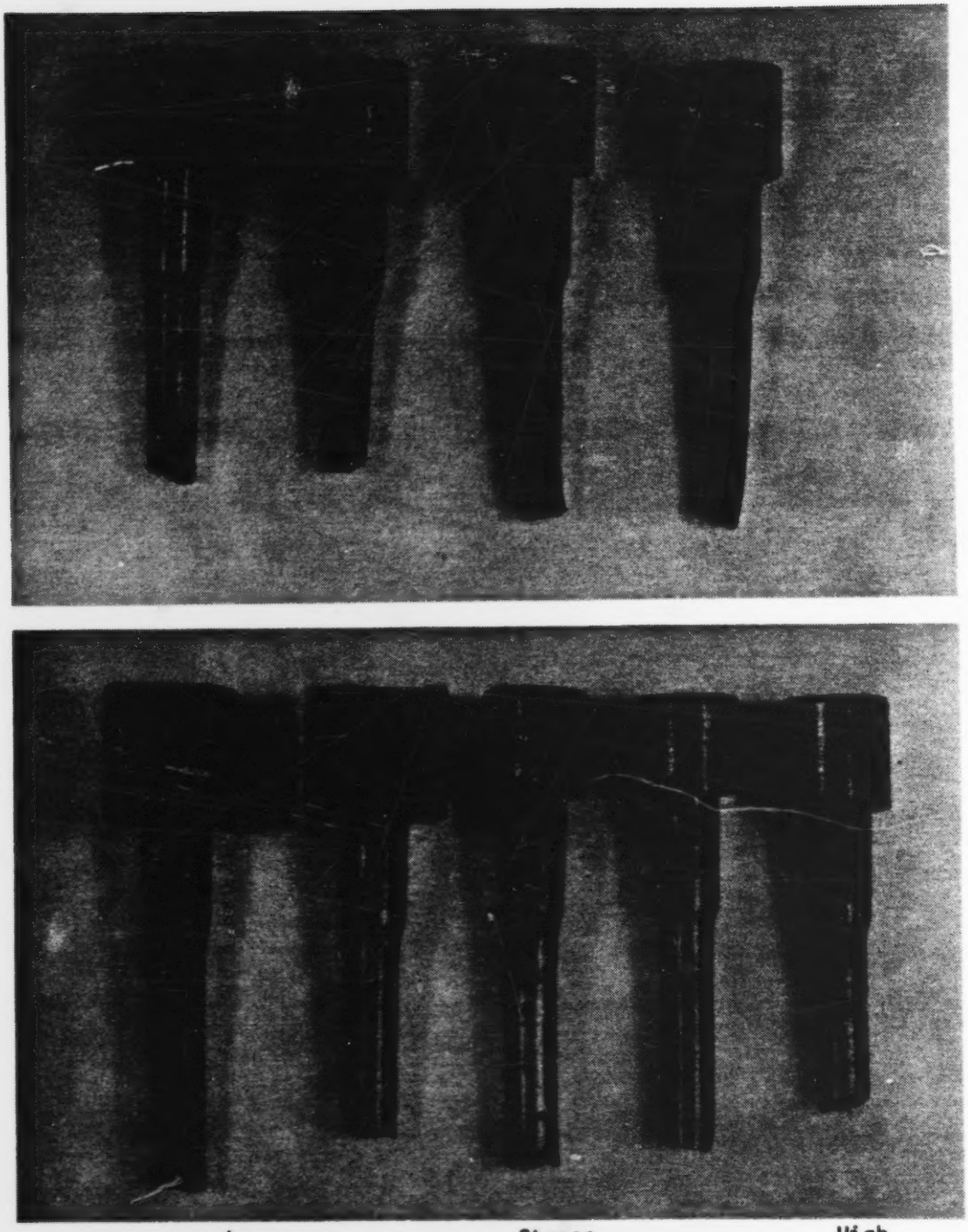

Figure 12 Appearance of Ruptured Stainless Alloy 310 and Cast Alloy HK40 Specimens After 800°C Tests in 2000 ppm SO_2 Synthetic Combustion Gas and Actual Bed Material

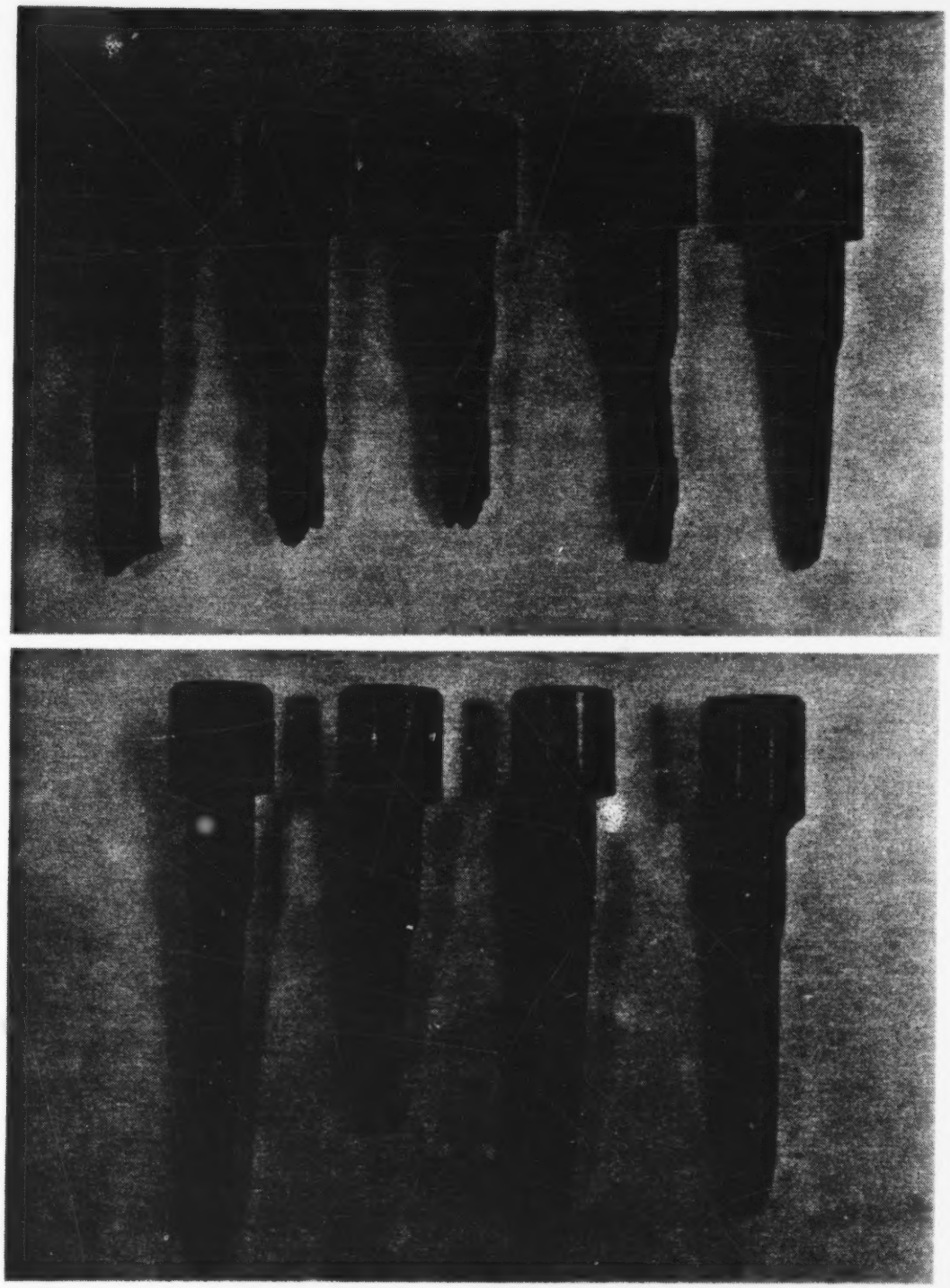

Figure 13 Appearance of Ruptured Incoloy 800H and Stainless Alloy 347H Specimens After 800°C Tests in 2000 ppm SO_2 Synthetic Combustion Gas and Actual Bed Material

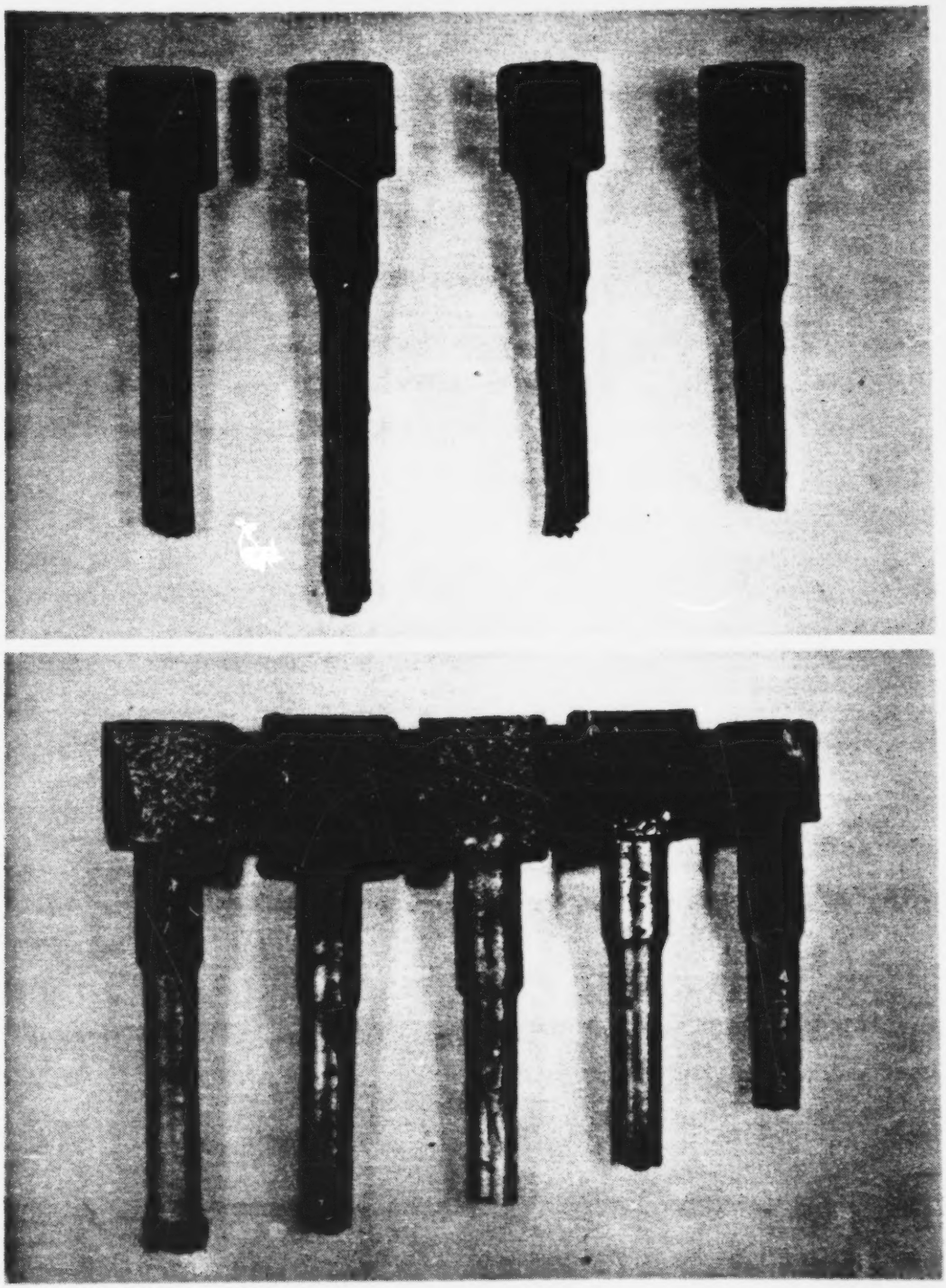

Figure 14 Appearance of Ruptured Stainless Alloy 310 and Cast Alloy HK40 Specimens After 900°C Tests in 2.0% SO_2 Synthetic Combustion Gas and Actual Bed Material

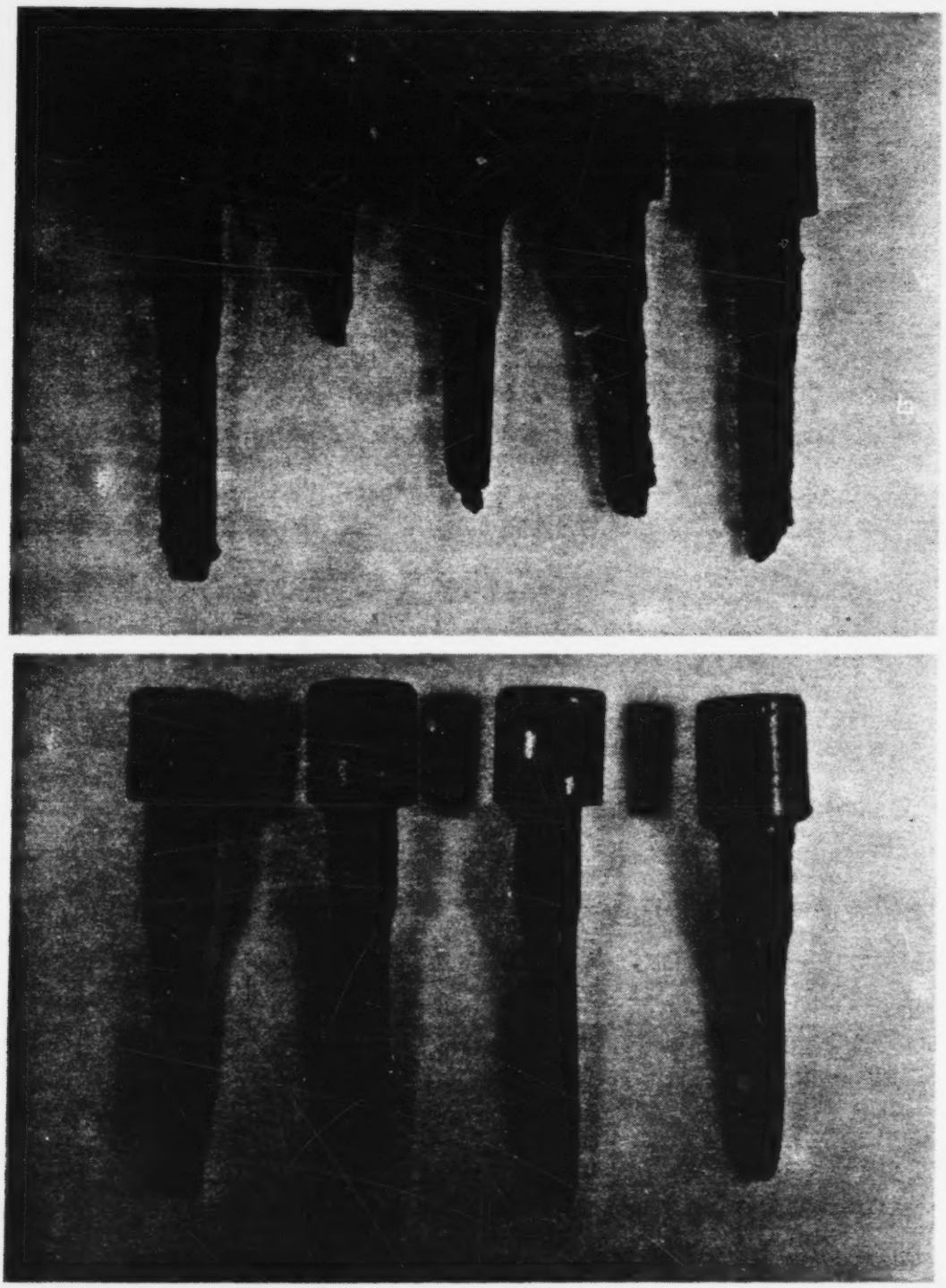

Figure 15 Appearance of Ruptured Incoloy 800H and Stainless Alloy 347H Specimens After 900°C Tests in 2.0% SO_2 Synthetic Combustion Gas and Actual Bed Material

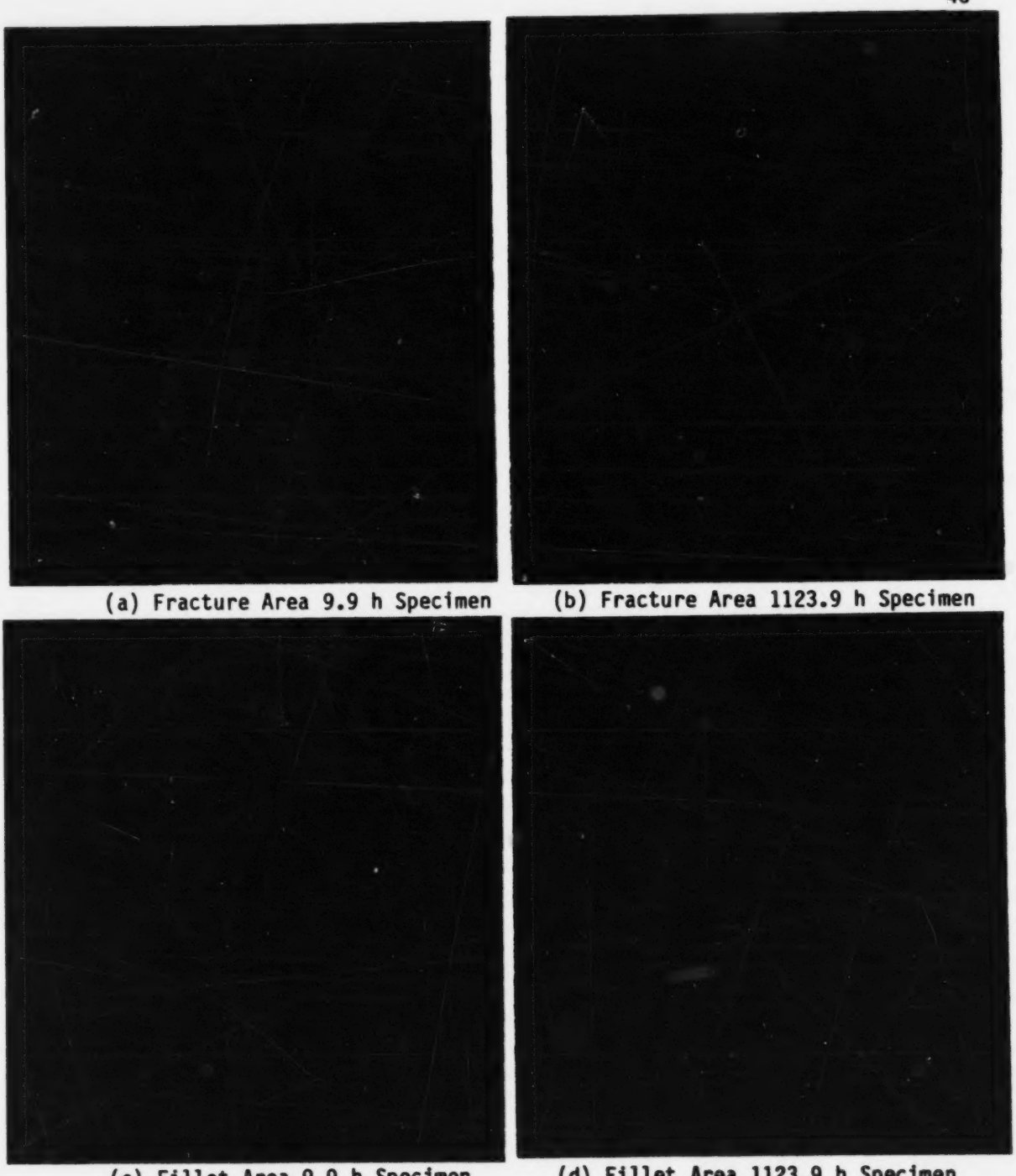

(a) Fracture Area 9.9 h Specimen

(b) Fracture Area 1123.9 h Specimen

(c) Fillet Area 9.9 h Specimen

(d) Fillet Area 1123.9 h Specimen

Figure 16 Sulphidation Observed in Stainless Alloy 347H Specimens After Rupture Lives of 9.9 and 1123 h at 800°C in 2000 ppm SO_2 Combustion Gas and Actual Bed Material

X100

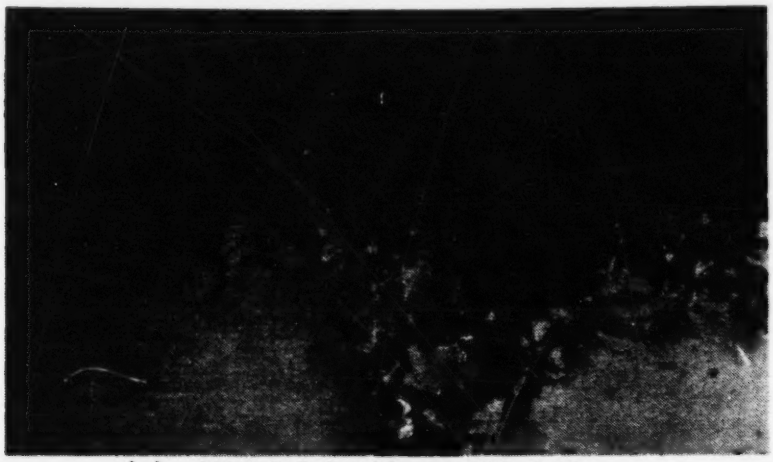

(a) 800H 9.7 h Life at 103.4 MPa

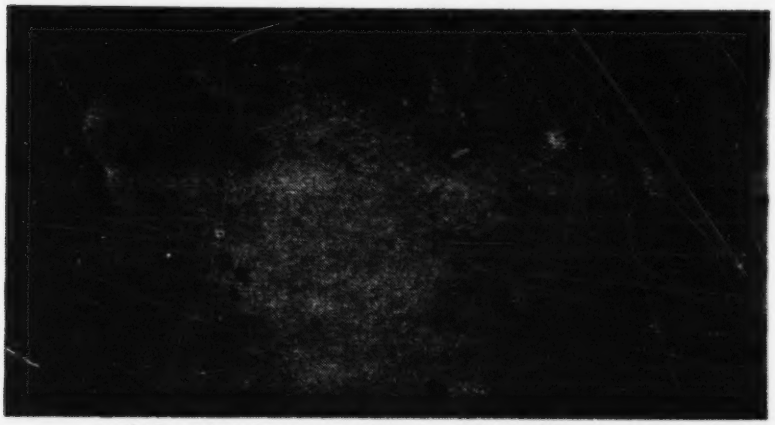

(b) 310 6.1 h Life at 96.5 MPa

(c) HK40 19.5 h Life at 134.4 MPa

Figure 17 Effect of Hot Corrosion on Incoloy 800H, Stainless Alloy 310 and Cast Alloy HK40 After Stress-Rupture Tests Using High Stress at 800°C in 2000 ppm SO_2 Combustion Gas and Actual Bed Material

X100

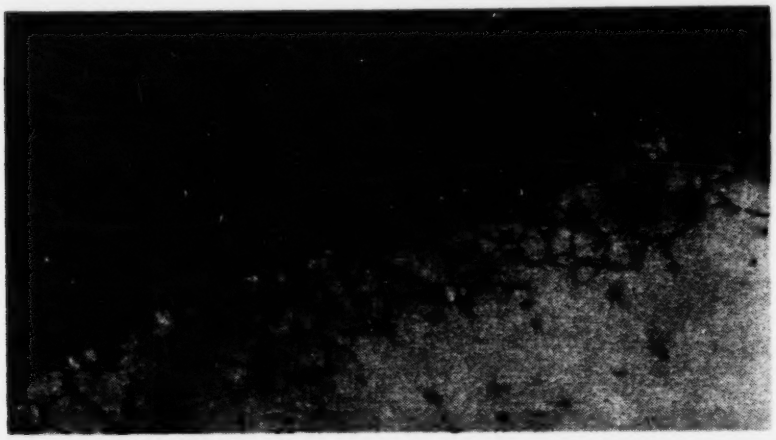

(a) 800H 745.5 h Life at 45.5 MPa

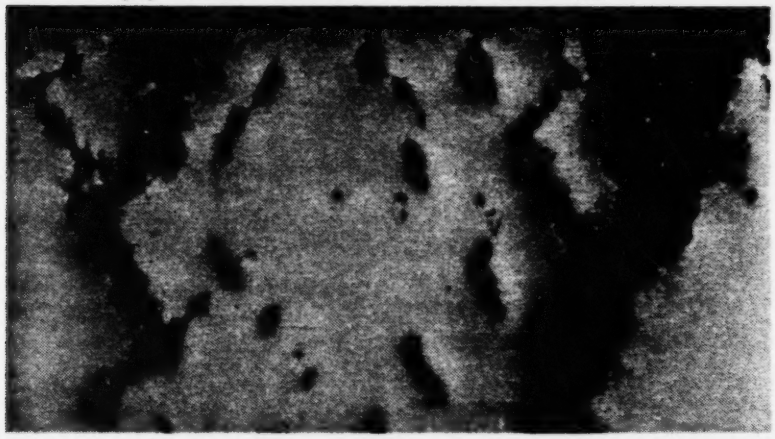

(b) 310 407.5 h Life at 34.1 MPa

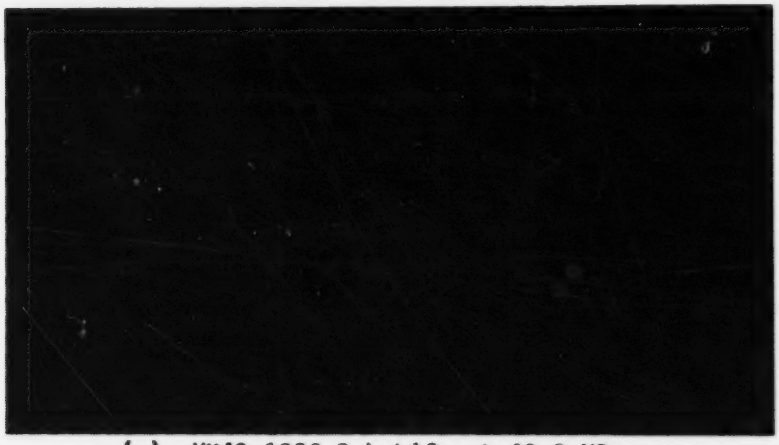

(c) HK40 1036.8 h Life at 49.0 MPa

Figure 18 Effect of Hot Corrosion on Incoloy 800H, Stainless Alloy 310 and Cast Alloy HK40 After Stress-Rupture Tests Using Low Stress at 800°C in 2000 ppm SO_2 Combustion Gas and Actual Bed Material

X100

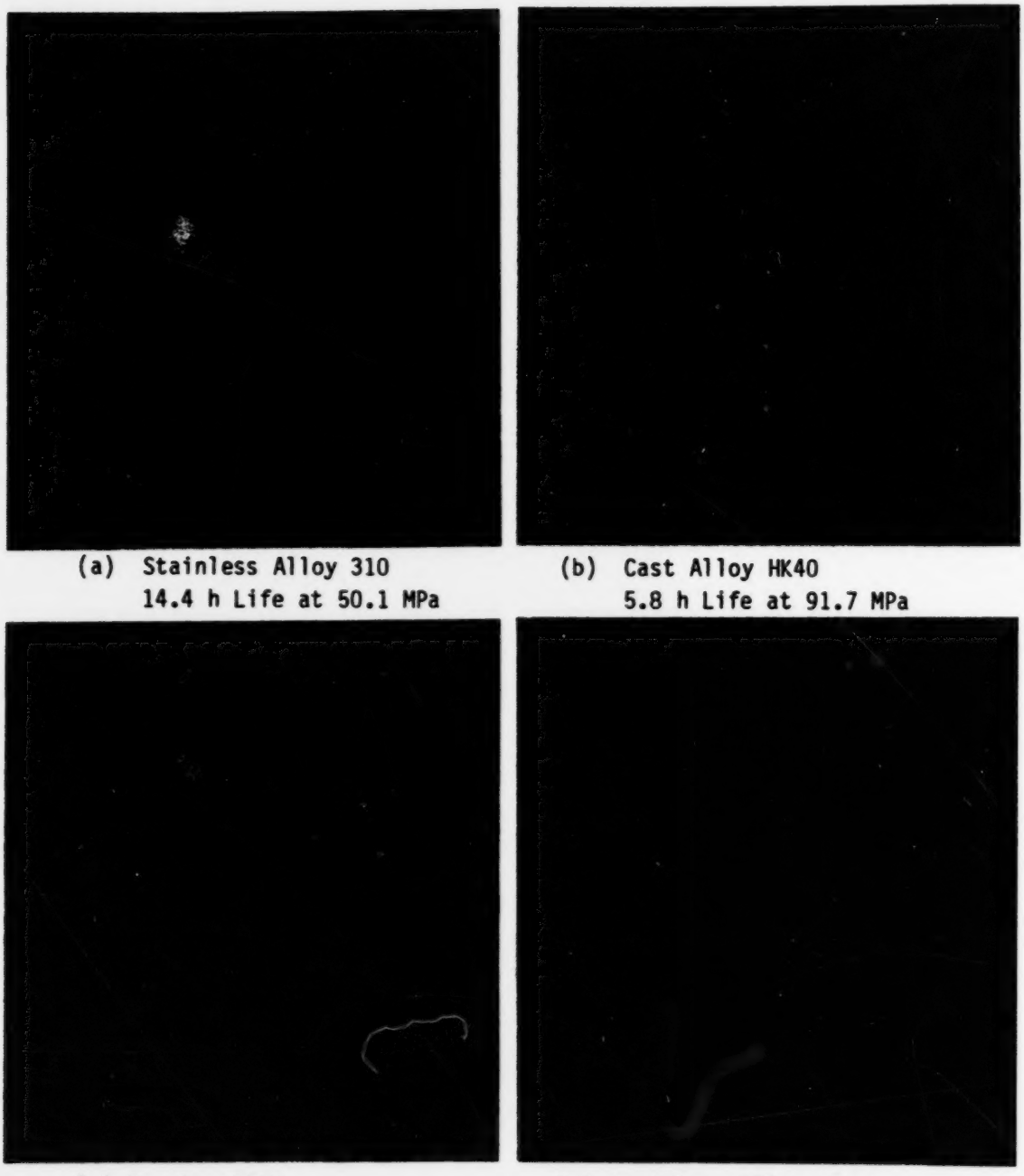

(a) Stainless Alloy 310
14.4 h Life at 50.1 MPa

(b) Cast Alloy HK40
5.8 h Life at 91.7 MPa

(c) Incoloy 800H
10.0 h Life at 53.0 MPa

(d) Stainless Alloy 347H
4.3 h Life at 59.0 MPa

Figure 19 Effect of Hot Corrosion on the Program Test Alloys After Stress-Rupture Tests Using High Stress at 900°C in 2.0% SO_2 Combustion Gas and Actual Bed Material
X100

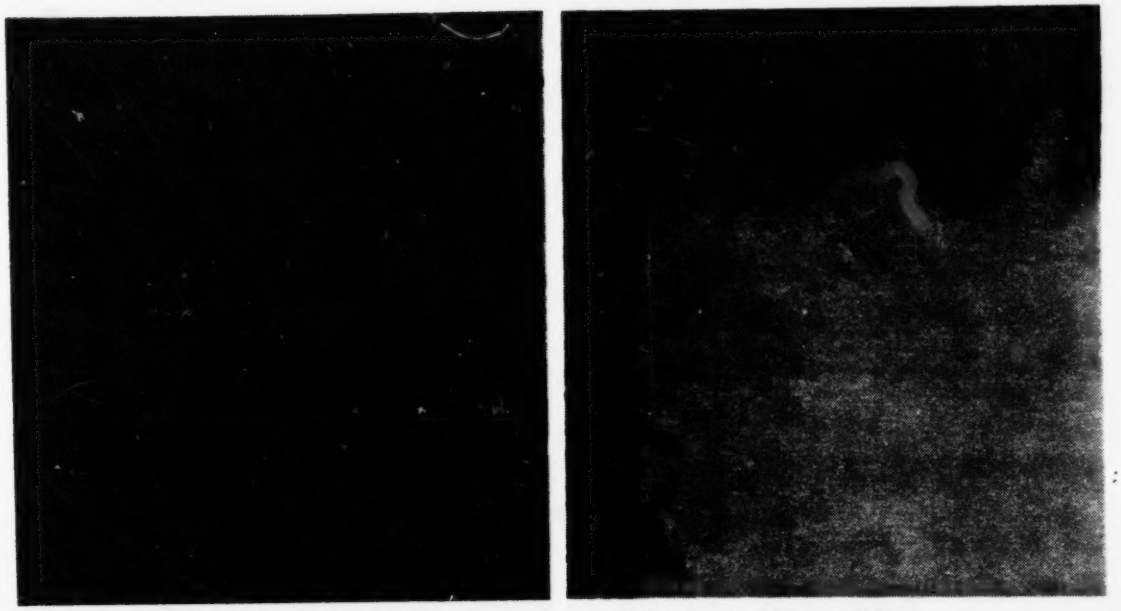

(a) Stainless Alloy 310
1756.5 h Life at 18.8 MPa

(b) Cast Alloy HK40
1070.3 h Life at 29.0 MPa

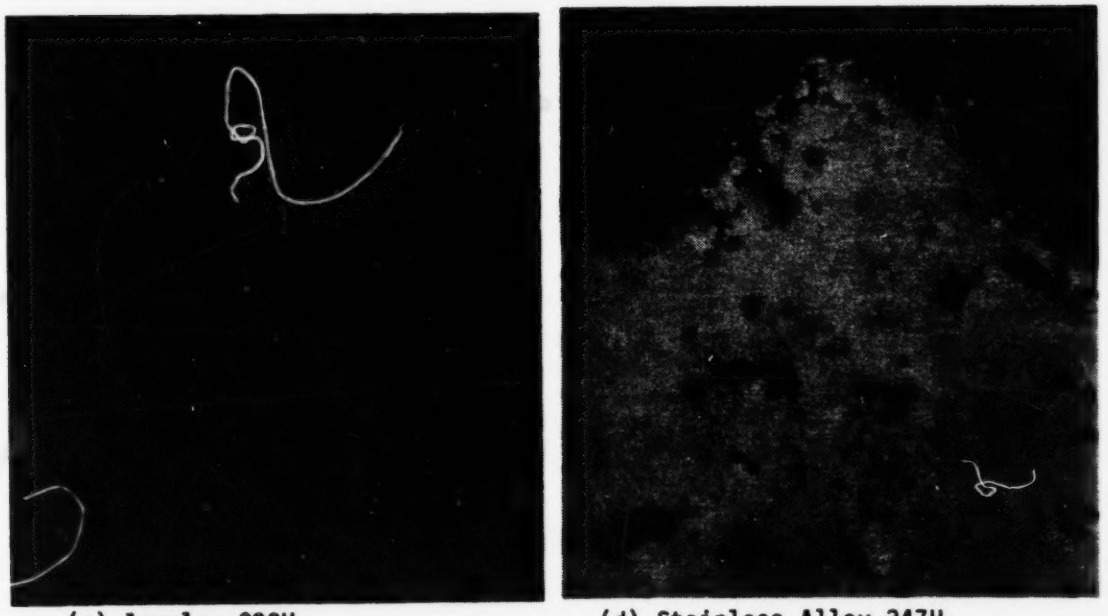

(c) Incoloy 800H
1320.9 h Life at 22.0 MPa

(d) Stainless Alloy 347H
1502.9 h Life at 13.1 MPa

Figure 20 Effect of Hot Corrosion on the Program Test Alloys After Stress-Rupture Tests Using Low Stress at 900°C in 2.0% SO_2 Combustion Gas and Actual Bed Material
X100

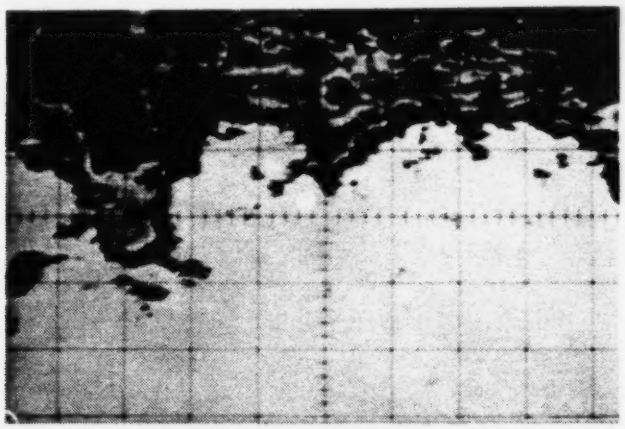

(a) Absorbed Electron Image

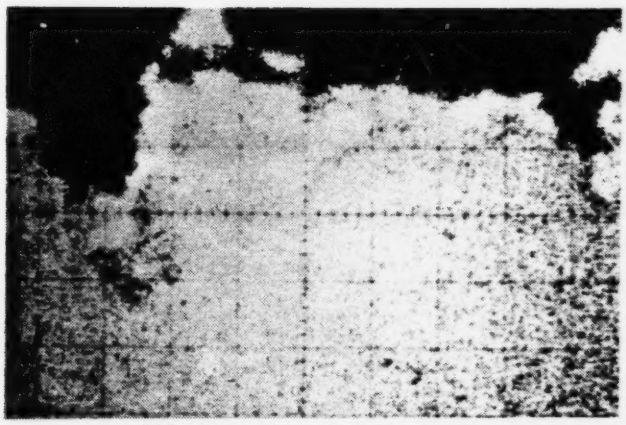

(b) Chromium X-Ray Image

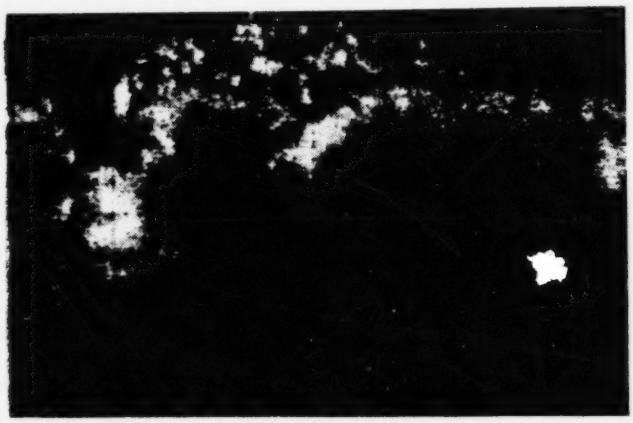

(c) Sulphur X-Ray Image

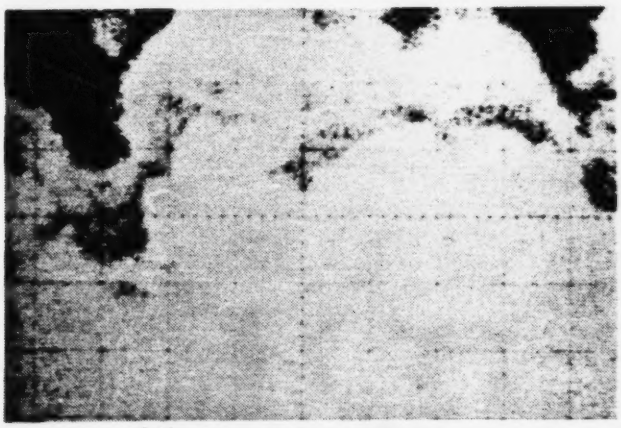

(d) Iron X-Ray Image

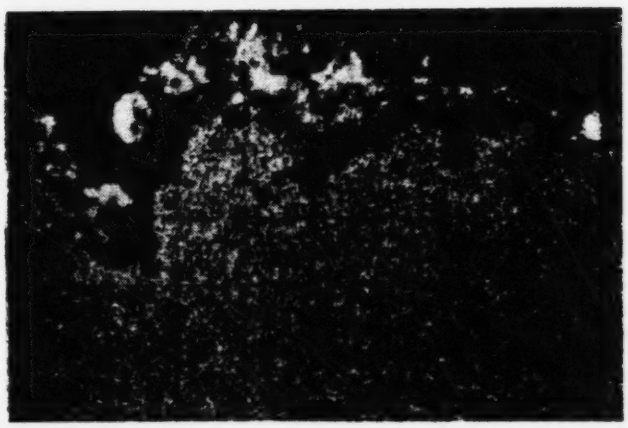

(e) Nickel X-Ray Image

Figure 21 Microprobe Analyses of Stainless Alloy 347H After 4.3 h Rupture Life at 900°C in 2.0% SO_2 Combustion Gas and Actual Bed Material

X400

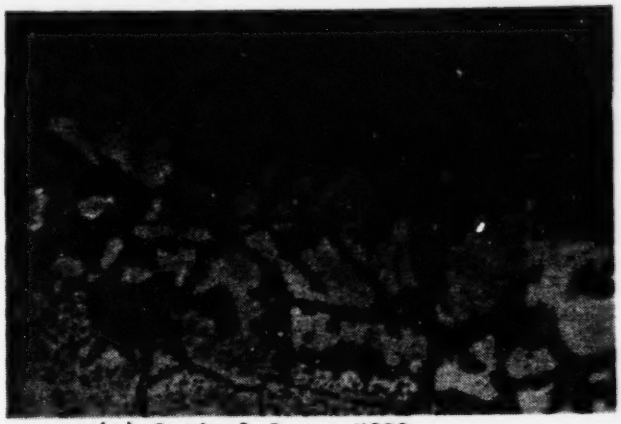

(a) Optical Image X200

(b) Absorbed Electron Image

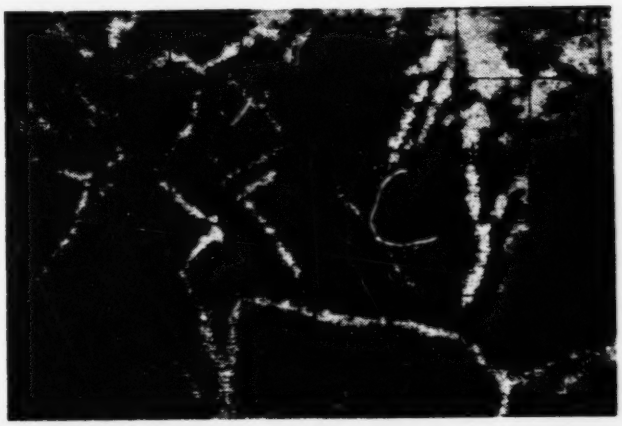

(c) Chromium X-Ray Image

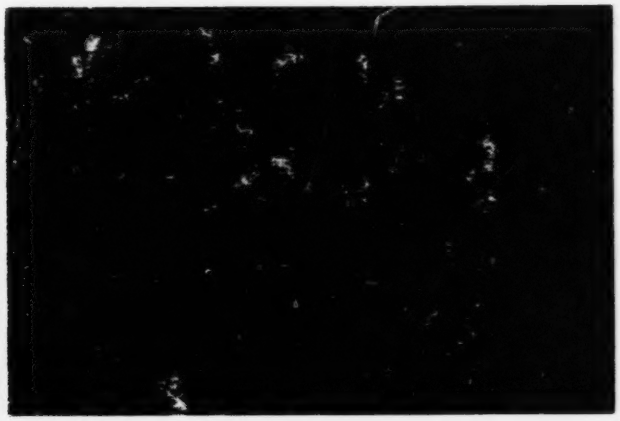

(d) Sulphur X-Ray Image

(e) Nickel X-Ray Image

(f) Iron X-Ray Image

Figure 22 Microprobe Analyses of Incoloy 800H After 333.7 h Rupture Life at 900°C in 2.0% SO_2 Combustion Gas and Actual Bed Material

X400

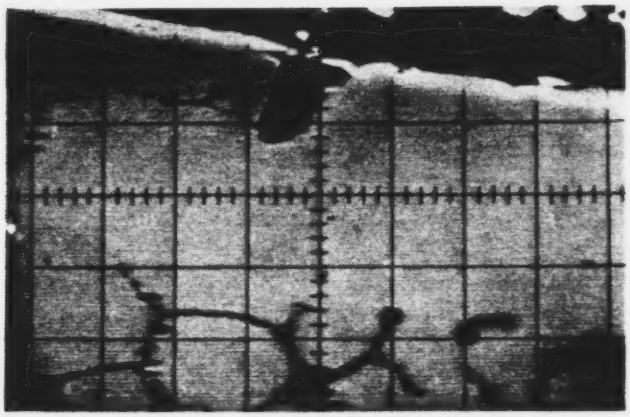

(a) Absorbed Electron Image

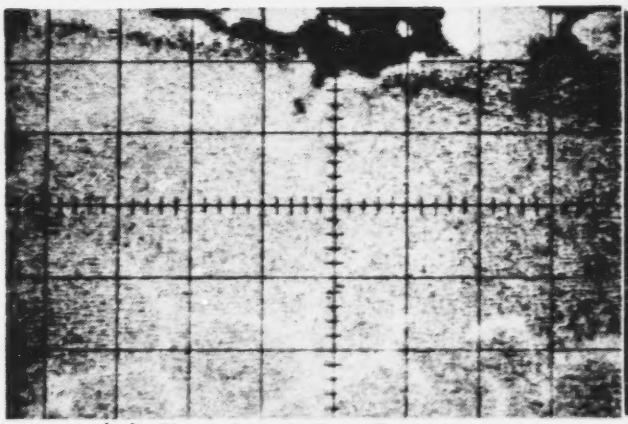

(b) Chromium X-Ray Image

(c) Sulphur X-Ray Image

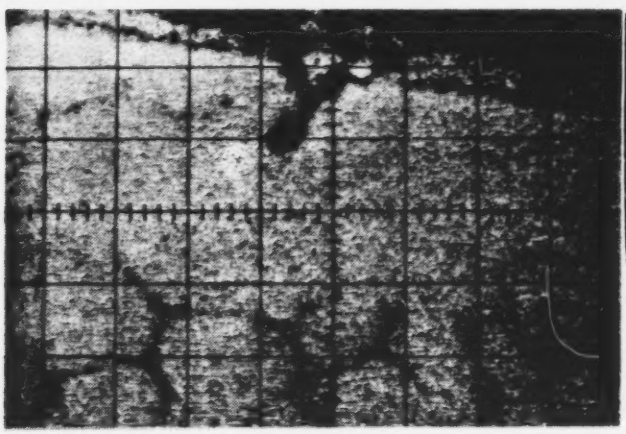

(d) Iron X-Ray Image

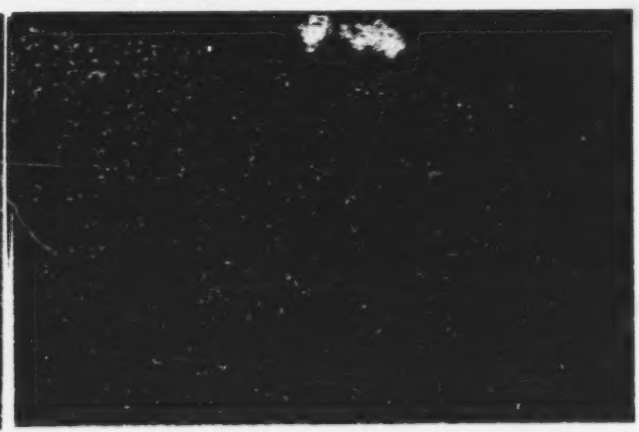

(e) Nickel X-Ray Image

Figure 23 Microprobe Analyses of Cast Alloy HK40 After 90 h Rupture Life at 800°C in 2000 ppm SO_2 Combustion Gas and Actual Bed Material

X400

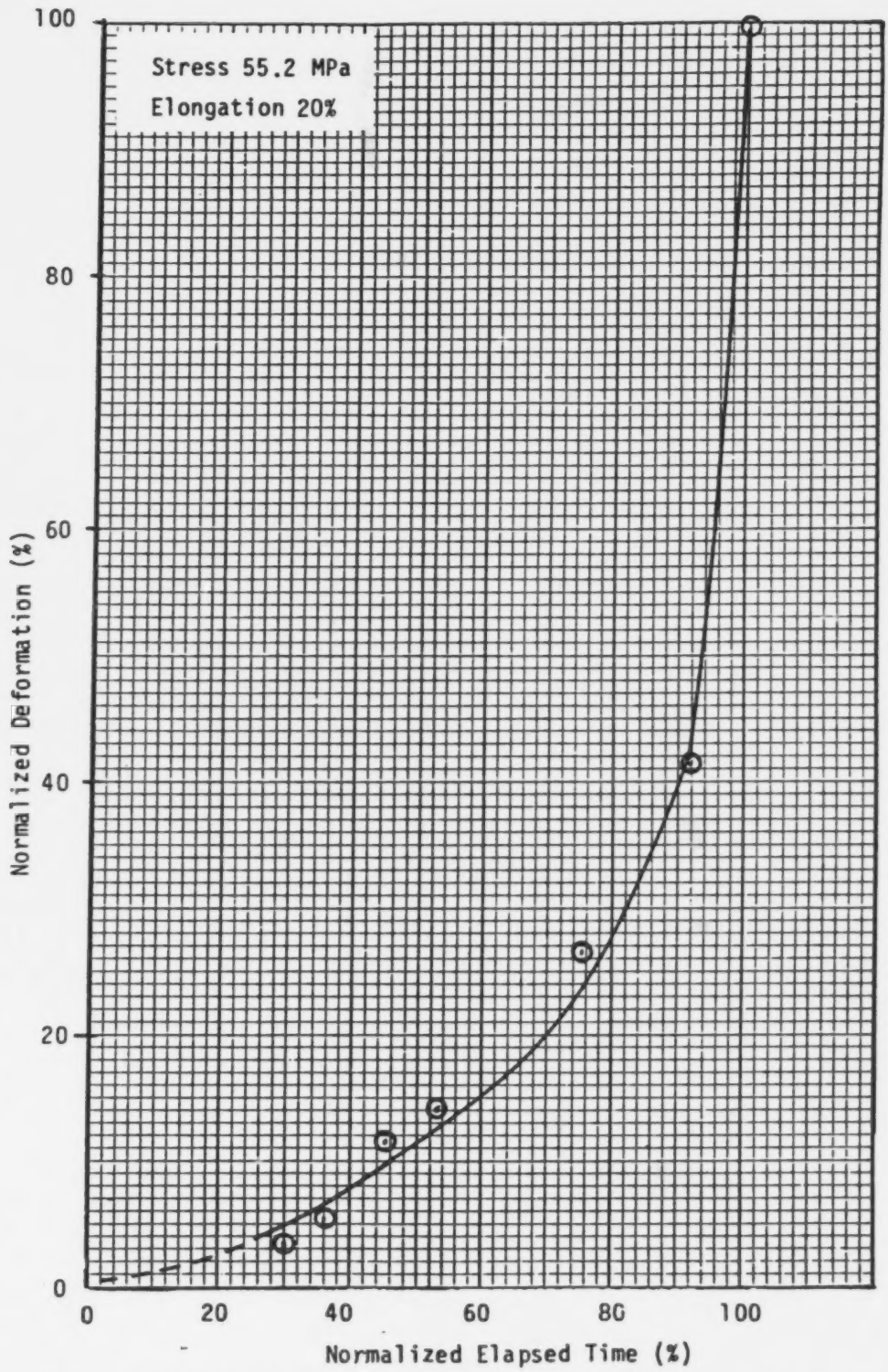

Figure 24 Simulated Creep Curve for Incoloy 800H as Determined During Stress-Rupture Test at 800°C in 2000 ppm SO_2 Combustion Gas and Actual Bed Material

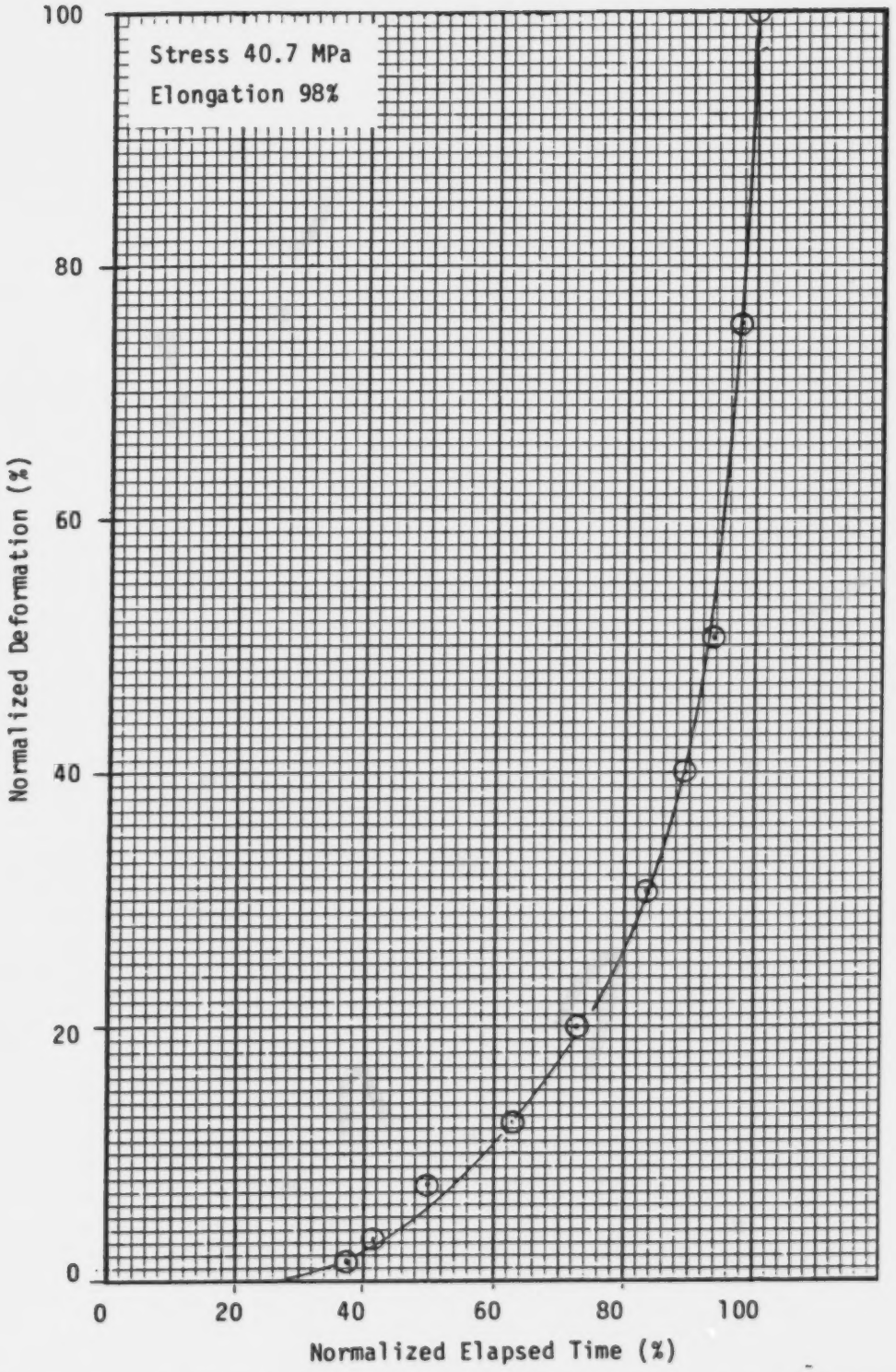

Figure 25 Simulated Creep Curve for Stainless Alloy 347H as Determined During Stress-Rupture Test at 800°C in 2000 ppm SO_2 Combustion Gas and Actual Bed Material

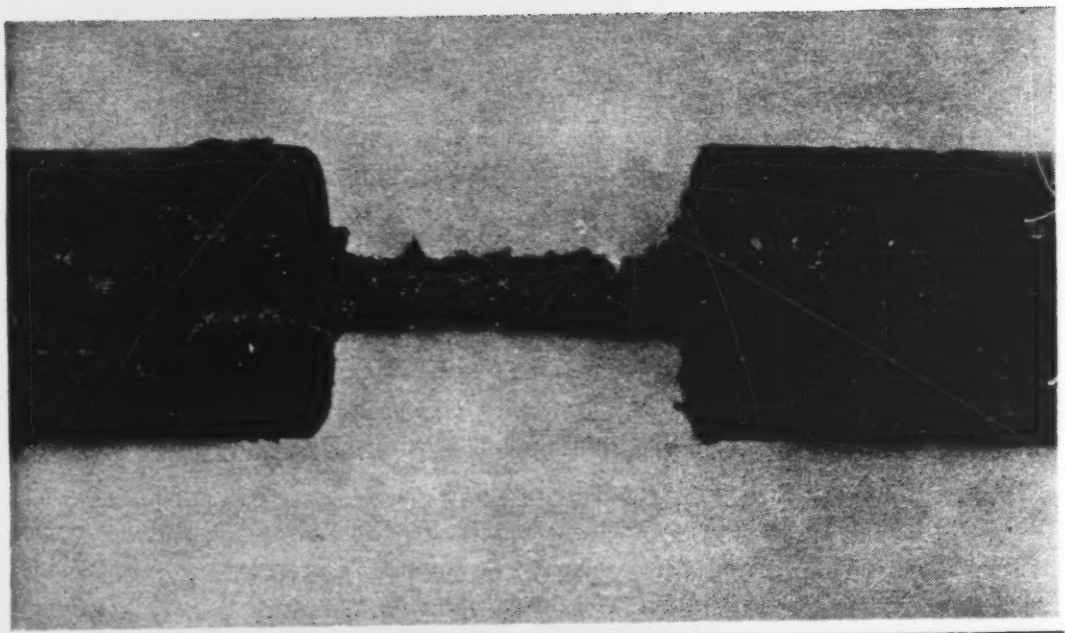

1.2X

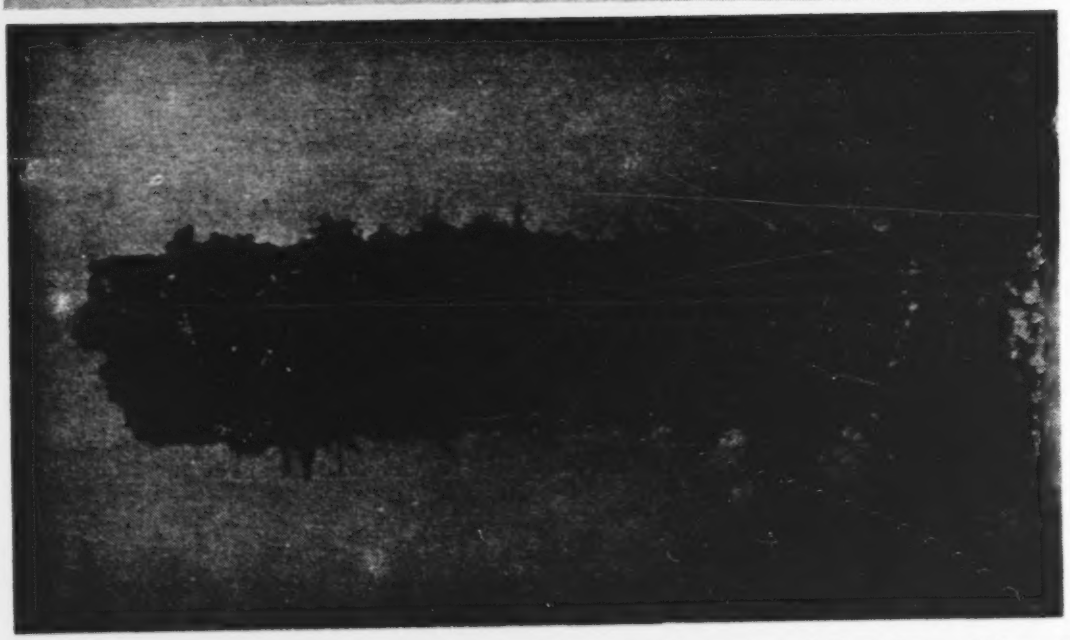

4X

Figure 26 Appearance of Cast Alloy HK40 Ruptured Specimen After Being Thermally Cycled During a 900°C Stress-Rupture Test in 2.0% SO_2 Combustion Gas

sherritt

2-905

Sherritt Gordon Mines Limited
Fort Saskatchewan, Alberta, Canada T8L 2P2 / Telephone 403 - 998 - 6911 / Telex 037 - 2290

Sherritt Research Centre

EVALUATION OF STRESS-RUPTURE PROPERTIES OF STAINLESS ALLOYS IN FLUIDIZED BED COMBUSTION ENVIRONMENTS PHASE 2 REPORT

For the Period
July 1, 1983 to June 30, 1984

K.G. Reid
M.J.H. Ruscoe

36 pp

MICROMEDIA
AUG 15 1988

Evaluation of Stress-Rupture Properties of Stainless Alloys in Fluidized Bed Combustion Environments

Phase 2 Report

by

Sherritt Research Centre
Sherritt Gordon Mines Limited
Fort Saskatchewan, Alberta
K.G. Reid, M.J.H. Ruscoe

Work on this project was conducted under the auspices of the Canada Centre for Mineral and Energy Technology, Energy, Mines and Resources, Canada

DSS FILE NUMBER	:	03SQ.23440-2-9053
DSS CONTRACT SERIAL NUMBER	:	OSQ82-00148
CANMET PROJECT NUMBER	:	430902
CANMET SCIENTIFIC AUTHORITY	:	Dr. D.C. Briggs

DATE: July 1, 1983 to June 30, 1984

This report should be cited as Contract Report No: OSQ82-00148

This work was performed for the Physical Metallurgy Research Laboratories of CANMET, Energy, Mines and Resources, Canada on Supply and Services Contract OSQ82-00148. The authors acknowledge the support received from Dr. David Briggs of PMRL in the scientific administration of the contract.

Any data presented, opinions, findings, conclusions or recommendations expressed in this report are those of the contractor and do not necessarily reflect the views of CANMET.

TABLE OF CONTENTS

		Page No
	SUMMARY	1
1.0	INTRODUCTION	2
2.0	EXPERIMENTAL	
2.1	Materials	3
	2.1.1 Alloys	3
	2.1.2 Synthetic Combustion Gas	3
2.2	Apparatus and Procedure	3
3.0	RESULTS AND DISCUSSION	
3.1	Stress-Rupture Data for 800°C Tests	12
	3.1.1 Stainless Alloy 310	12
	3.1.2 Cast Alloy HK40	12
	3.1.3 Incoloy 800H	15
	3.1.4 Stainless Alloy 347H	15
3.2	Metallographic and Microprobe Examination of 800°C Ruptured Specimens	18
3.3	Stress-Rupture Data for 900°C Tests	31
	3.3.1 Stainless Alloy 310	31
	3.3.2 Cast Alloy HK40	34
	3.3.3 Incoloy 800H	37
	3.3.4 Stainless Alloy 347H	37
3.4	Metallographic and Microprobe Examination of 900°C Ruptured Specimens	40

LIST OF TABLES

		Page No
Table 1	Chemical Analyses of Test Alloys	4
Table 2	Physical Properties of Test Alloys	5
Table 3	Stress-Rupture Data for Stainless Alloy 310 Tested at 800°C in Synthetic Combustion Gas and Simulated Fluidized Bed Deposit	12
Table 4	Stress-Rupture Data for Cast Alloy HK40 Tested at 800°C in Synthetic Combustion Gas and Simulated Fluidized Bed Deposit	15
Table 5	Stress-Rupture Data for Incoloy 800H Tested at 800°C in Synthetic Combustion Gas and Simulated Fluidized Bed Deposit	15
Table 6	Stress-Rupture Data for Stainless Alloy 347H Tested at 800°C in Synthetic Combustion Gas and Simulated Fluidized Bed Deposit	18
Table 7	Stress-Rupture Data for Stainless Alloy 310 Tested at 900°C in Synthetic Combustion Gas (2.0% SO_2)	34
Table 8	Stress-Rupture Data for Cast Alloy HK40 Tested at 900°C in Synthetic Combustion Gas (2.0% SO_2)	37
Table 9	Stress-Rupture Data for Incoloy 800H Tested at 900°C in Synthetic Combustion Gas (2.0% SO_2)	37
Table 10	Stress-Rupture Data for Stainless Alloy 347H Tested at 900°C in Synthetic Combustion Gas (2.0% SO_2)	40

LIST OF FIGURES

		Page No
Figure 1	Appearance of Alloy 310 and Inconel 713C Clevises After Long Term Exposure to High SO_2 Combustion Gas	6
Figure 2	Appearance of 310 Retort Liner After Long Term Exposure to Synthetic Combustion Gas	8
Figure 3	Sulphidation Observed in 800H after 232 h Exposure to High SO_2 Combustion Gas at 900°C	10
Figure 4	Appearance of Aluminum Diffusion Coated 800H After 232 h Exposure to High SO_2 Combustion Gas at 900°C	11
Figure 5	Stress-Rupture Tests for Alloy 310 at 800°C in Synthetic Combustion Gas	13
Figure 6	Stress-Rupture Tests for Alloy HK40 at 800°C in Synthetic Combustion Gas	14
Figure 7	Stress-Rupture Tests for Incoloy 800H at 800°C in Synthetic Combustion Gas	16
Figure 8	Stress-Rupture Tests for Alloy 347H at 800°C in Synthetic Combustion Gas	17
Figure 9	Appearance of 347H and 800H After Testing in Contact with Simulated Deposit in Synthetic Combustion Gas at 800°C	19
Figure 10	Appearance of 310 and HK40 After Testing in Contact with Simulated Deposit in Synthetic Combustion Gas at 800°C	20
Figure 11	Hot Corrosion Observed in Incoloy 800H After 800°C Test at 103.4 MPa for 12.4 h	21
Figure 12	Hot Corrosion Observed in Incoloy 800H After 800°C Test at 56.5 MPa for 83.0 h	22
Figure 13	Electron Microprobe Analyses of Corrosion Deposit in a Stress Crack of Incoloy 800H After 800°C Test at 56.5 MPa for 83 h	24
Figure 14	Photomicrographs Showing Appearance of 800H After 800°C Test at 37.2 MPa for 1445 h in Synthetic Combustion Gas	25

LIST OF FIGURES

		Page No
Figure 15	Electron Microprobe Analyses of Upper Corrosion Layer on 800H After 800°C Test at 37.2 MPa for 1445 h	26
Figure 16	Electron Microprobe Analysis of Lower Corrosion Layer on 800H After 800°C Test at 37.2 MPa for 1445 h	27
Figure 17	Comparative X-ray Energy Spectra from 800H Matrix and Area Near Corrosion Layer-Base Alloy Interface	28
Figure 18	Corrosion Observed in 310, 347H and HK40 After 800°C Tests in Contact with Simulated Deposit at High Stress	29
Figure 19	Corrosion Observed in 310, 347H and HK40 After 800°C Tests in Contact with Simulated Deposit at Low Stress	30
Figure 20	Anomalous "Coating" on HK40 After 800°C Test in Contact with Simulated Deposit Using 108.3 MPa for 51.8 h	32
Figure 21	Electron Microprobe Analyses of HK40 After 800°C Test in Contact with Simulated Deposit Using 56.9 MPa for 424 h	33
Figure 22	Comparative Microstructures of Ruptured 310 Samples After 900°C Tests Using 21.0 MPa	35
Figure 23	Stress-Rupture Tests for Alloy 310 at 900°C in Synthetic Combustion Gas	36
Figure 24	Stress-Rupture Tests for Alloy HK40 at 900°C in Synthetic Combustion Gas	38
Figure 25	Stress-Rupture Tests for Incoloy 800H at 900°C in Synthetic Combustion Gas	39
Figure 26	Stress-Rupture Tests for Alloy 347H at 900°C in Synthetic Combustion Gas	41
Figure 27	Appearance of Ruptured Specimens of 800H and 347H After 900°C Tests in Synthetic Combustion Gas Combustion Gas (2.0% SO_2)	42

LIST OF FIGURES

		Page No
Figure 28	Appearance of Ruptured Specimens of 310 and HK40 After 900°C Tests in Synthetic Combustion Gas (2.0% SO_2)	43
Figure 29	Comparative Corrosive Attack of 800H and 347H After 900°C Tests for ~1200 h in Synthetic Combustion Gas (2.0% SO_2)	44
Figure 30	Hot Corrosion Observed in HK40, 310 and 347H After 900°C Tests for ~10 h in Synthetic Combustion Gas (2.0% SO_2)	45
Figure 31	Microprobe Analyses of Underlying Matrix of 800H After 900°C Test for ~1200 h in Synthetic Combustion Gas (2.0% SO_2)	46
Figure 32	Microprobe Analyses of Corrosion Layer on 800H After 900°C Test for ~1200 h in Synthetic Combustion Gas (2.0% SO_2)	47

SUMMARY

Phase 2 of the Contract was successfully completed according to the Statement of Work.

Stress-rupture tests were carried out on four alloys at 800 and 900°C in a synthetic coal combustor atmosphere. The alloys tested were Stainless 310 and 347H, Cast Alloy HK40 and Incoloy 800H. For the 800°C tests, the alloys were tested in contact with a simulated fluidized bed combustor deposit in addition to the synthetic combustion gas of Phase 1. During the 900°C tests no deposit was used and the sulphur dioxide content of the synthetic combustion gas was increased from 0.2 to 2.0%. In general, rupture lives of the alloys tested in contact with the deposit were similar to the results obtained in Phase 1 using only the synthetic combustion gas. Rupture lives at 900°C were also similar to those reported from tests in Phase 1 using the lower content sulphur dioxide synthetic combustion gas. As reported in Phase 1, 800H was shown to be the least suited for service in the combustion gas atmosphere. For the iron base alloys, HK40 and 347H appeared to be the least affected by the corrosive environment.

1.0 INTRODUCTION

This is an interim report which covers the work conducted during the period July 1, 1983 to June 30, 1984 under Phase 2 of the stress-rupture test program. In the previous interim report for Phase 1, data were presented which compared the stress-rupture properties of the four program test alloys, when tested at 800 and 900°C in a synthetic combustion gas, to the stress-rupture properties of the alloys when tested in air. The Phase 1 data for the 900°C tests indicated that the test alloys (800H, 347H, 310 and HK40) in general had rupture lives similar to those expected when testing the alloys in air. This finding was attributed to the gas having an oxidizing potential at 900°C. At the lower test temperature of 800°C and at low stress, lives were generally shorter than comparable tests in air. This was attributed to the gas having a sulphidizing potential at 800°C.

In the original statement of work for the stress-rupture test program, Phase 2 had as its objective to essentially repeat Phase 1 except that the program alloys were to be tested with a simulated fluidized bed deposit enveloping the gauge length of the stress-rupture test specimen. However, in consultation with the program scientific officer, it was decided that a sulphidizing potential should be established at 900°C by redefining the synthetic gas composition. Accordingly, Phase 2 was revised to accommodate the change in scope. Part 1 of revised Phase 2 consisted of 800°C stress-rupture tests conducted using the synthetic combustion gas of Phase 1 and with each alloy having the simulated fluidized bed deposit enveloping the specimen gauge length. In Part 2 of revised Phase 2, 900°C stress-rupture tests were conducted using uncoated test specimens in the new gas.

2.0 EXPERIMENTAL

2.1 Materials

2.1.1 Alloys

The alloys used for the stress-rupture tests at 800 and 900°C were from the same heats as those used in Phase 1. The chemical and room temperature physical properties of the alloys are shown in Tables 1 and 2, respectively. Specimen preparation techniques conformed to the ASTM E8-81 designation, sections 6.1 and 6.4.

2.1.2 Synthetic Combustion Gas

The synthetic combustion gas for Phase 2 was purchased from Matheson of Canada. For the 800°C tests the nominal gas composition was the same as used for Phase 1, namely, 200 ppm CO, 2000 ppm SO_2, 20% CO_2 and balance N_2. The gas composition contained in each cylinder was certified by Matheson to be within the preparation tolerance. An additional requirement for Phase 2 testing was that the gas be certified to contain $\leq$10 ppm O_2.

Synthetic combustion gas for the 900°C tests had a nominal composition of 540 ppm CO, 2.0% SO_2, 18% CO_2, $\leq$30 ppm O_2 and balance N_2. A certificate of analyses was provided for the gas contained in each cylinder.

2.2 Apparatus and Procedure

Stress-Rupture evaluations for Phase 2 were carried out using the apparatus as described in the Phase 1 interim report, except that the bill of material for the specimen clevises and pull rods was later changed. Although the useful life of the Inconel 713C clevises and pull rods in the synthetic combustion gas had been increased by first oxidizing at 1000°C in air, considerable corrosive attack was evident after long term tests. This degradation of 713C was particularly marked when used in the 2.0% SO_2 gas at 900°C and the bill of material was changed to stainless alloy 310. The appearance of both alloys after long term use in the 2.0% SO_2 gas at 900°C is shown in Figure 1. Note the pitting of 310.

Table 1 Chemical Analyses of Test Alloys

	Analyses (%)											
	Incoloy 800H			310			HK40			347H		
	Min	Max	Actual	Min	Max	Actual	Min	Max	Actual	Min	Max	Actual
Al	0.15	0.6	0.31	ns	ns	-	ns	ns	-	ns	ns	-
C	0.05	0.10	0.08	-	0.15	0.12	0.35	0.45	0.45	0.04	0.10	0.07
Cb+Ta	ns	ns	-	ns	ns	-	ns	ns	-	8xC	1.0	0.90
Cr	19.0	23.0	20.17	24.0	26.0	24.37	23.0	27.0	24.81	17.0	19.0	18.2
Cu		0.75	0.61	ns	ns	-	ns	ns	-	ns	ns	-
Mn		1.50	0.94	-	2.00	1.69	-	1.50	0.73	-	2.00	1.83
Mo	ns	ns	-	ns	ns	-	-	0.50	0.052	ns	ns	-
Ni	30.0	35.0	32.9	19.0	22.0	19.01	19.0	22.0	20.69	9.0	13.0	10.77
P	ns	ns	-	-	0.040	0.031	-	0.040	0.019	-	0.040	0.030
S		0.015	0.001	-	0.030	0.006	-	0.040	0.012	-	0.030	0.007
Si		1.0	0.60	-	0.75	0.66	0.50	2.00	1.11	-	1.00	0.48
Fe	39.5	ns	43.95	ns	ns	-	ns	ns	-	ns	ns	-
Ti	0.15	0.60	0.45	ns	ns	-	ns	ns	-	ns	ns	-
ASTM: UNS:	B-408-77 N08810			A249-80 S31000			A608-79 J94224			A479-80a S34709		
Supplier	Inco Alloys Canada Ltd			Specialty Steels			Fahramet			Atlas Alloys		
Heat No:	(4) HH0898A M1989			40477			75016			A11330		

ns: Not specified

Table 2 Physical Properties of Test Alloys*

Alloy	Supplier	Heat No	Reference ASTM	Short Term Tensile			Hardness R_B	Grain Size ASTM
				YS(MPa)	UTS(MPa)	Elongation(%)		
310 Stainless	Specialty Steels	40477	A249-80	282(205)	642(515)	44(35)	80(90max)	8-9
347H	Atlas Alloys	A11330**	A479-80a	482(205)	662(515)	46(35)	99(ns)	9-10
HK40	Fahramet	75016	A608-79	ns***	ns			
800H	Inco Alloys Canada Ltd	HH0898A M1989	B408-77	179(170)	568(450)	56(30)	78(ns)	4.5

* Bracketed numbers represent minimum values, except as noted, from reference data

** Alloy heated to 1066°C min for sufficient time to dissolve carbides then quenched in water

*** As outlined in ASTM A608 Section 8 "tensile tests at room temperature are not recommended as acceptance criteria"

ns: Not specified

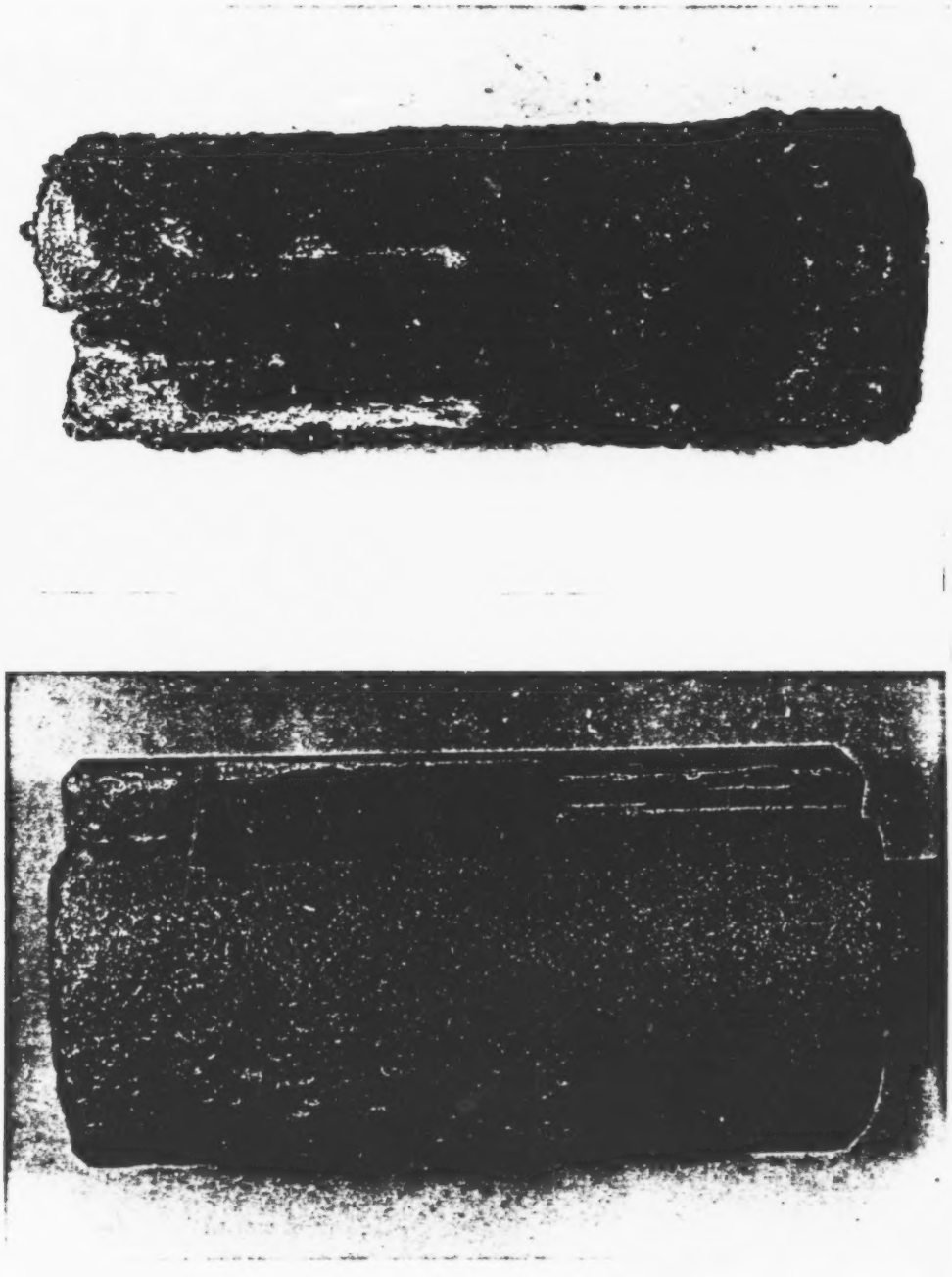

Figure 1 Appearance of Alloy 310 and Inconel 713C Clevises After Long Term Exposure to High SO_2 Combustion Gas

As noted in the Phase 1 report, the original Inconel 713 retort liner was also changed to 310 in an effort to prolong liner life. The 310 liner however was also severely attacked during Phase 2 testing. The attack was characterized by a massive layer of built up corrosion products on the inside of the liner at the centre of the furnace hot zone. An example of this attack is illustrated in Figure 2. Some of this deposit was invariably found on the upper surface of the bottom retort cover after completion of each stress-rupture test. It was not determined if this material had spalled off the liner during heating or cooling or if it was inadvertently knocked off during removal of the test sample, clevises and pull rods at the conclusion of the test. It was difficult to judge the relative degree of liner degradation and, as a consequence, the liners were probably changed more often than was actually necessary. However, it was deemed prudent to change the liner rather than to jeopardize a 1000 h test!

Synthetic combustion gas flow rates for the 800°C tests remained unchanged from those of Phase 1 but the gas velocity over the specimen was reduced to 75 mm/min for the 900°C tests. It should be pointed out that use of the high SO_2 content gas at 900°C resulted in the formation of a yellow colored deposit on the inner surface of the water cooled top of the retort. Microprobe energy dispersive X-ray analyses of the deposit showed only sulphur. This finding was confirmed by X-ray diffraction which indicated the presence of orthorhombic sulphur. Analyses of the inlet and outlet gas taken during the 900°C tests however showed that the gas composition remained unchanged and suggested that decomposition of SO_2 during stress-rupture testing was minimal.

The initial stress levels for each alloy were chosen with reference to data obtained during Phase 1 stress-rupture testing. Additional stress levels were selected using the Phase 1 data together with a least squares analysis of the actual Phase 2 results.

The application of the simulated fluidized bed combustor deposit to the test specimen for the 800°C tests was conducted using the procedure described in the Phase 1 report. Briefly, a blend of six parts calcium sulphate and one part calcium oxide (both chemically pure substances) was loosely packed into an amorphous refractory silicon dioxide cloth (refrasil) bag which surrounded the specimen gauge length. Platinum-rhodium thermocouple wire was used to secure the bag to the test sample. In all cases the deposit containment bag was found to be intact upon completion of the stress-rupture test.

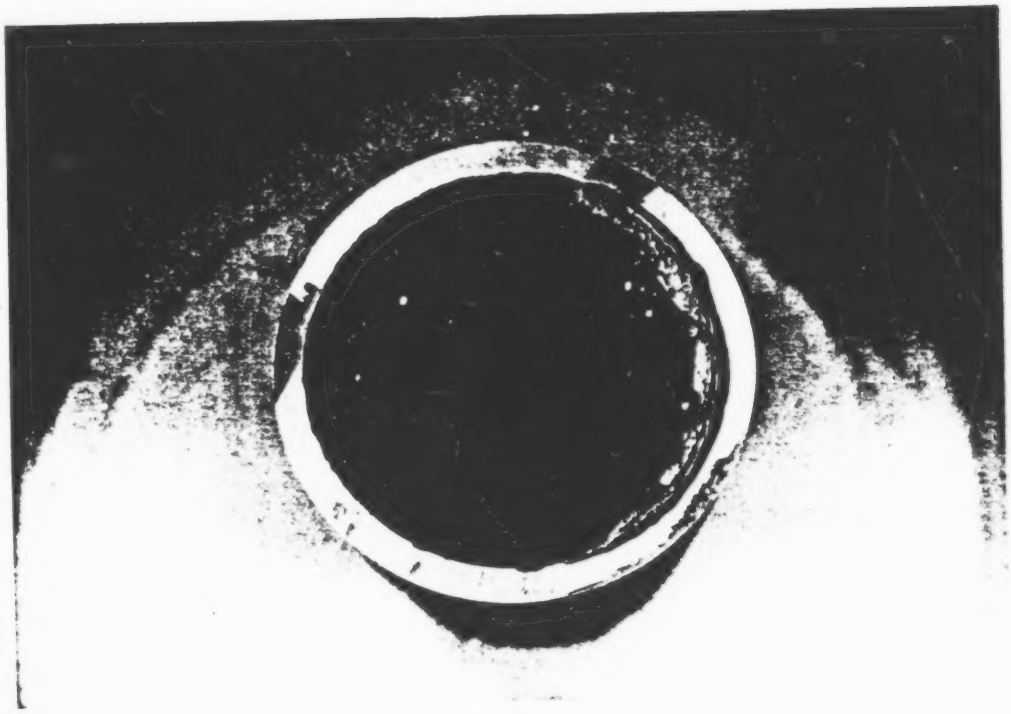

Figure 2 Appearance of 310 Retort Liner After Long Term Exposure to Synthetic Combustion Gas

During Phase 2 testing, an experiment was conducted to evaluate the degree of protection that could be gained by applying a diffusion coating of aluminum to the test alloys prior to exposure to the combustion gas. For these tests, short lengths of each of the four alloys plus Incoloy MA956* were pack alonized for 2.5 h in a mixture of Al, Al_2O_3 and NH_4Cl at 950°C in H_2. The small treated pieces together with uncoated controls were positioned in one stress-rupture retort and subjected to a 232 h exposure to the high SO_2 content gas at 900°C.

Metallographic examination of the uncoated and aluminum diffusion coated alloys after the 232 h heat treatment showed that neither the coated nor the uncoated samples of HK40, 310 or 347H were attacked significantly. Some porosity in the diffusion coating was observed with 347H showing the most and 310 the least. The degree of porosity correlated roughly with the width of what appeared to be a diffusion zone in the alloy. Microprobe traces would have to be done to confirm this correlation.

Uncoated MA956 and 800H showed some areas of sulphidation with the effect being more pronounced for 800H. For the aluminum diffusion coated alloys, the integrity of the coating on MA956 was similar to 347H while the coating on 800H had little porosity and exhibited an excellent bond to the alloy. An example of sulphidation observed in uncoated 800H is shown in Figure 3. As shown in the photomicrograph, the sulphidation was flanked by areas which appeared to have undergone very little or no attack. The metallographic examination of diffusion coated 800H did not reveal any areas of hot corrosive attack of the underlying alloy. Some surface attack was observed, but this appeared to be related to a surface defect in the alloy as shown in Figure 4. Note that although no inward sulphide penetration had occurred some cracks had developed in the coating.

Collectively, the above results suggested that aluminum diffusion coatings offered some protection against the corrosive environment of the synthetic combustion gas, especially for 800H, but more work would be required to establish whether the coatings would be effective over longer exposure times and when subjected to stress.

---

* An oxide (0.5% Y_2O_3) dispersion strengthened iron(74)-chromium(20)-aluminum(4.5) alloy produced by mechanical alloying

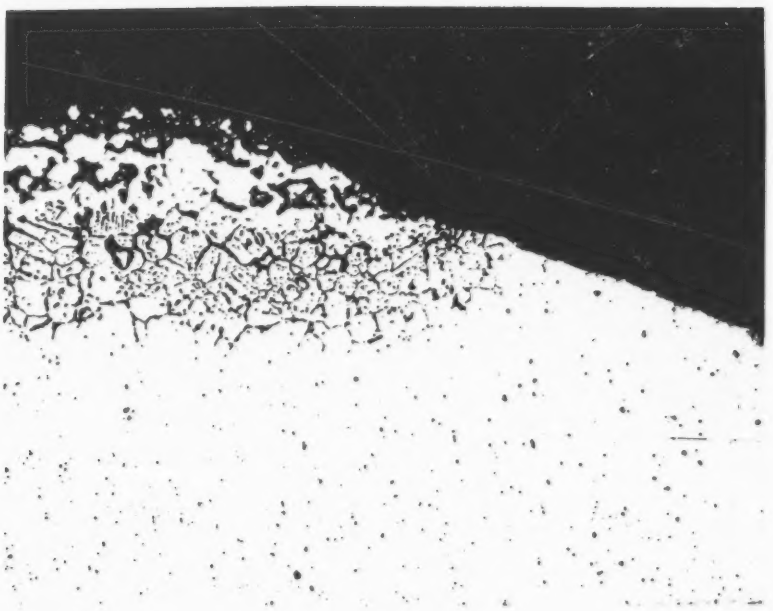

X50

Figure 3 Sulphidation Observed in 800H after 232 h Exposure to High SO_2 Combustion Gas at 900°C

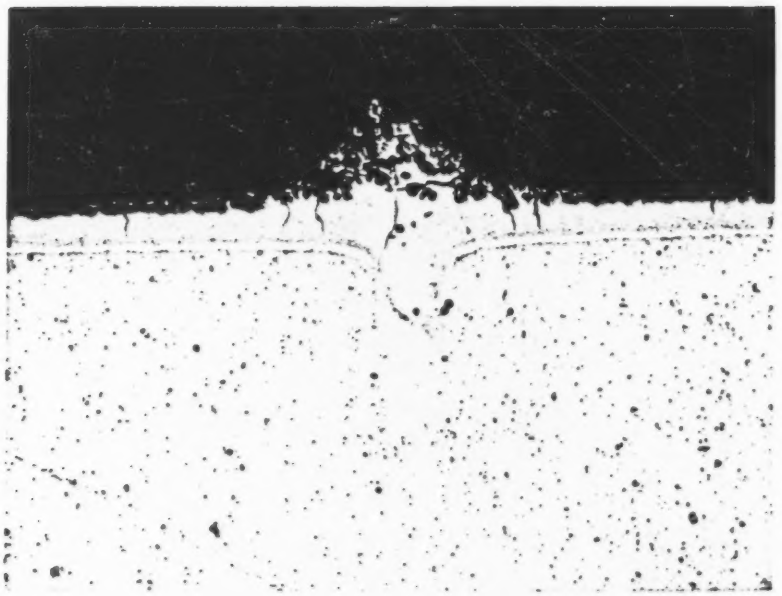

X50

Figure 4 Appearance of Aluminum Diffusion Coated 800H After 232 h Exposure to High SO_2 Combustion Gas at 900°C

3.0 RESULTS AND DISCUSSION

3.1 Stress-Rupture Data for 800°C Tests

3.1.1 Stainless Alloy 310

The stress-rupture data for 310 are shown in Table 3. As indicated in the Table, six tests were conducted instead of the five required by the contract. The sixth test was carried out because of the unexpectedly short time to rupture (109.2 h) which occurred when using a stress of 50.3 MPa. The retest resulted in a life of 148.4 h.

The data of Table 3 are compared to Phase 1 results in Figure 5 and show that the simulated deposit in the synthetic combustion gas did not have a marked affect on the stress to rupture behavior of the alloy (the dashed lines in the Figure represent the minimum and maximum expected results for comparable tests conducted in air without the deposit and are based on data from the literature).

Table 3 Stress-Rupture Data for Stainless Alloy 310 Tested at 800°C in Synthetic Combustion Gas and Simulated Fluidized Bed Deposit

Stress (MPa)	Time to Rupture (h)	Elongation (%)
89.6	15.6	40
71.0	55.2	25
62.1	106.6	18
50.3	109.2	29
50.3*	148.4	29
32.8	787.7	26

* Retest

3.1.2 Cast Alloy HK40

Data obtained for the 800°C stress-rupture behavior of HK40 are shown in Table 4 and compared to Phase 1 results in Figure 6. It should be noted that the stress chosen for the last long term test shown in the Table was based on the previous four and was expected to cause rupture after approximately 1000 h. The 423.8 h actual result implied a much shorter life compared to Phase 1 data. Metallographic examination of the 423.8 h specimen however did not reveal catastrophic sulphidation and comparatively little difference between this and previously tested specimens was observed. After consultation with the scientific officer it was decided that this anomalous result would be resolved during Phase 3 by conducting an additional long term test.

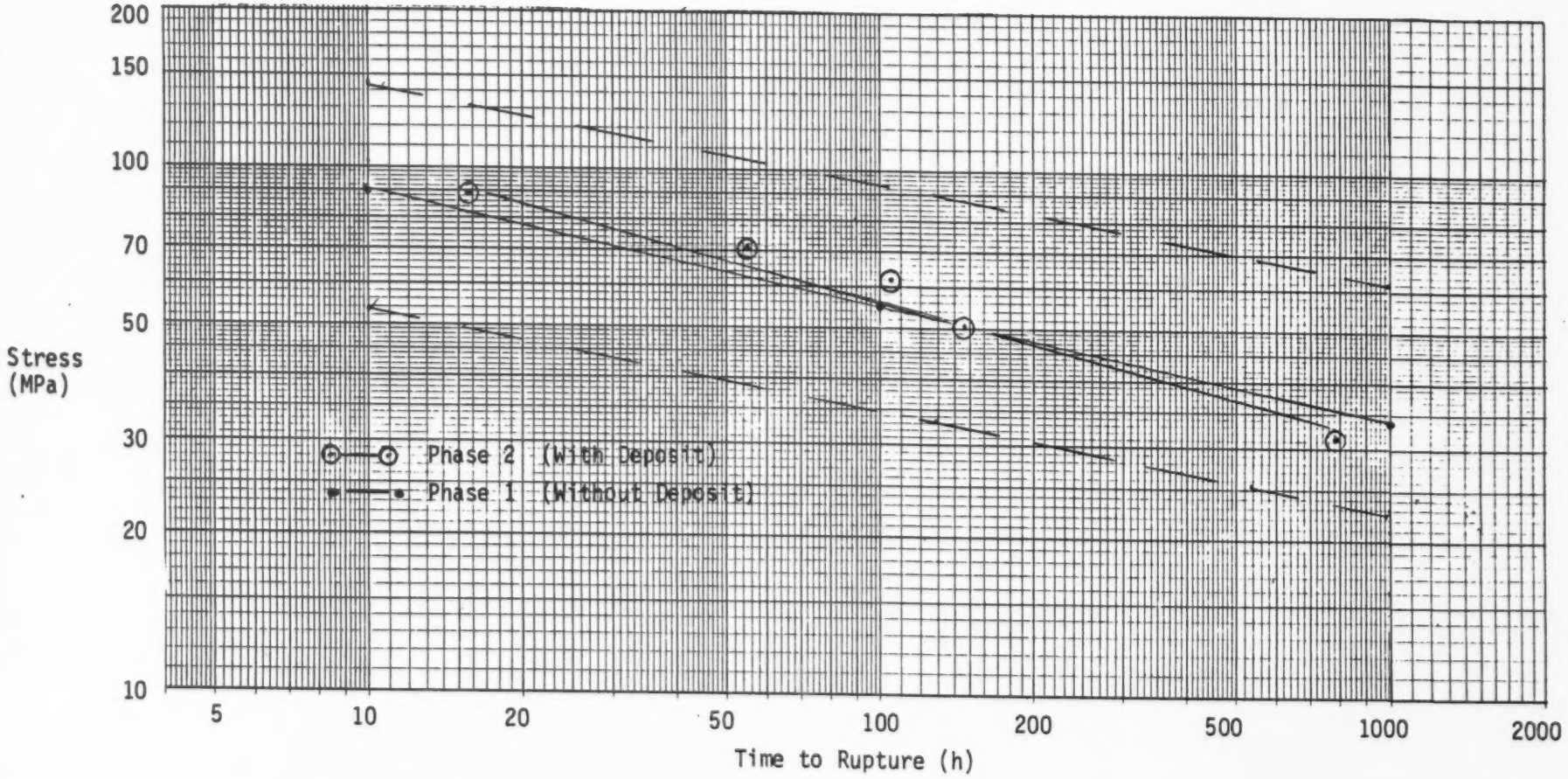

Figure 5 Stress-Rupture Tests for Stainless Alloy 310 at 800°C in Synthetic Combustion Gas

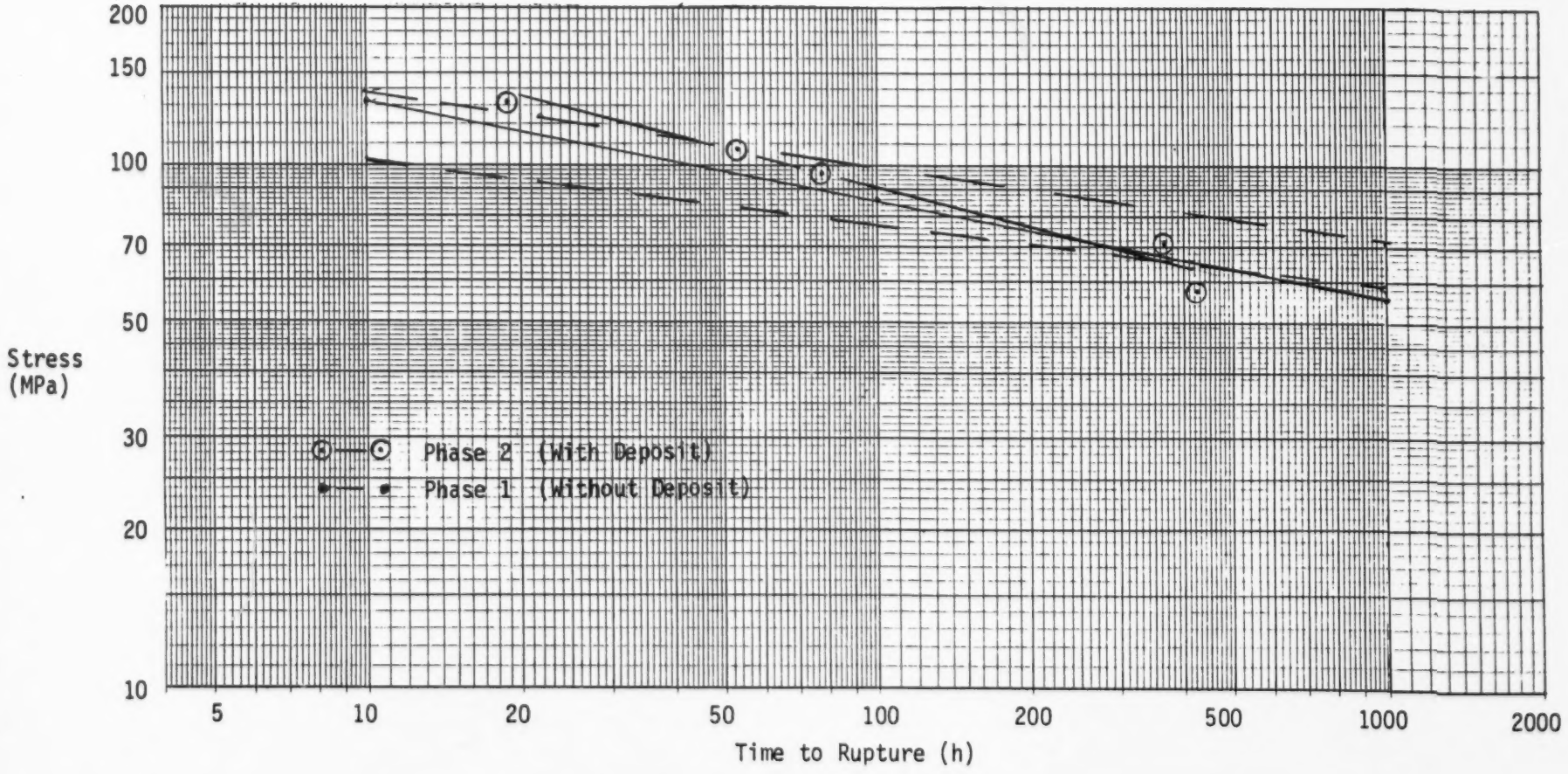

Figure 6 Stress-Rupture Tests for Cast Alloy HK40 at 800°C in Synthetic Combustion Gas

Table 4 Stress-Rupture Data for Cast Alloy HK40 Tested at 800°C in Synthetic Combustion Gas and Simulated Fluidized Bed Deposit

Stress (MPa)	Time to Rupture (h)	Elongation (%)
133.8	19.0	13
108.3	51.8	6
96.5	78.1	6
70.3	367.3	3
56.9	423.8	4

3.1.3 Incoloy 800H

Although 800H was characterized by heavy corrosion during the 800°C tests (in some instances the attack obliterated the gauge marks) little difference in the stress-rupture curve was evident when compared to Phase 1 data. The results in Table 5 and Figure 7 however show some scatter and an additional test designed to cause rupture in approximately 300 h is scheduled for Phase 3.

Table 5 Stress-Rupture Data for Incoloy 800H Tested at 800°C in Synthetic Combustion Gas and Simulated Fluidized Bed Deposit

Stress (MPa)	Time to Rupture (h)	Elongation (%)
103.4	12.4	63
89.6	17.7	59
76.6	96.3	nd
56.5	83.0	40
37.2	1445.1	nd

nd Not done, heavy corrosion obliterated gauge marks

3.1.4 Stainless Alloy 347H

Stress-rupture data for 347H showed no anomalies (Table 6) and compared very well with previous Phase 1 results (Figure 8).

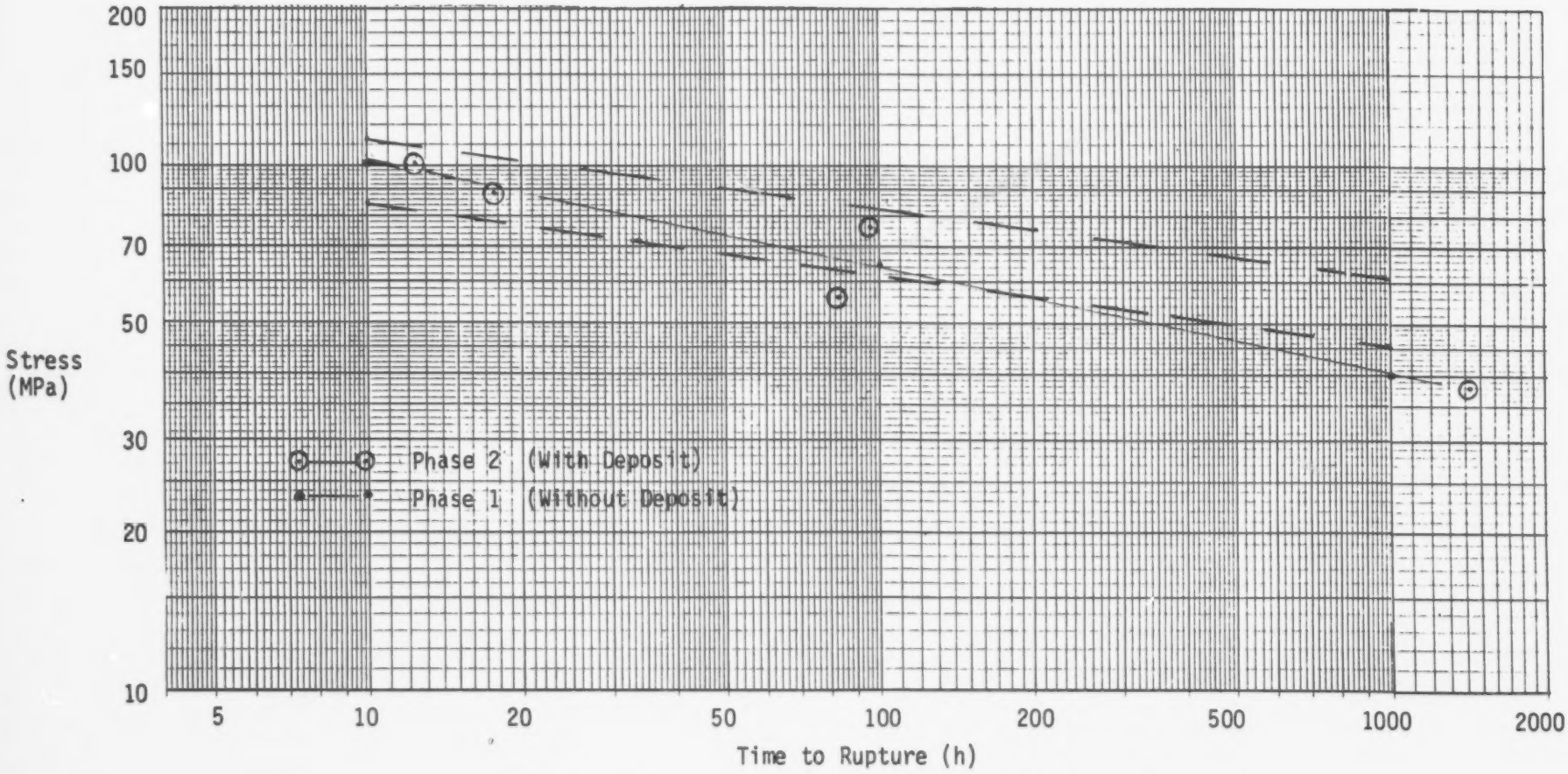

Figure 7 Stress-Rupture Tests for Incoloy 800H at 800°C in Synthetic Combustion Gas

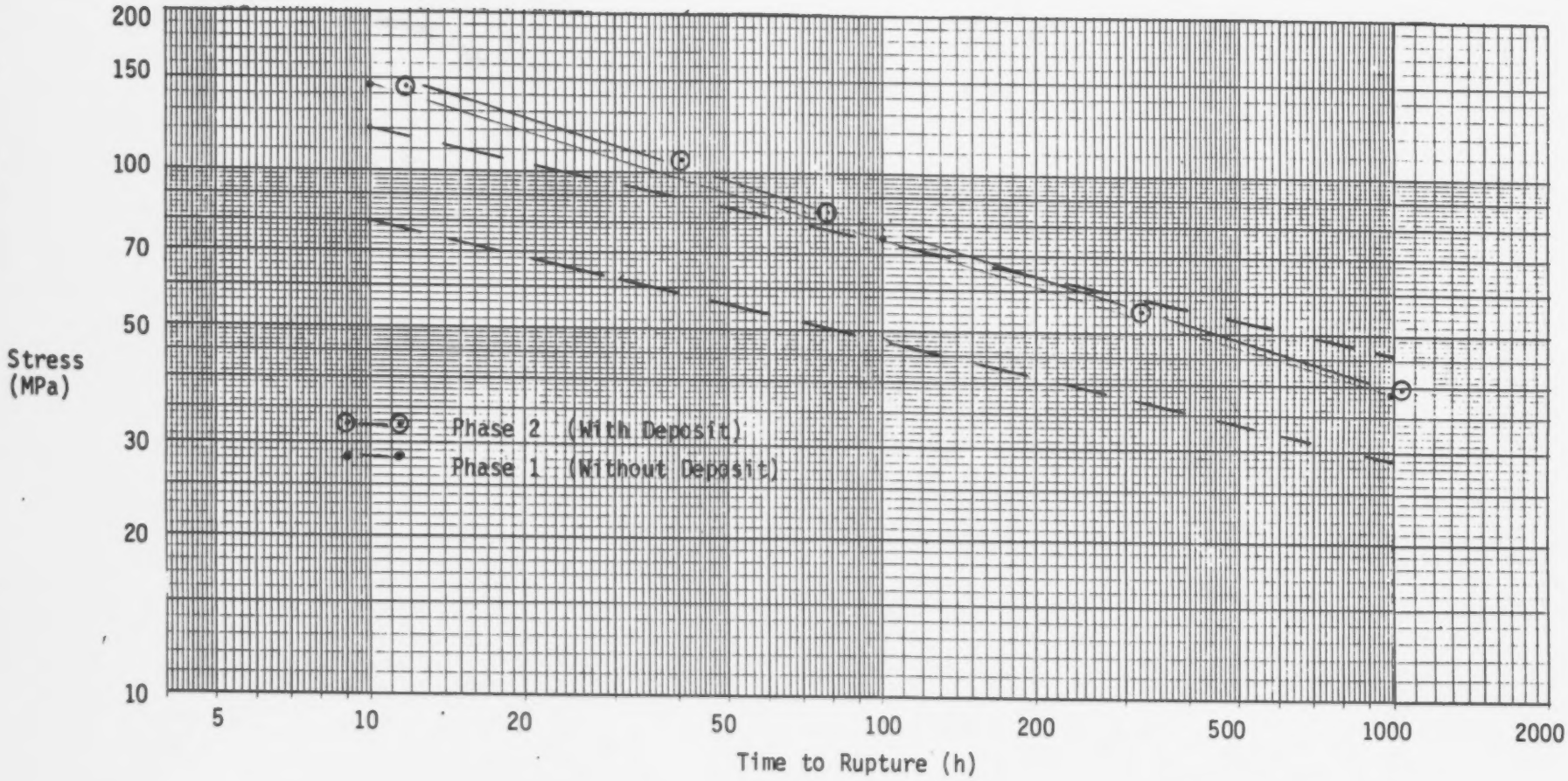

Figure 8 Stress-Rupture Tests for Stainless Alloy 347H at 800°C in Synthetic Combustion Gas

Table 6 Stress-Rupture Data for Stainless Alloy 347H Tested at 800°C in Synthetic Combustion Gas and Simulated Fluidized Bed Deposit

Stress (MPa)	Time to Rupture (h)	Elongation (%)
145.5	11.9	37
106.2	40.7	50
84.1	78.4	67
54.5	320.0	67
39.7	1031.4	100

3.2 Metallographic and Microprobe Examination of 800°C Ruptured Specimens

Figures 9 and 10 show the appearance of the specimens after stress-rupture testing. Comparatively, 800H showed the most corrosion and 347H the least. Alloys 310 and HK40 were similar although 310 appeared to be characterized by more pitting.

In the Phase 1 report, metallographic examination of 800H indicated that increased surface attack appeared to correlate with areas of high deformation. However this correlation was not as well defined in the ruptured specimens of Phase 2 800°C testing. For example, Figure 11 shows both high and low magnifications of the specimen tested using a stress of 103.4 MPa, life to rupture was 12.4 h. In the low magnification photomicrograph of the area near the fracture, very little evidence of corrosion can be observed although the base of the stress cracks appear rounded. Some indication of hot corrosion was apparent however and as shown in the high magnification photomicrograph sulphidation appeared to be following stress cracks into the alloy. This was similar to the Phase 1 800H results.

In ruptured specimens of 800H which had been tested for longer times at lower stress more corrosion was evident. A large proportion of the observed corrosion did not appear to be related to stress cracks. The corrosion observed on the specimen after a life of 83 h at 56.5 MPa is illustrated in Figure 12 and the high magnification photomicrograph shows this effect very clearly. Corrosion associated with stress cracks was also observed in this specimen. An example of the distribution of the major elements in the deposit of a stress crack and in the adjacent alloy is illustrated by the electron microprobe analyses in Figure 13. In this Figure, the absorbed electron image shows the deposit at the base of a stress crack in the surrounding matrix of 800H alloy (darker grey). The distribution of sulphur, nickel, iron and chromium relative

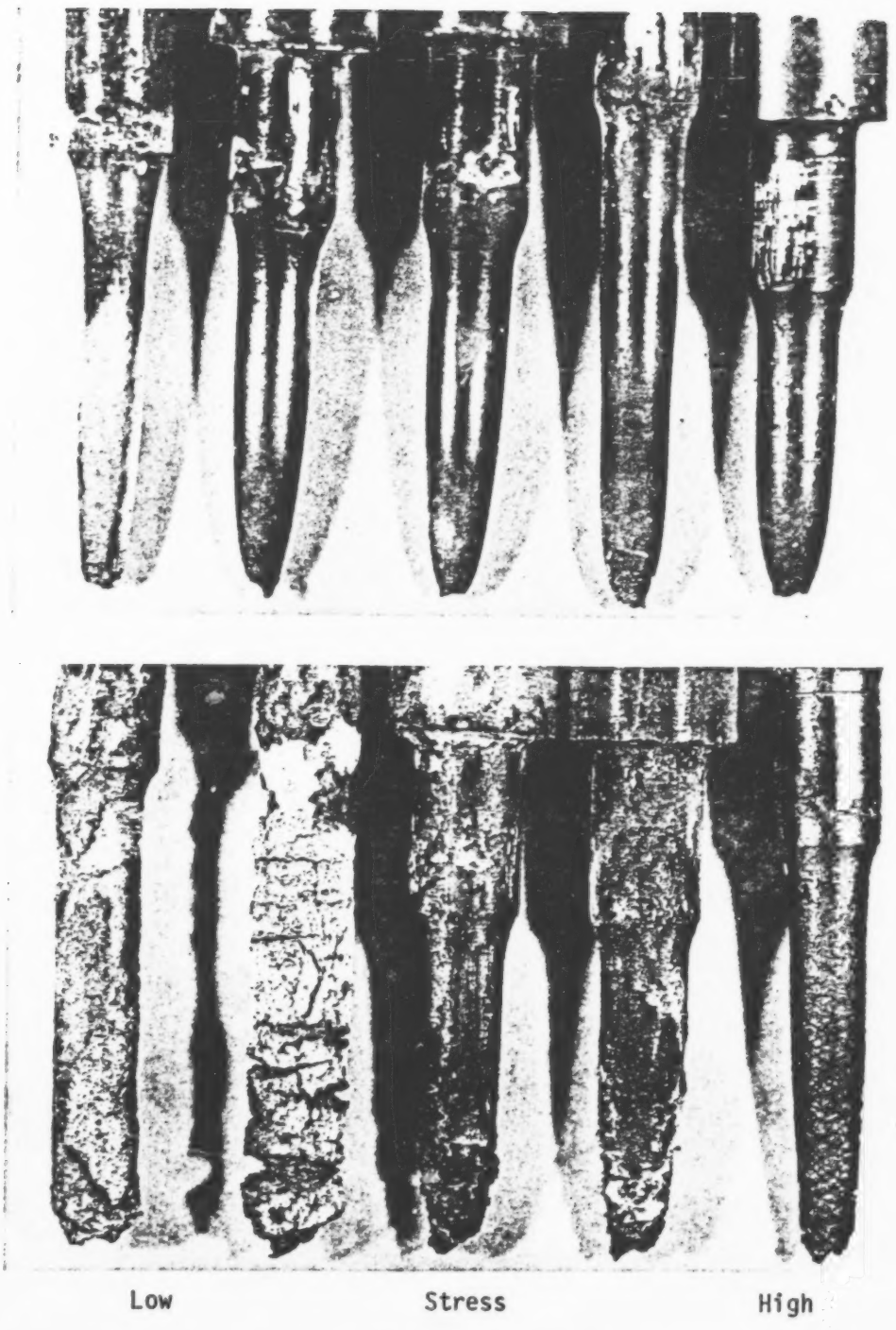

Figure 9 Appearance of 347H and 800H After Testing in Contact with Simulated Deposit in Synthetic Combustion Gas at 800°C

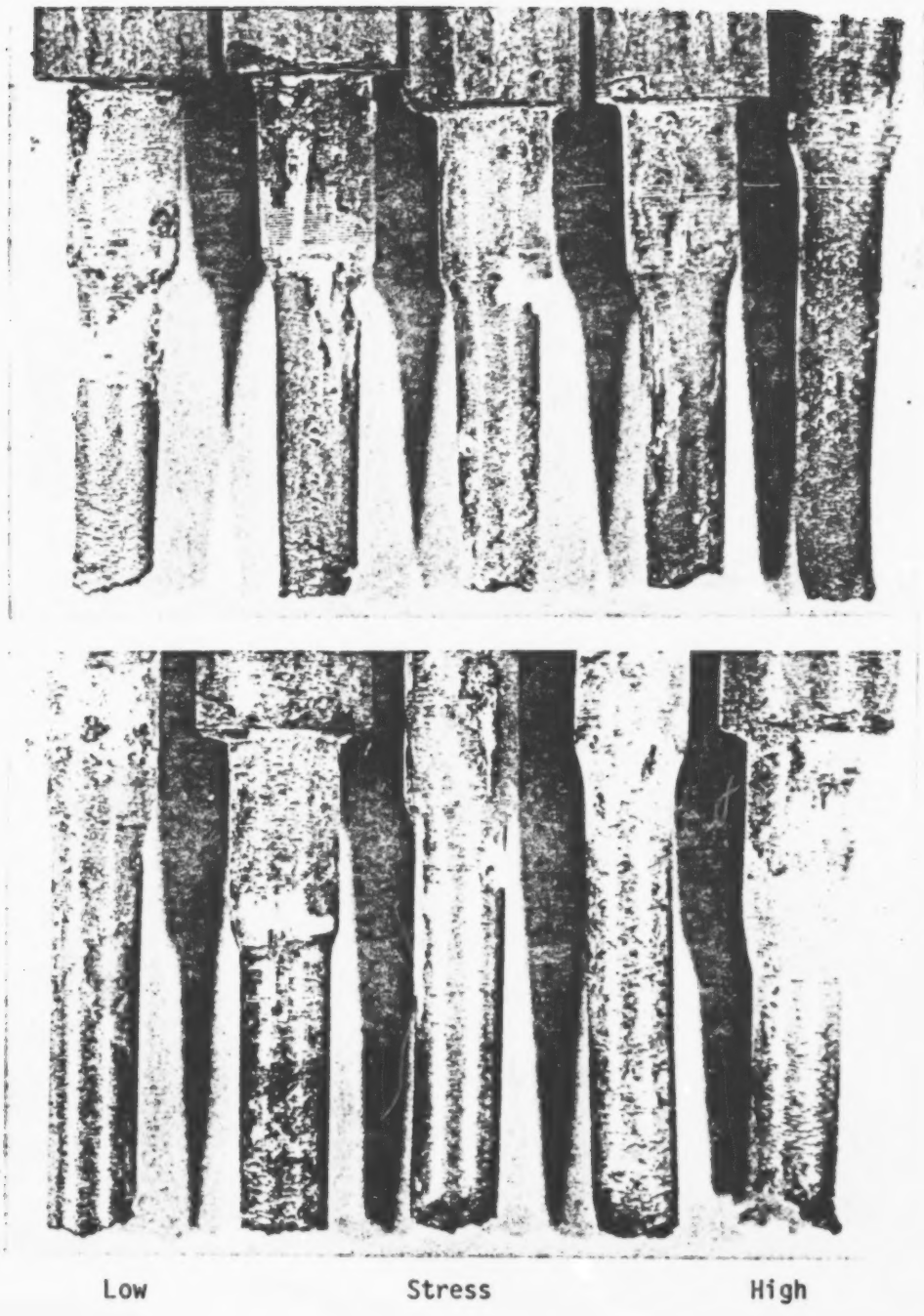

Figure 10 Appearance of 310 and HK40 After Testing in Contact with Simulated Deposit in Synthetic Combustion Gas at 800°C

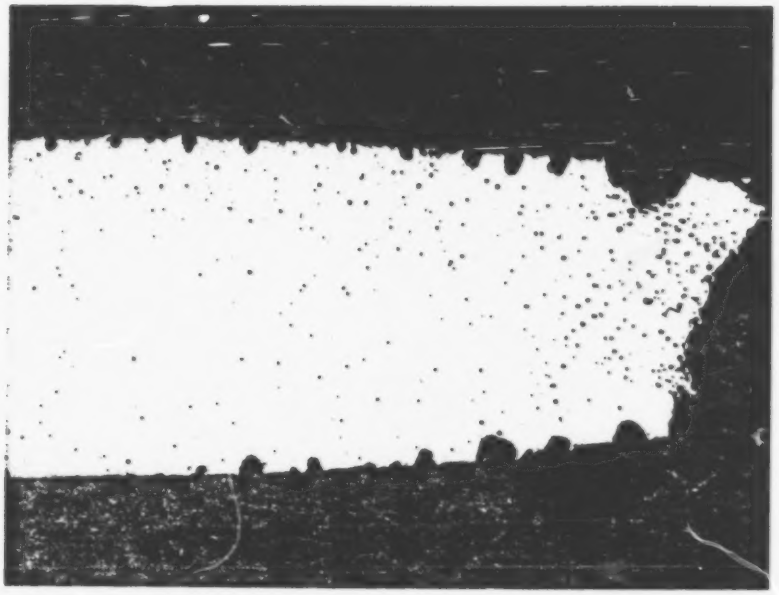

X10

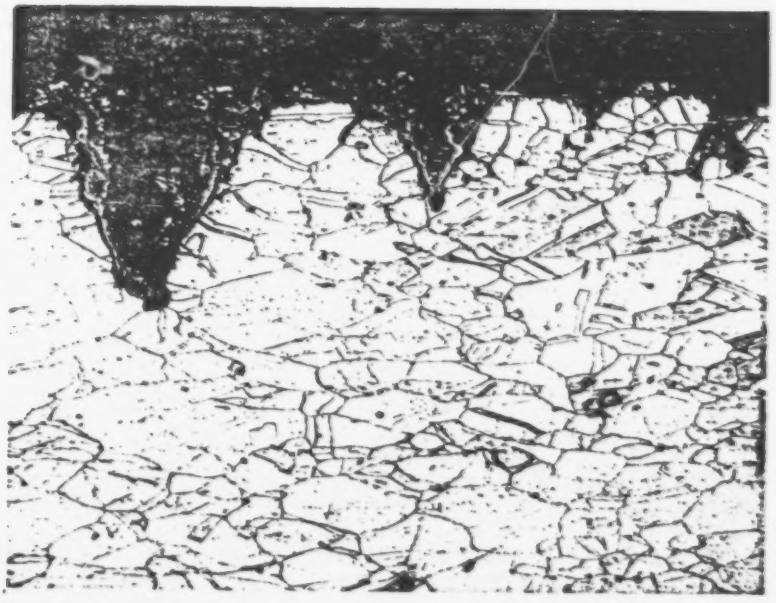

X100

Figure 11 Hot Corrosion Observed in Incoloy 800H After 800°C Test at 103.4 MPa for 12.4 h

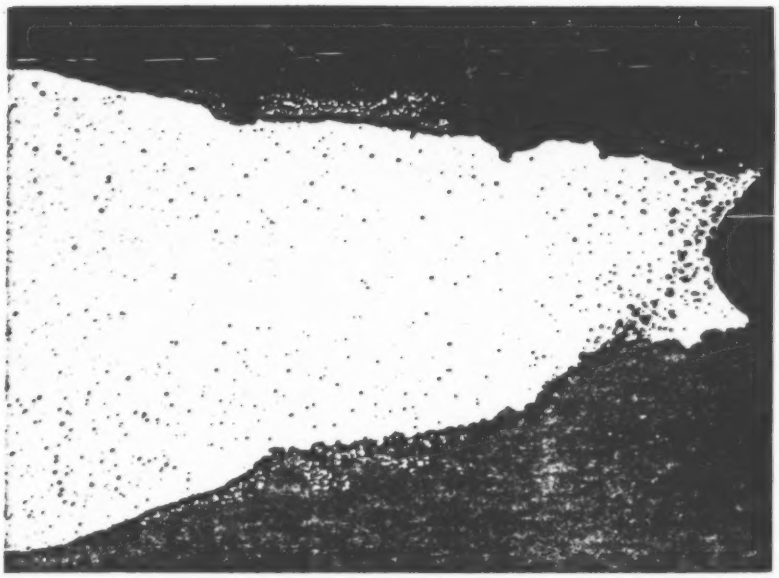

X10

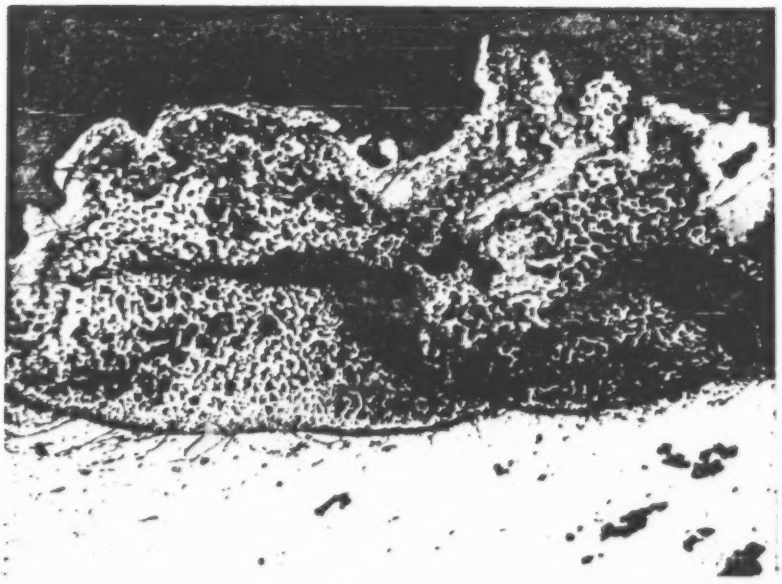

X100

Figure 12 Hot Corrosion Observed in Incoloy 800H After 800°C Test at 56.5 MPa for 83.0 h

to the absorbed electron image is indicated by the white dots making up the X-ray maps for each element. These X-ray element maps show that sulphur appears to be associated in the deposit both with nickel and chromium but not with iron. Very little sulphur is contained in the surrounding base alloy although high concentrations appear to delineate the stress crack.

Photomicrographs of the ruptured 800H specimen which was tested using 37.2 MPa and which had a life of 1445 h are shown in Figure 14. The lower magnification photomicrograph shows the ductile fracture and the heavy corrosion on the alloy surface while the higher magnification photomicrograph shows the corrosion scale and the underlying alloy in greater detail. Electron microprobe analyses indicated that in general sulphur concentrations in the upper regions of the corrosion scale were low although some small pockets of high sulphur were found. These sulphur concentrations correlated well with areas of high chromium and, as well, with areas of low iron and nickel. Nickel and iron were associated with one another while massive regions of high chromium appeared to be devoid of sulphur and were presumably oxide as shown in Figure 15. The electron microprobe analysis showed that in the lower regions of the corrosion scale sulphur was more abundant and was associated preferentially with chromium and iron rather than with nickel. An example of the distribution of the major elements in one of these areas is shown in Figure 16. In the area where the corroded surface bordered the alloy, sulphur concentrations were generally low while chromium concentrations were higher than in the alloy matrix, Figure 17, suggesting outward diffusion of the element. (The X-ray energy dispersive spectra of Figure 17 represent the relative element concentrations in a rectangular area equivalent to that of the absorbed electron image of Figure 16.).

Compared to 800H, less corrosion was observed in 310, HK40 and 347H after being tested in contact with the simulated deposit. This was similar to the trend established in Phase 1. Examples of the corrosion observed in these alloys after testing under conditions of high and low stress are shown in Figures 18 and 19 respectively. As illustrated in the photomicrographs, more corrosion was associated with areas of high deformation in the specimens. Alloy 310 appeared to be affected the most. HK40 was characterized by only limited attack of all specimens, regardless of the stress employed. This finding was probably related to the characteristically low elongations (typically 3 to 10%) exhibited by the cast material.

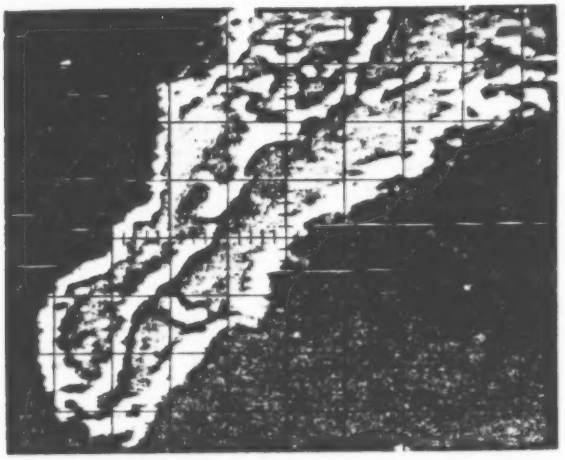

(a) Absorbed Electron Image

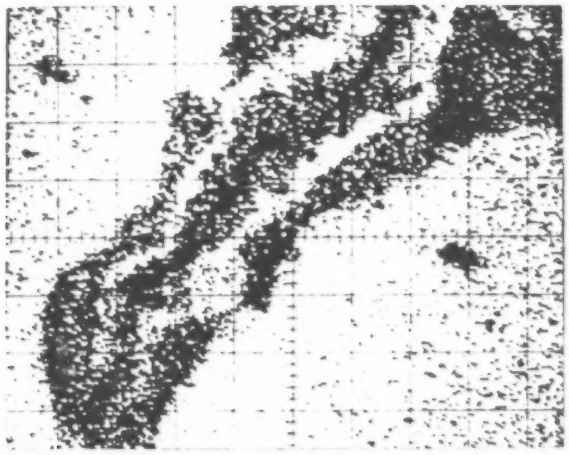

(b) Iron X-Ray Image

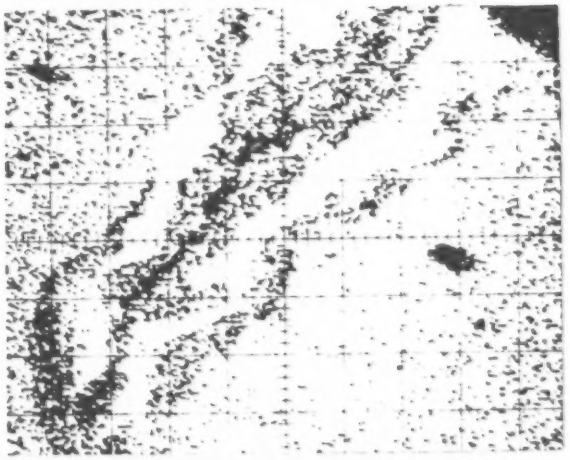

(c) Chromium X-Ray Image

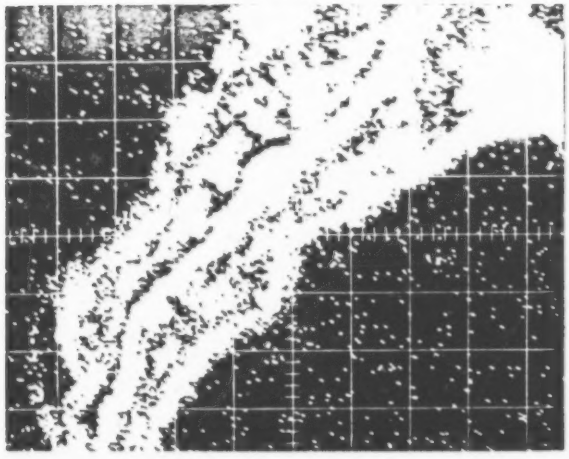

(d) Sulphur X-Ray Image

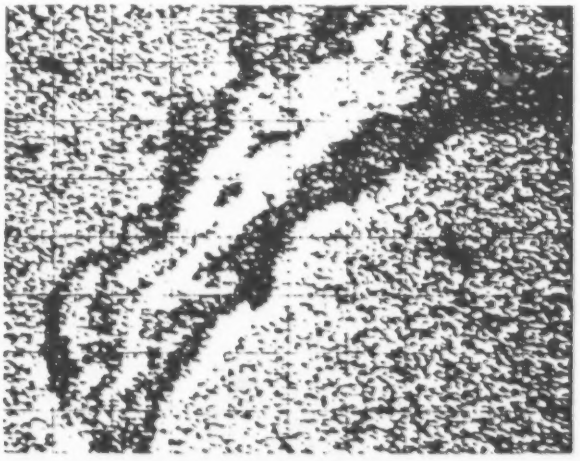

(e) Nickel X-Ray Image

Figure 13 Electron Microprobe Analyses of Corrosion Deposit in a Stress Crack of Incoloy 800H After 800°C Test at 56.5 MPa for 83 h X400

X10

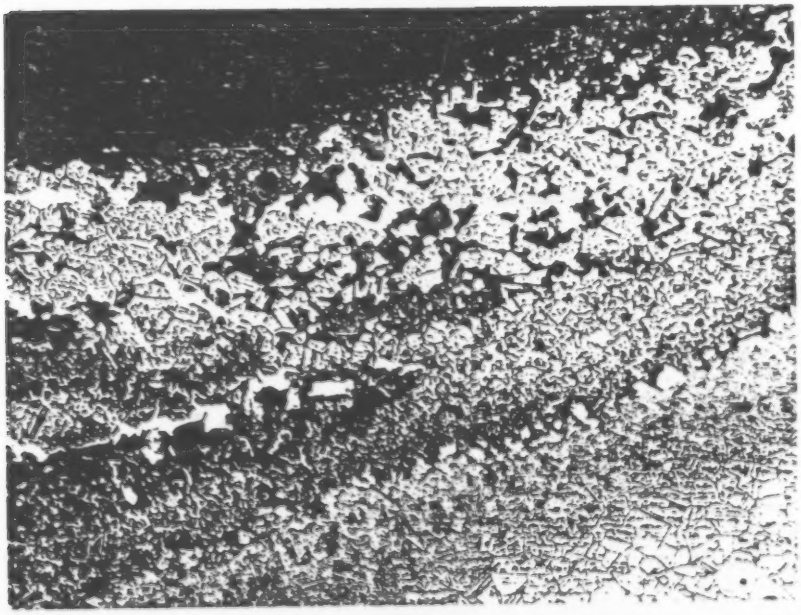

X100

Figure 14 Photomicrographs Showing Appearance of 800H After 800°C Test at 37.2 MPa for 1445 h in Synthetic Combustion Gas

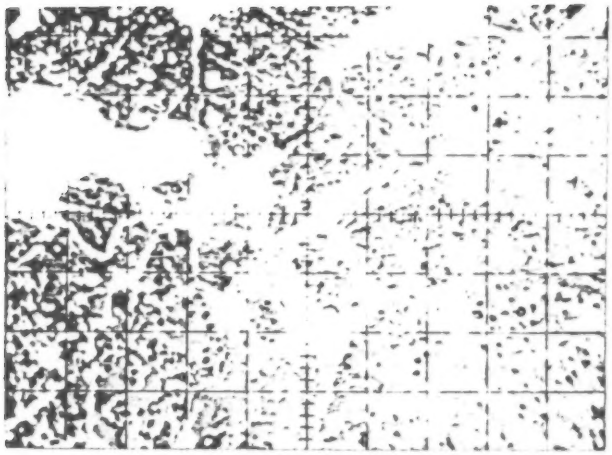

(a) Absorbed Electron Image

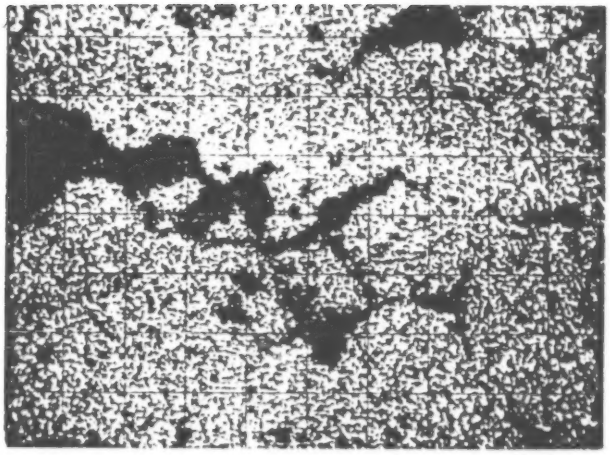

(b) Iron X-Ray Image

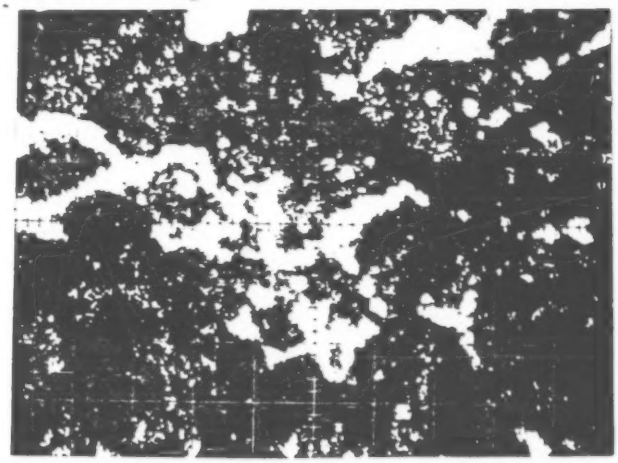

(c) Chromium X-Ray Image

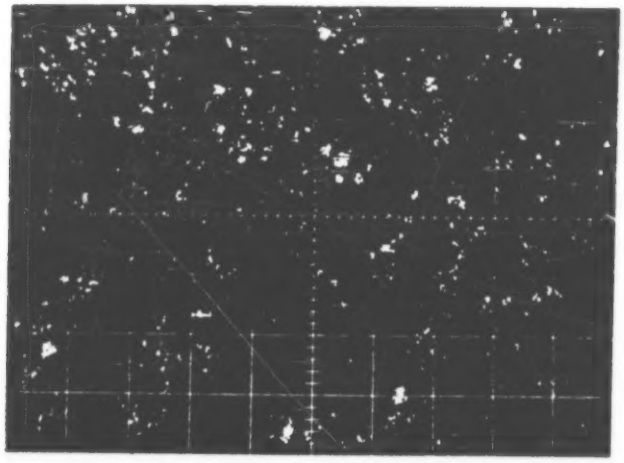

(d) Sulphur X-Ray Image

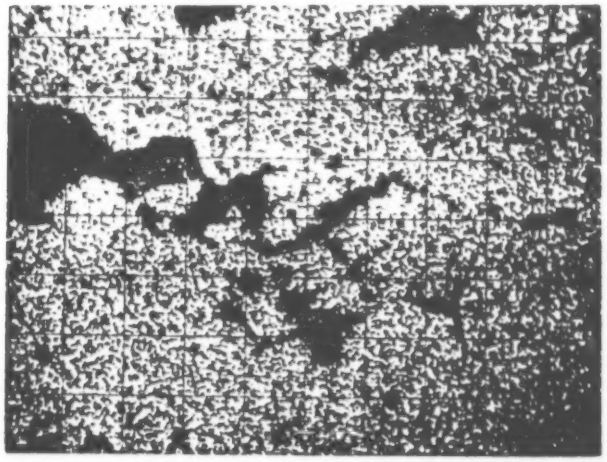

(e) Nickel X-Ray Image

Figure 15 Electron Microprobe Analyses of Upper Corrosion Layer on 800H After 800°C Test at 37.2 MPa for 1445 h
X400

(a) Absorbed Electron Image

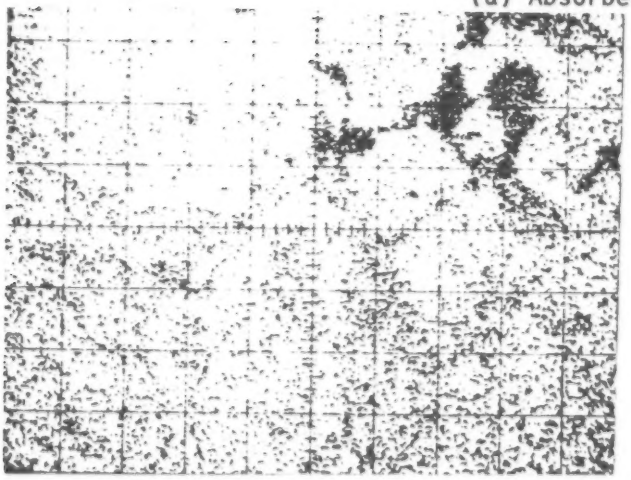

(b) Iron X-Ray Image

(c) Chromium X-Ray Image

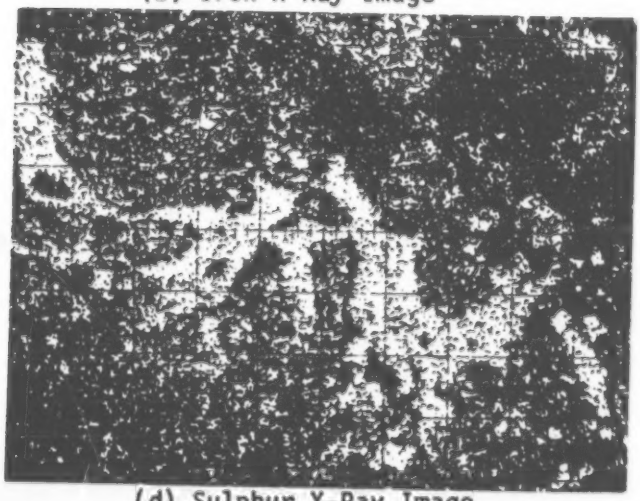

(d) Sulphur X-Ray Image

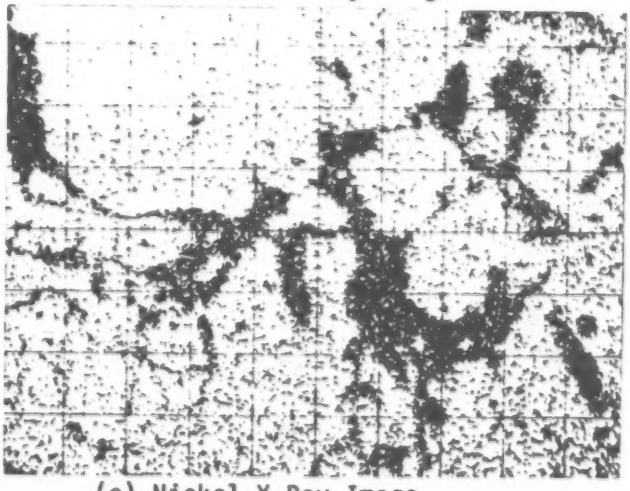

(e) Nickel X-Ray Image

Figure 16 Electron Microprobe Analysis of Lower Corrosion Layer on 800H After 800°C Test at 37.2 MPa for 1445 h
X400

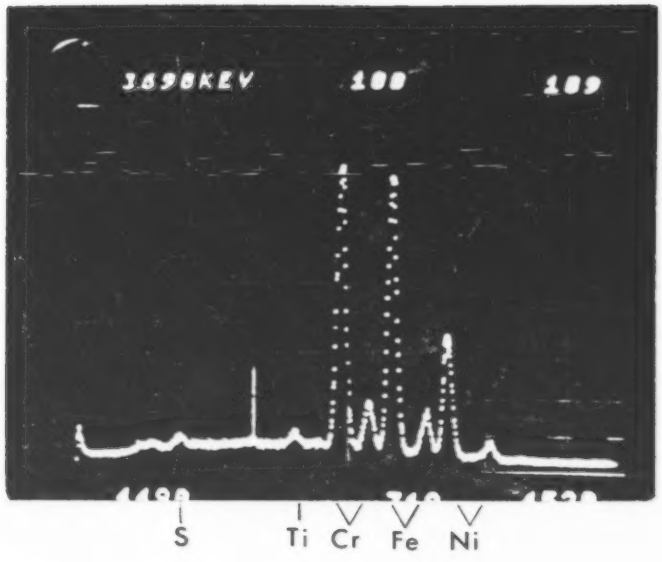

(a) Near Interface

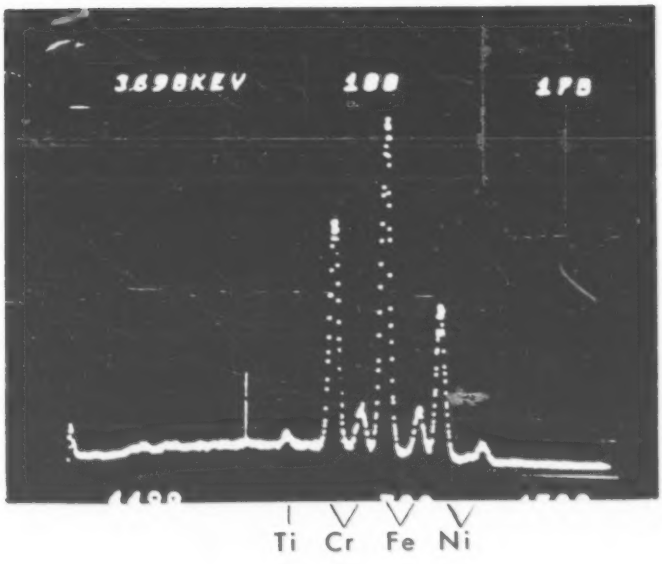

(b) Matrix

Figure 17 Comparative X-ray Energy Spectra from 800H Matrix and Area Near Corrosion Layer - Base Alloy Interface

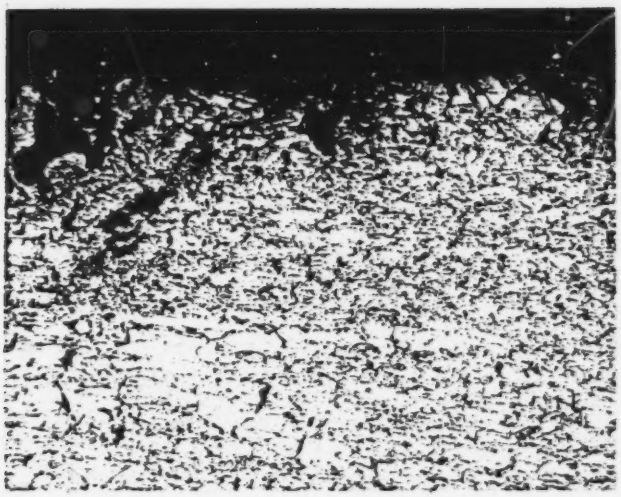

310
90 MPa for 16 h
X100

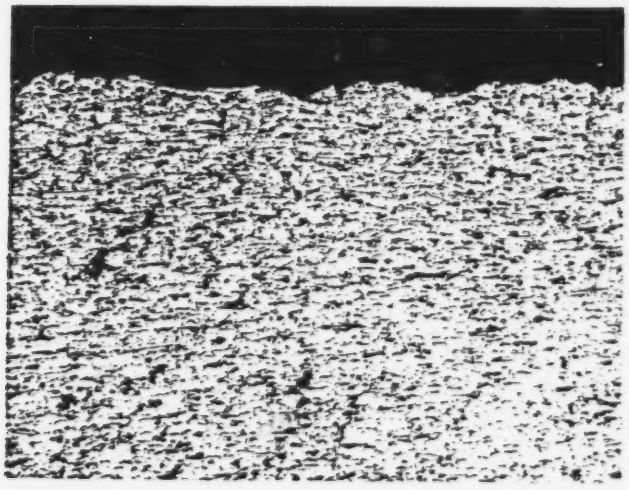

347 H
145 MPa for 12 h
X100

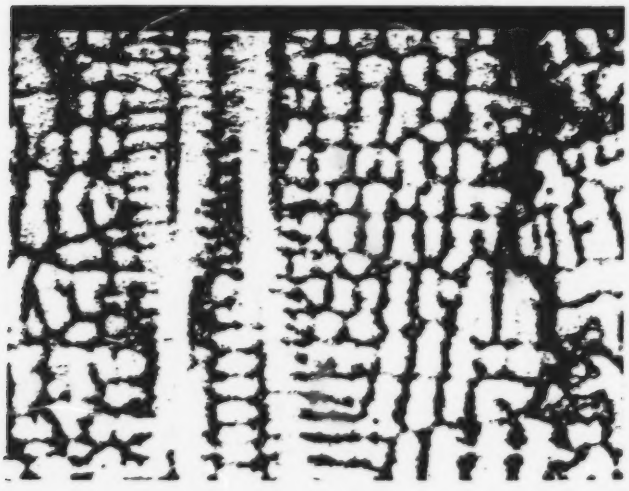

HK40
134 MPa for 19 h
X100

Figure 18 Corrosion Observed in 310, 347H and HK40 After 800°C Tests in Contact with Simulated Deposit at High Stress

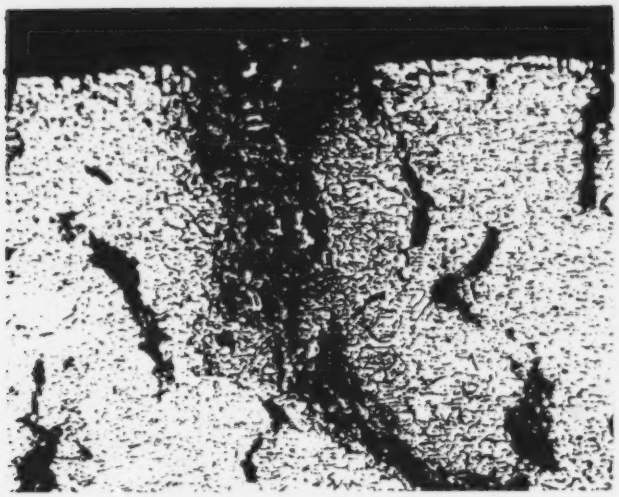

310
33 MPa for 899 h
X100

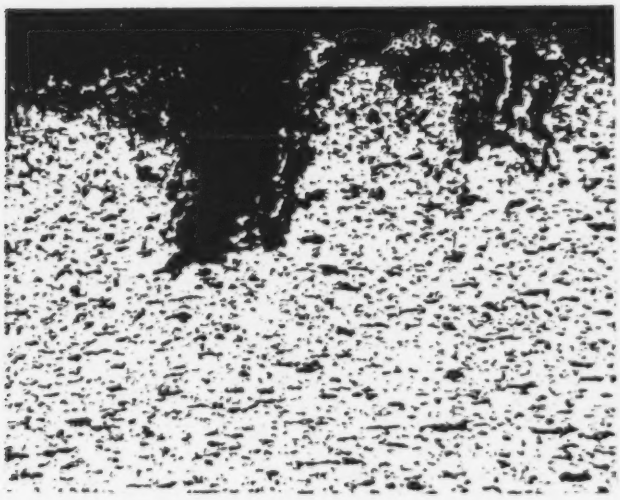

347 H
40 MPa for 1031 h
X100

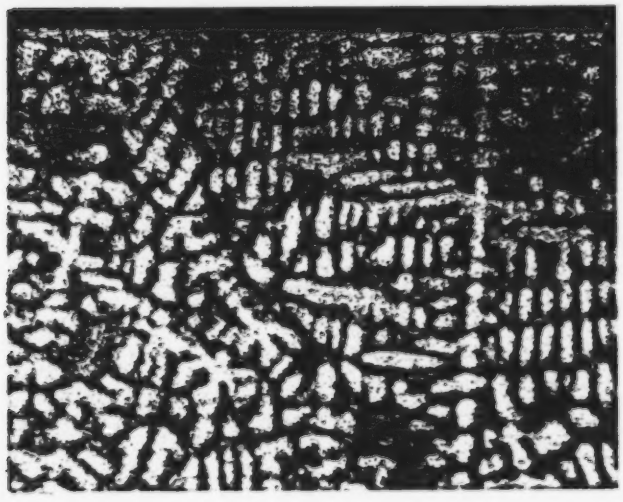

HK40
57 MPa for 424 h
X100

Figure 19 Corrosion Observed in 310, 347H and HK40 After 800°C Tests in Contact with Simulated Deposit at Low Stress

Looking at the photomicrographs of HK40 in Figure 18 and 19, and perhaps better illustrated in Figure 20, a near continuous anomalous "coating" of the ruptured HK40 can be seen. Note the "blister" above the stress crack in Figure 20. Electron microprobe analyses of HK40 tested using a stress of 56.9 MPa for 424 h were conducted. The analysis covered an area which contained a "blister" similar to the one in Figure 20. The element X-ray distribution maps of Figure 21 show that chromium had diffused to the alloy surface. With reference to the grid lines of the X-ray maps, it can be seen that the high concentration of chromium at the surface was outside the fully dense alloy. Note also that this chromium appeared to be below the indicated sulphur location except in the area of the stress crack and that calcium was associated with both chromium and sulphur in these areas. The analyses showed that iron had diffused to the surface as well, but like nickel, remained in the base alloy beneath the high chromium and calcium concentrations except in the area of the stress crack. The microprobe analyses suggested that the outward diffusion of chromium resulted in a protective coating of the alloy. Hot corrosion appeared to occur where the coating had become discontinuous such as in the area of the stress crack as evidenced by outward diffusion of nickel and iron in this location. The nickel and iron in this region appeared to be unassociated with sulphur and suggested the formation of an oxide.

In summary, the metallographic and microprobe examinations have shown that hot corrosion of all alloys occurred during 800°C stress-rupture testing. Incoloy 800H was attacked the most while for the iron base alloys the degree of attack appeared to be related to the amount of deformation which occurred i.e. stainless alloy 310 was attacked more than either HK40 or 347H. However, the stress-rupture data showed that hot corrosion due to the combined use of the simulated deposit and the synthetic combustion gas had little effect on the stress-rupture properties of the alloys when compared to Phase 1 results.

3.3 Stress-Rupture Data for 900°C Tests

3.3.1 Stainless Alloy 310

As shown in Table 7, six stress-rupture tests were conducted to complete the time to rupture requirement. This was done because of the anomalous result obtained when using a stress of 21.0 MPa. The retest was carried out using 20.9 MPa and resulted in a life of 901 h; this was much closer to the expected 1000 h life predicted from the shorter term tests.

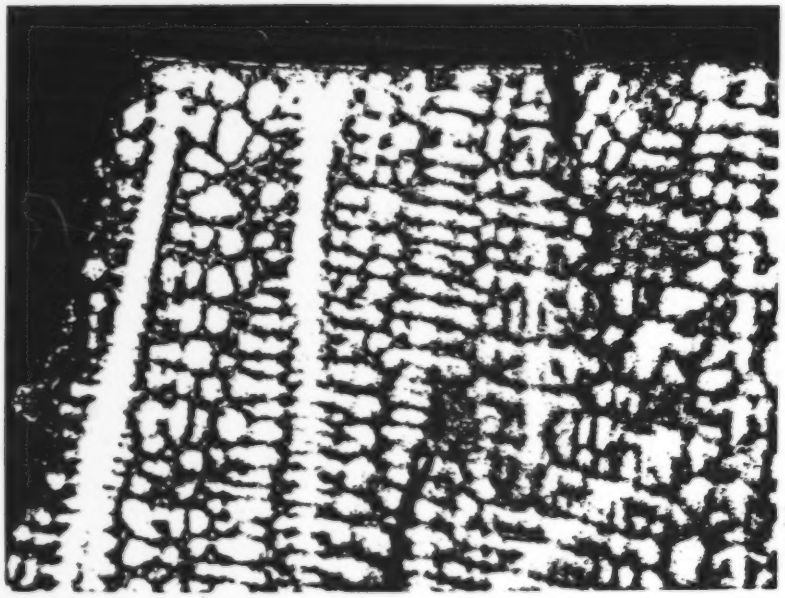

X100

Figure 20 Anomalous "Coating" on HK40 After 800°C Test in Contact with Simulated Deposit Using 108.3 MPa for 51.8 h

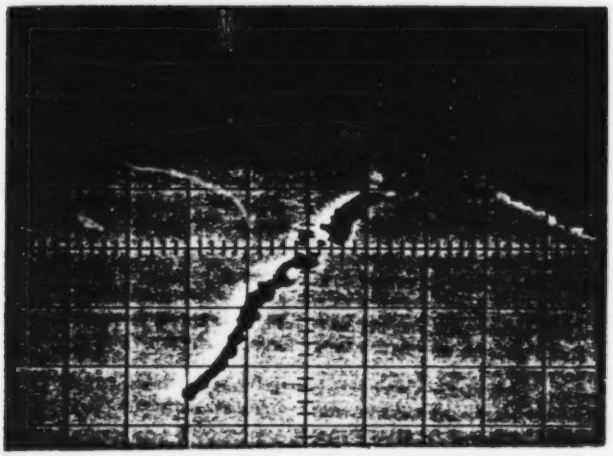

(a) Absorbed Electron Image

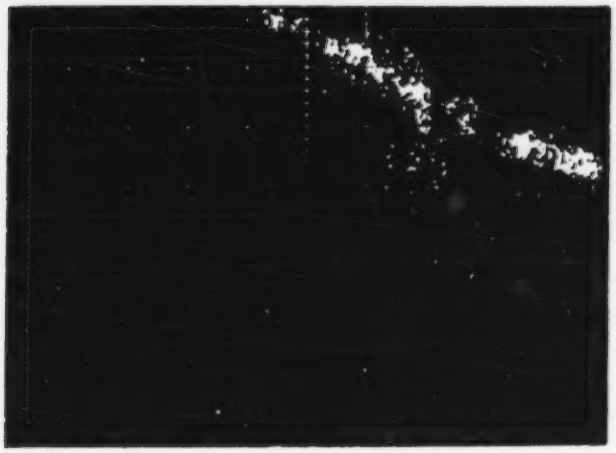

(b) Sulphur X-Ray Image

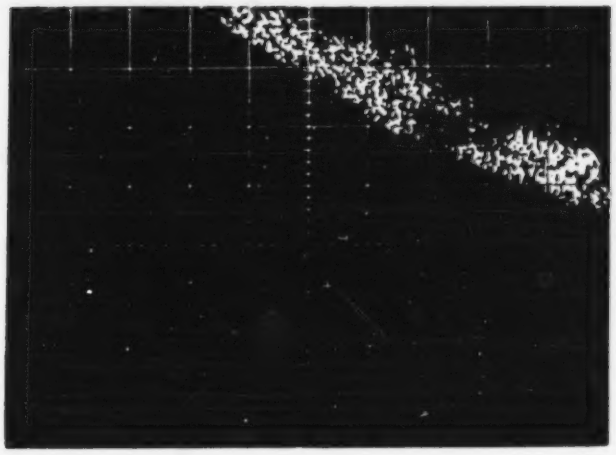

(c) Calcium X-Ray Image

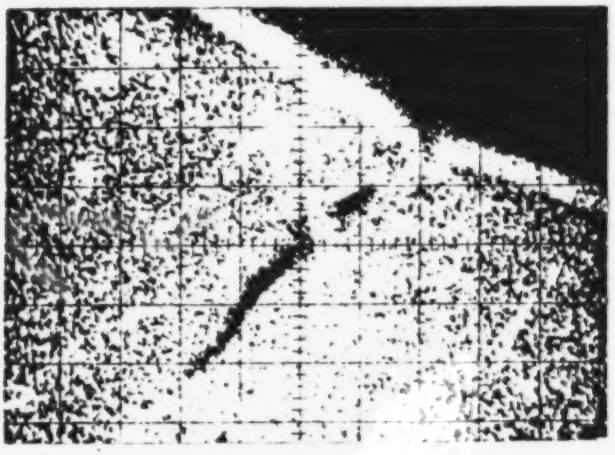

(d) Chromium X-Ray Image

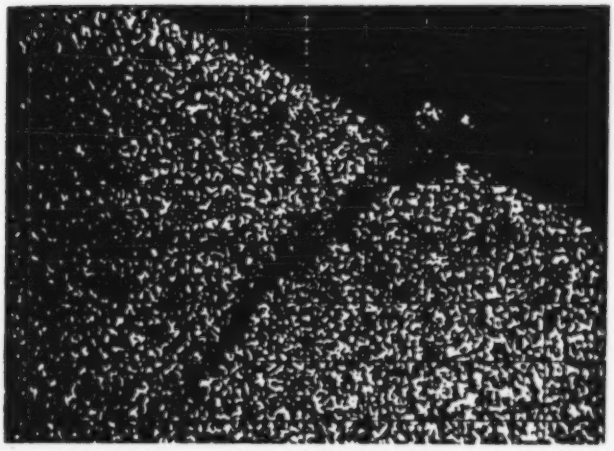

(e) Nickel X-Ray Image

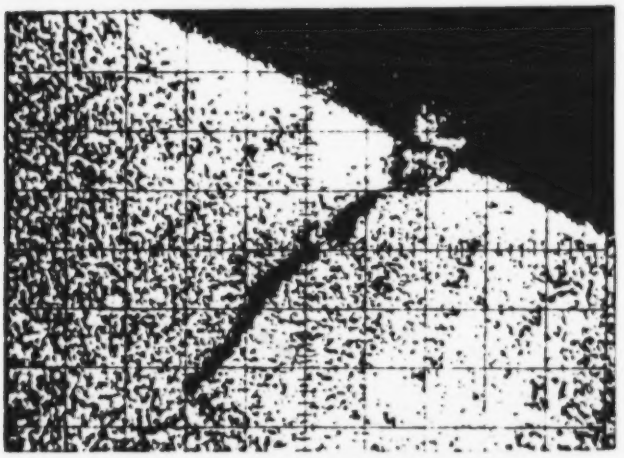

(f) Iron X-Ray Image

Figure 21 Electron Microprobe Analyses of HK40 After 800°C Test in Contact with Simulated Deposit Using 56.9 MPa for 424 h
X400

Table 7 Stress-Rupture Data for Stainless Alloy 310 Tested at 900°C in Synthetic Combustion Gas (2.0% SO_2)

Stress (MPa)	Time to Rupture (h)	Elongation (%)
54.0	11.6	37
39.3	50.7	28
34.3	69.4	28
27.8	293.2	25
21.0	264.6	30
20.9	901.0	23

It was interesting to note that the elongation obtained for the retest fitted the trend of decreasing elongation with decreasing stress. Although the elongation for the anomalous test was much greater than expected, metallographic examination failed to provide an unequivocal explanation for the early failure. Massive sulphidation was observed in and near the fracture but both longer and shorter term tests were characterized in a similar manner. It was possible that a grain size variation existed but, as shown in Figure 22, little difference in the grain sizes of the two ruptured specimens was observed.

In Figure 23, the present 900°C stress-rupture data for 310 are compared to the results obtained in Phase 1. The comparison indicates a near parallel shift of the stress-rupture curve to longer rupture lives for the alloy when tested using the high SO_2 synthetic combustion gas.

3.3.2 Cast Alloy HK40

The stress-rupture data for HK40 are shown in Table 8 and compared to Phase 1 results in Figure 24. As shown in Table 8, duplicate tests using 44 MPa were done. The initial test was conducted using one 310 and one 713C clevis to support the specimen in the hot zone. After the unexpected short rupture life of 120 h, inspection of the specimen indicated that rupture had occurred outside the gauge marks and near the filet end which was supported by the 713C clevis. Although the specimen gauge length and opposite end showed little hot corrosion, massive corrosion had occurred where the HK40 had contacted the 713C clevis. It appeared that the 713C (high Ni alloy) had reacted vigorously with the synthetic combustion gas to form a low melting point sulphide which in turn reacted with the HK40. Retesting using the same stress level but employing two 310 clevises yielded a rupture life of ~260 h which was much closer to the initial targeted life of 300 h. Stainless alloy 310 clevises were used for all subsequent tests.

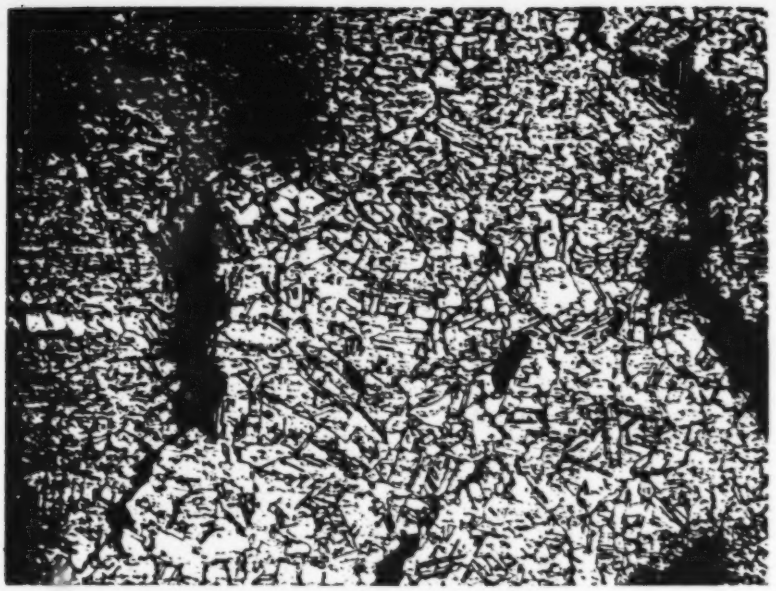

(a) Rupture Life 901 h

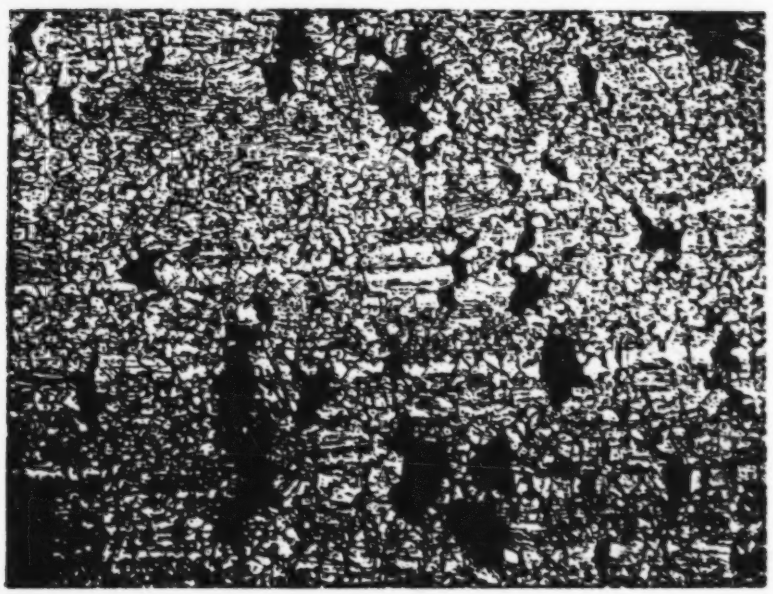

(b) Rupture Life 265 h

Figure 22 Comparative Microstructures of Ruptured 310 Samples After 900°C Tests Using ~21 MPa
X100

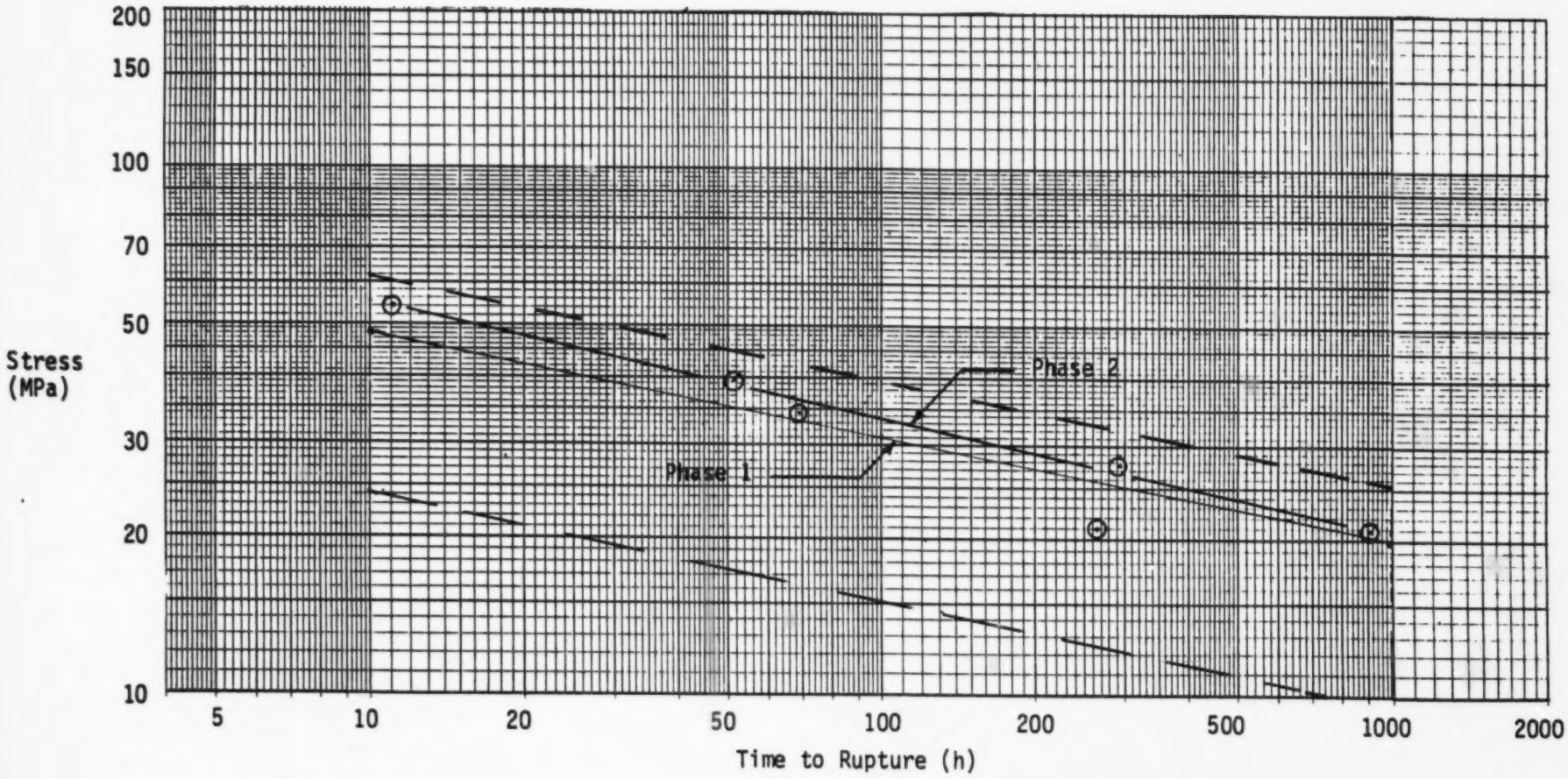

Figure 23 Stress-Rupture Tests for Stainless Alloy 310 at 900°C in Synthetic Combustion Gas

Based on the first four tests in Table 8 it was expected that use of 33.5 MPa would cause rupture in ~1000 h. The actual life of 482.5 h at this stress suggested a possible discontinuity in the rupture curve and therefore an additional test was done using a stress of 30.5 MPa. The life to rupture was 835.6 h indicating a slightly shorter life compared to Phase 1 data.

Table 8 Stress-Rupture Data for Cast Alloy HK40 Tested at 900°C in Synthetic Combustion Gas (2.0% SO_2)

Stress (MPa)	Time to Rupture (h)	Elongation (%)
82.7	13.5	6
63.6	57.7	6
54.0	95.9	3
44.0	259.5	5
(44.0)	(120.3)	Not Measured*
33.5	482.5	3
30.5	835.6	6

* Apparent reaction of SO_2 with Inconel 713C clevis caused premature rupture

3.3.3 Incoloy 800H

Incoloy 800H was again characterized by heavy corrosion during the 900°C tests. When the stress-rupture data in Table 9 are compared to Phase 1 data as shown in Figure 25 however, it is apparent that there is little difference for the short term tests and that lives are actually somewhat longer at lower stresses.

Table 9 Stress-Rupture Data for Incoloy 800H Tested at 900°C in Synthetic Combustion Gas (2.0% SO_2)

Stress (MPa)	Time to Rupture (h)	Elongation (%)
52.0	14.2	43
40.0	31.3	14
35.9	93.3	13
27.6	575.0	19
23.0	1219.5	20

3.3.4 Stainless Alloy 347H

Analogous to the 800°C Phase 2 data, the stress-rupture results for 347H tested at 900°C show no anomalies (Table 10) and compare very well with Phase 1 data as shown in Figure 26.

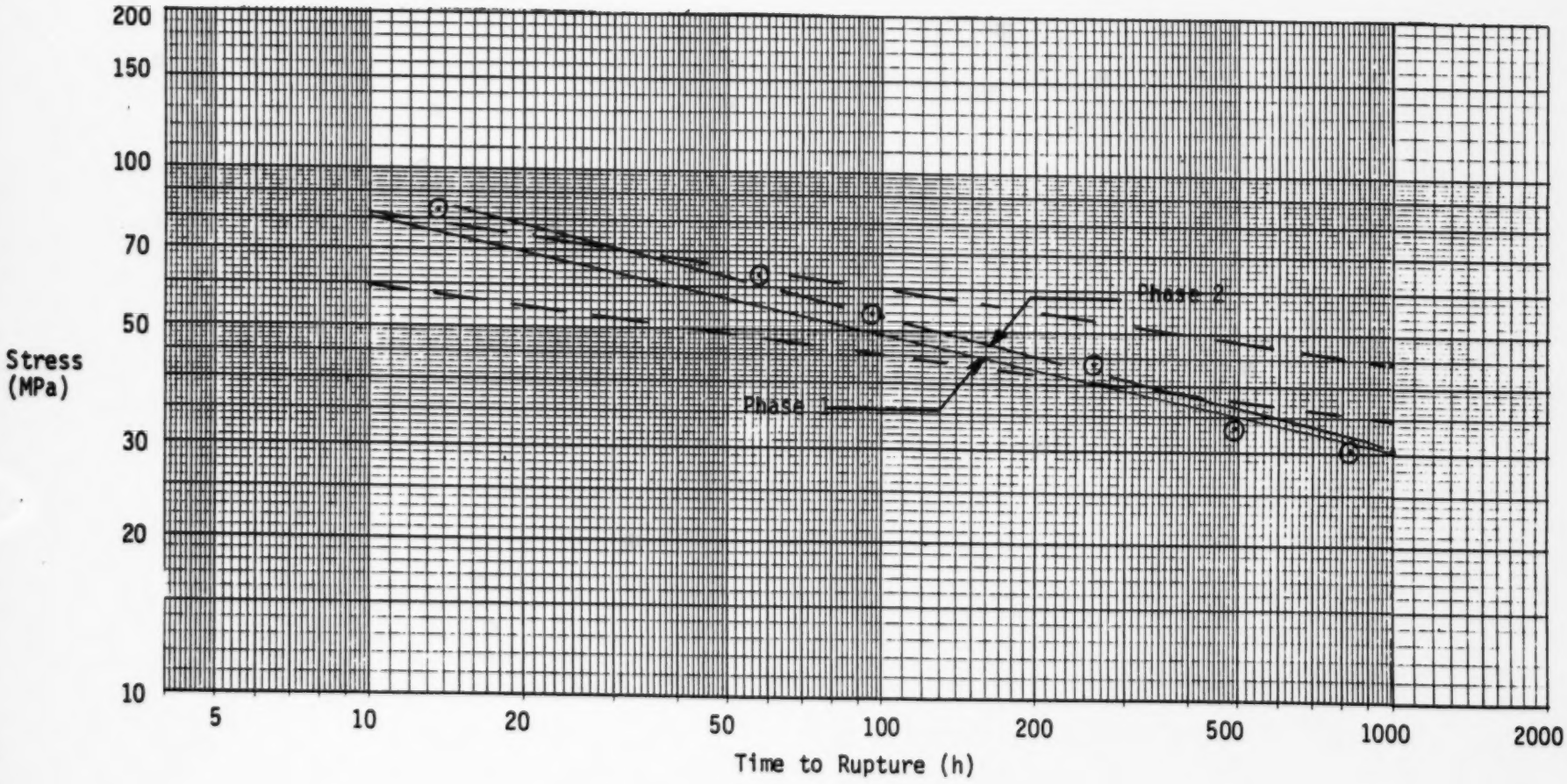

Figure 24 Stress-Rupture Tests for Cast Alloy HK40 at 900°C in Synthetic Combustion Gas

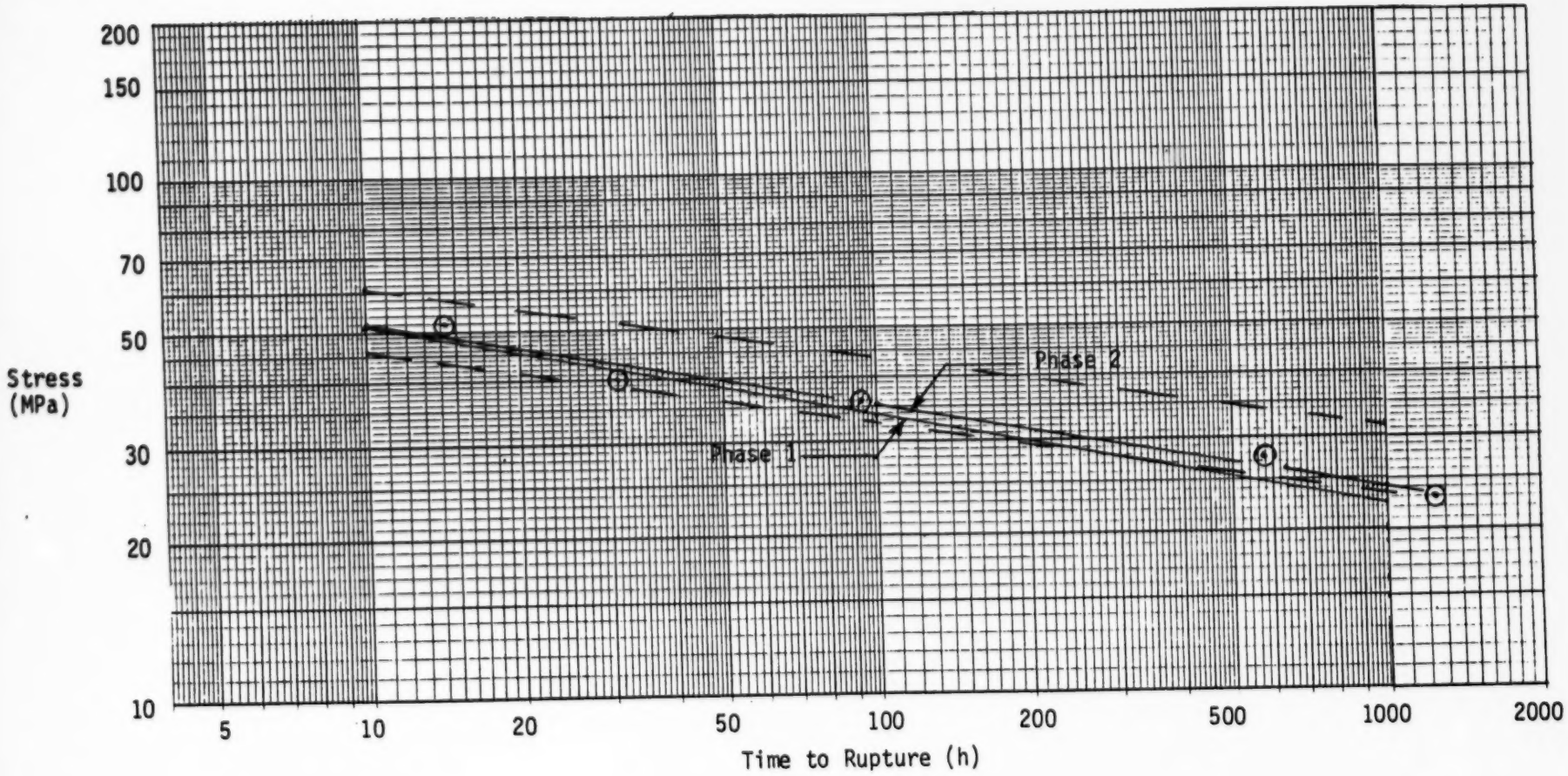

Figure 25 Stress-Rupture Tests for Incoloy 800H at 900°C in Synthetic Combustion Gas

Table 10 Stress-Rupture Data for Stainless Alloy 347H Tested at 900°C in Synthetic Combustion Gas (2.0% SO_2)

Stress (MPa)	Time to Rupture (h)	Elongation (%)
48.0	10.8	21
35.2	34.5	95
26.2	89.2	73
18.6	260.0	82
12.6	1181.1	98

3.4 Metallographic and Microprobe Examination of 900°C Ruptured Specimens

The appearance of the stress-rupture specimens after testing at 900°C in the high SO_2 gas are shown in Figures 27 and 28. The photographs indicate that 800H was attacked the most while HK40 and 347H appear to be the least affected. The difference in degree of attack after ~1200 h tests for 800H and 347H is illustrated in Figure 29 and shows the typical heavy corrosion of the former contrasted with the very limited attack of the latter. Hot corrosion was also observed in the iron base alloys after testing for short times using higher stress levels. Typical examples of the corrosion exhibited in specimens tested for ~10 h are shown in Figure 30.

Microprobe evaluation of selected specimens showed some interesting results. For example, Figure 31 shows the element distribution in an area of the matrix of 800H. This area was located slightly below the heavily corroded surface of the sample which failed after ~1200 h. The X-ray maps showed chromium concentrated at the grain boundaries while sulphur was conspicuous by its absence in the area. Note that the small black triangular feature in the absorbed electron image was found to contain only titanium and was presumably present as a carbide. Figure 32 shows a portion of the corroded surface above the area shown in Figure 31. The X-ray maps relative to this area showed that chromium was severely depleted within the grains but concentrated at what appeared to be grain boundaries and in the corrosion layer. Sulphur showed high concentrations in areas where a portion of the chromium was also concentrated while nickel and iron were primarily associated with one another immediately below the corrosion layer. These two Figures illustrate the manner in which chromium moves to the alloy surface in an attempt to combat hot corrosion.

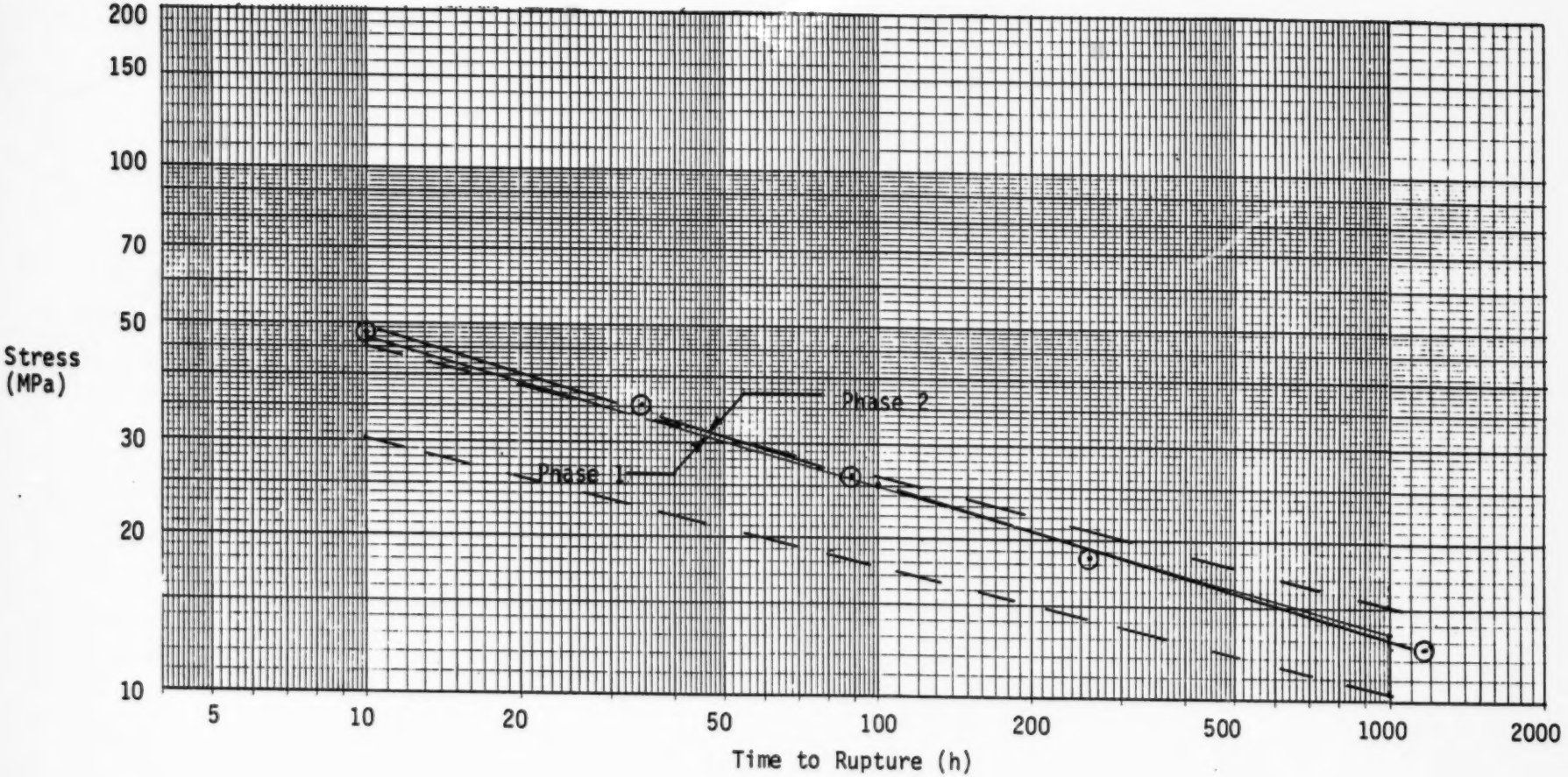

Figure 26 Stress-Rupture Tests for Stainless Alloy 347H at 900°C in Synthetic Combustion Gas

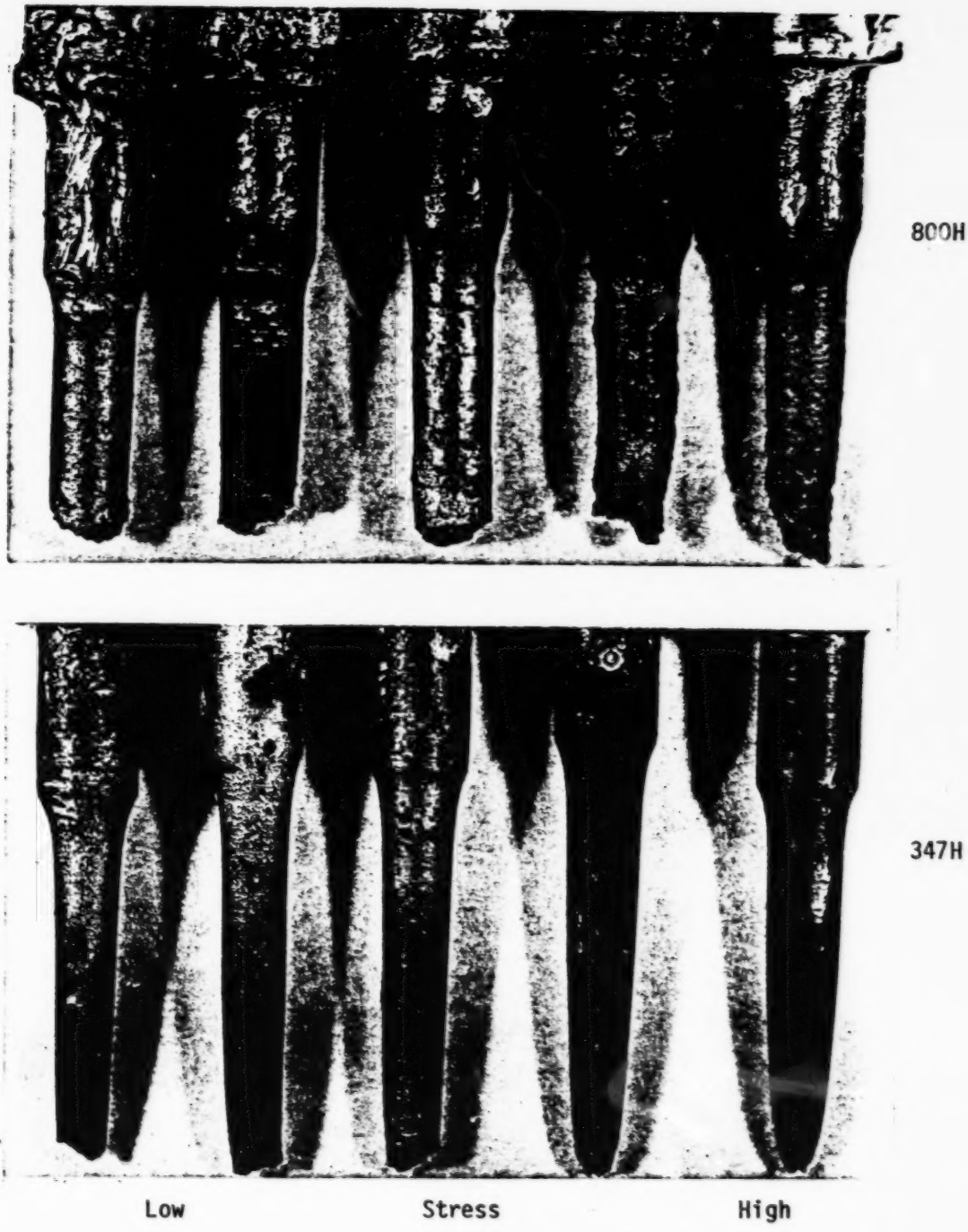

Figure 27 Appearance of Ruptured Specimens of 800H and 347H After 900°C Tests in Synthetic Combustion Gas (2.0% SO_2)

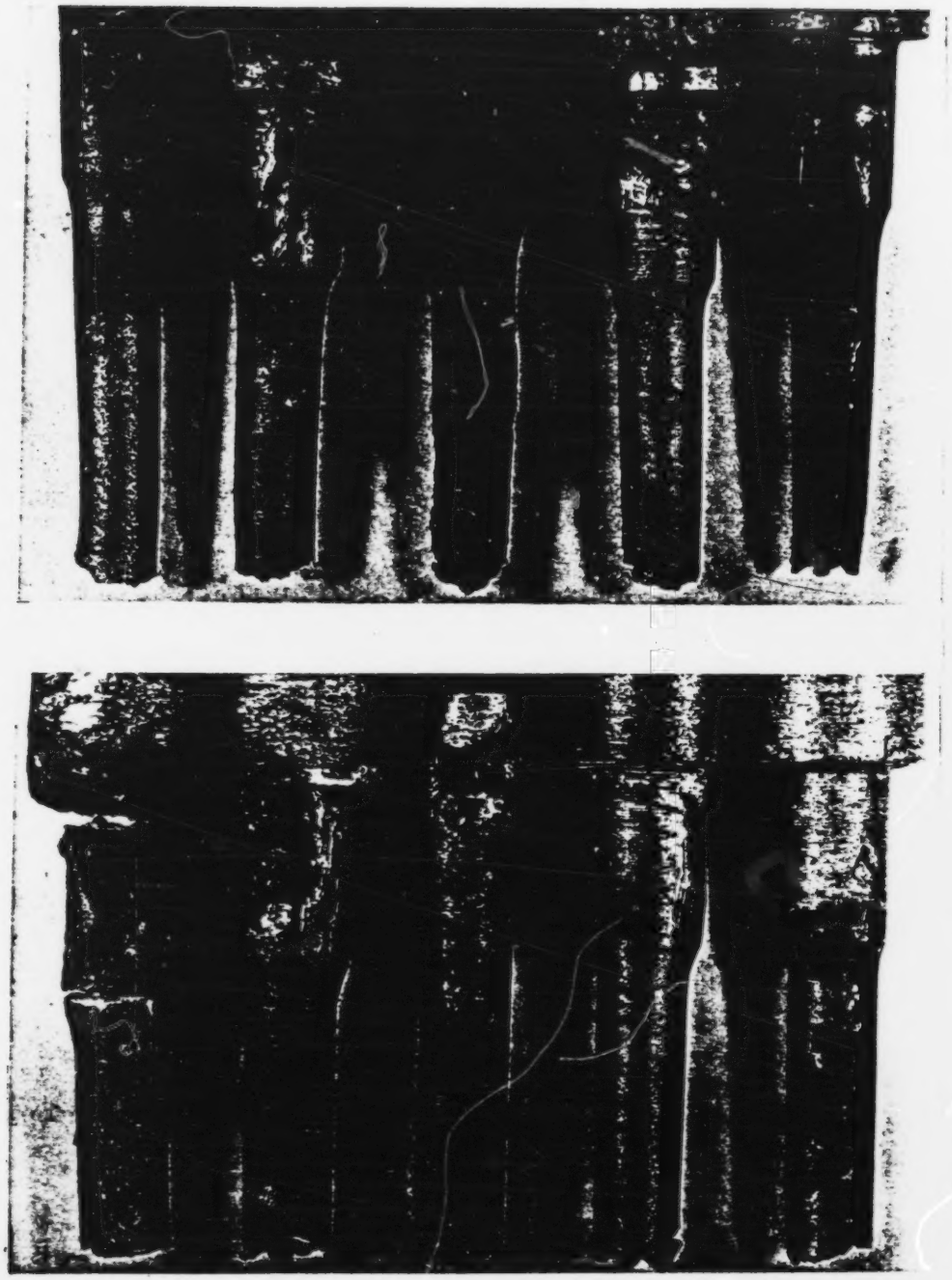

Figure 28 Appearance of Ruptured Specimens of 310 and HK40 After 900°C Tests in Synthetic Combustion Gas (2.0% SO_2)

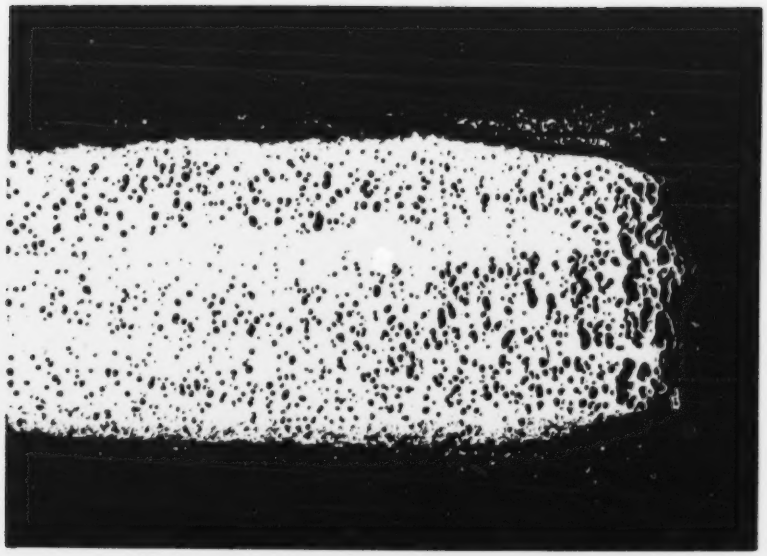

(a) Incoloy 800H

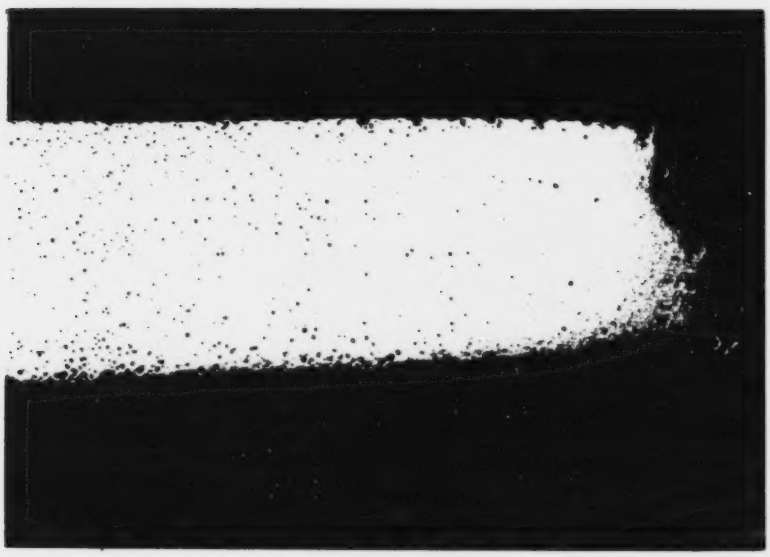

(b) Alloy 347H

Figure 29 Comparative Corrosive Attack of 800H and 347H After 900°C Tests for ~1200 h in Synthetic Combustion Gas (2.0% SO_2) X10

HK40
Rupture Life
13 h at 83 MPa

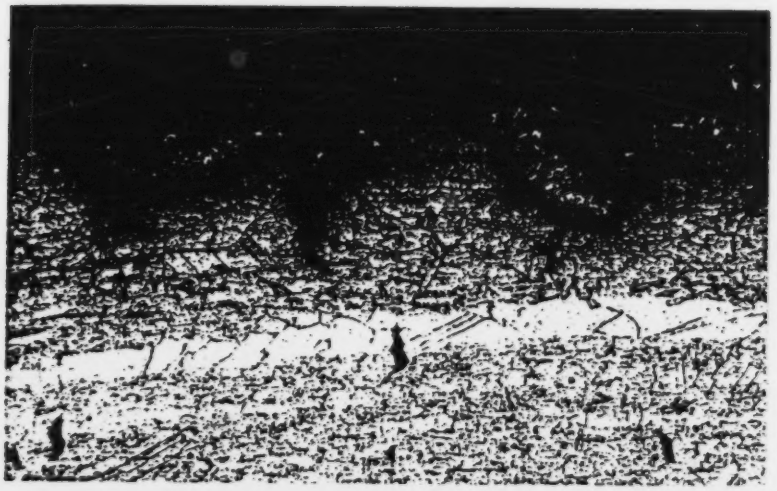

310
Rupture Life
12 h at 54 MPa

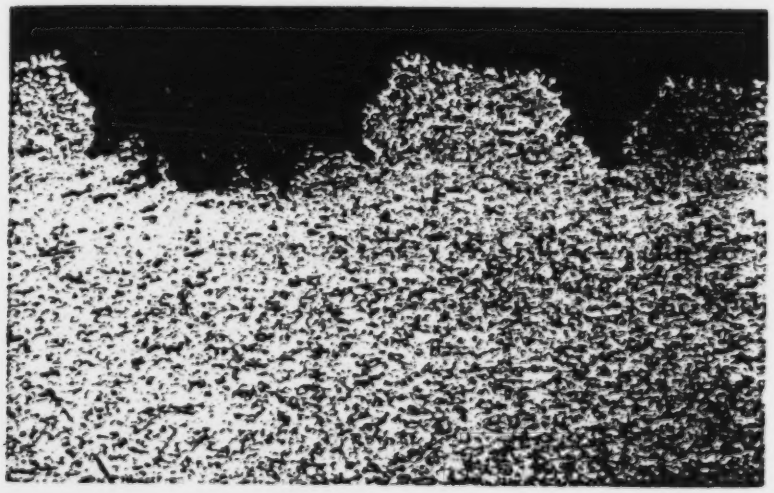

347H
Rupture Life
11 h at 48 MPa

Figure 30 Hot Corrosion Observed in HK40, 310 and 347H After 900°C Tests for ~10 h in Synthetic Combustion Gas (2.0% SO_2)
X100

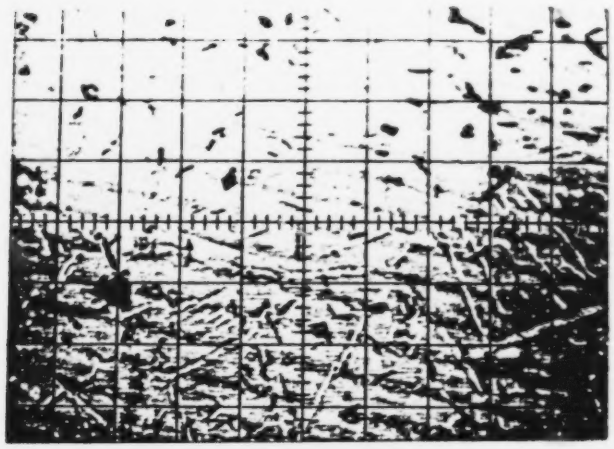

(a) Absorbed Electron Image

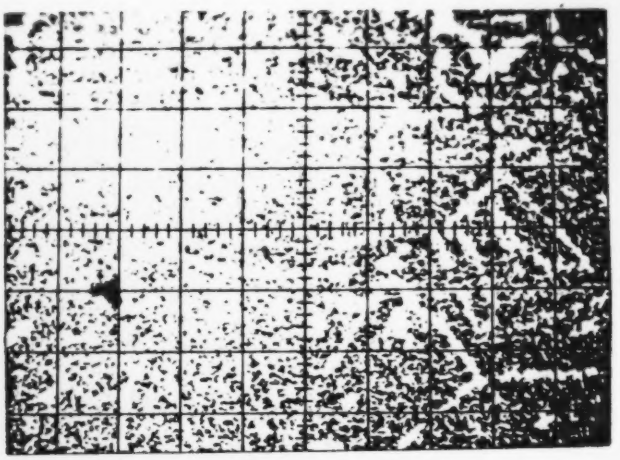

(b) Chromium X-Ray Image

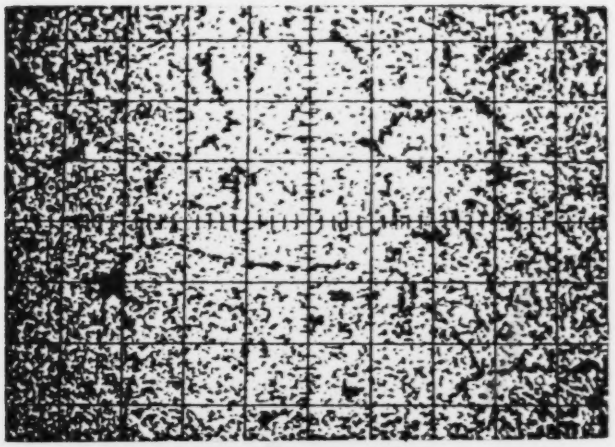

(c) Nickel X-Ray Image

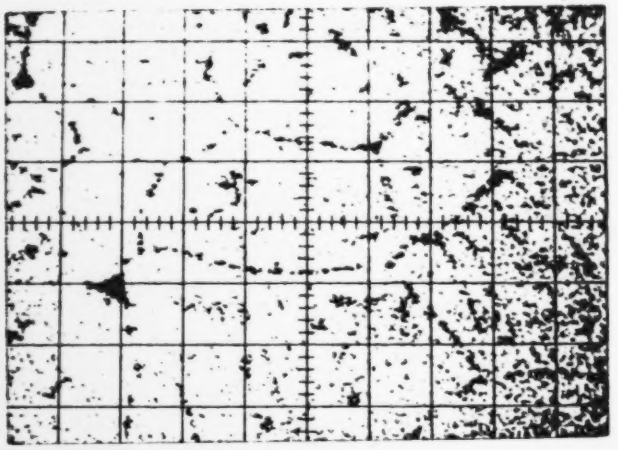

(d) Iron X-Ray Image

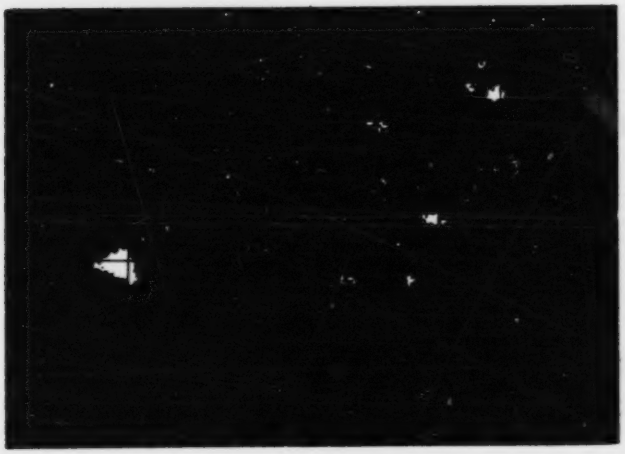

(e) Titanium X-Ray Image

(f) Sulphur X-Ray Image

Figure 31 Microprobe Analyses of Underlaying Matrix of 800H After 900°C Test for ~1200 h in Synthetic Combustion Gas (2.0% SO_2) X400

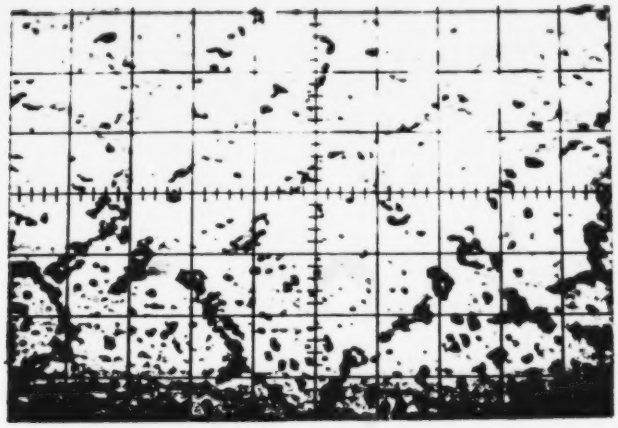

(a) Absorbed Electron Image

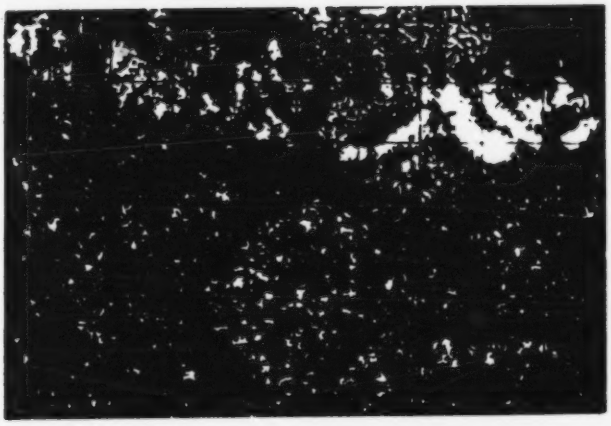

(b) Sulphur X-Ray Image

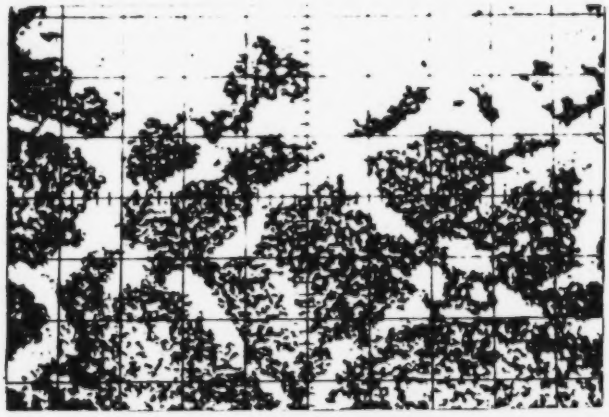

(c) Chromium X-Ray Image

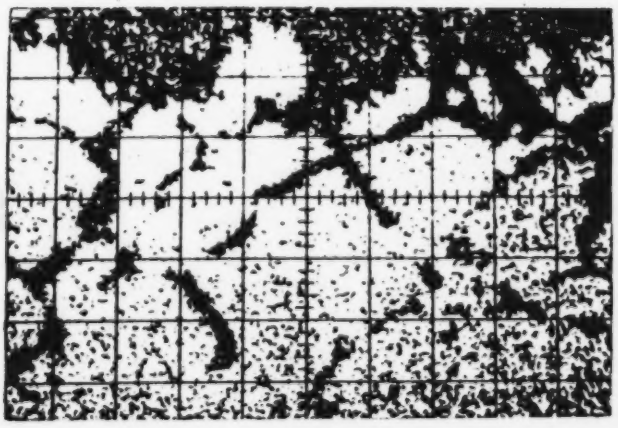

(d) Nickel X-Ray Image

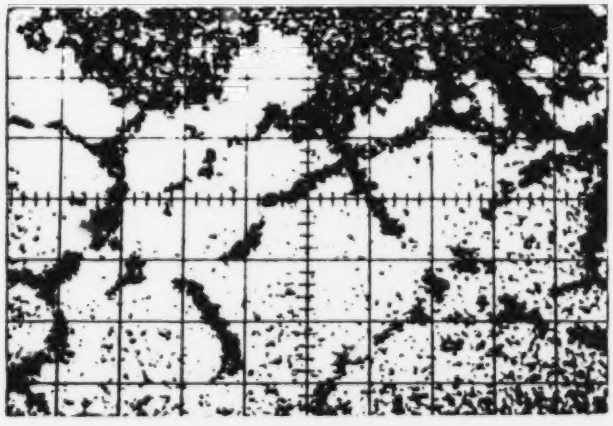

(e) Iron X-Ray Image

Figure 32 Microprobe Analyses of Corrosion Layer on 800H After 900°C Test for ~1200 h in Synthetic Combustion Gas (2.0% SO_2)
X400

In conclusion, although the metallographic and microprobe evaluations showed that some of the 900°C test specimens exhibited massive corrosive attack during stress-rupture testing, when compared to Phase 1 results, the corrosion induced by the high SO_2 concentration in the combustion gas did not appear to adversely affect the stress-rupture properties of the alloys.

sherritt

Sherritt Gordon Mines Limited
Fort Saskatchewan, Alberta, Canada T8L 2P2 / Telephone 403 - 998 - 6911 / Telex 037 - 2290

Sherritt Research Centre

EVALUATION OF STRESS-RUPTURE PROPERTIES OF STAINLESS ALLOYS IN FLUIDIZED BED COMBUSTION ENVIRONMENTS INTERIM REPORT FOR PHASE 3 PARTS 1 and 2

For the Period
April 1, 1984 to June 1, 1985

K.G. Reid
M.J.H. Ruscoe

33pp

MICROMEDIA

sherritt

Evaluation of Stress-Rupture Properties of Stainless Alloys in Fluidized Bed Combustion Environments

Phase 3, Parts 1 and 2

by

Sherritt Research Centre
Sherritt Gordon Mines Limited
Fort Saskatchewan, Alberta
K.G. Reid, M.J.H. Ruscoe

Work on this project was conducted under the auspices of the Canada Centre for Mineral and Energy Technology, Energy, Mines and Resources, Canada

DSS FILE NUMBER	:	03SQ.23440-2-9053
DSS CONTRACT SERIAL NUMBER	:	0SQ82-00148
CANMET PROJECT NUMBER	:	430902
CANMET SCIENTIFIC AUTHORITY	:	Dr. D.C. Briggs

DATE: April 1, 1984 to June 1, 1985

This report should be cited as Contract Report No: 0SQ82-00148

AUG 15 1988
MICROMEDIA

This work was performed for the Physical Metallurgy Research Laboratories of CANMET, Energy, Mines and Resources, Canada on Supply and Services Contract OSQ82-00148. The authors acknowledge the support received from Dr. David Briggs of PMRL in the scientific administration of the contract.

Any data presented, opinions, findings, conclusions or recommendations expressed in this report are those of the contractor and do not necessarily reflect the views of CANMET.

TABLE OF CONTENTS

		Page No
	SUMMARY	1
1.0	INTRODUCTION	2
2.0	EXPERIMENTAL	3
2.1	Materials	3
2.1.1	Alloys	3
2.1.2	Synthetic Combustion Gas	3
2.2	Apparatus and Procedure	3
3.0	RESULTS AND DISCUSSION	7

LIST OF TABLES

		Page No
Table 1	Chemical Analyses of Test Alloys	4
Table 2	Physical Properties of Test Alloys	5
Table 3	Stress-Rupture Data for Stainless Alloy 310 Tested at 900°C in Synthetic Combustion Gas and Simulated Fluidized Bed Deposit	8
Table 4	Stress-Rupture Data for Cast Alloy HK40 Tested at 900°C in Synthetic Combustion Gas and Simulated Fluidized Bed Deposit	8
Table 5	Stress-Rupture Data for Incoloy 800H Tested at 900°C in Synthetic Combustion Gas and Simulated Fluidized Bed Deposit	9
Table 6	Stress-Rupture Data for Stainless Alloy 347H Tested at 900°C in Synthetic Combustion Gas and Simulated Fluidized Bed Deposit	9
Table 7	Stress-Rupture Data for Incoloy 800H Tested at 800°C in Synthetic Combustion Gas and Simulated Fluidized Bed Deposit	14
Table 8	Stress-Rupture Data for Cast Alloy HK40 Tested at 800°C in Synthetic Combustion Gas and Simulated Fluidized Bed Deposit	14

LIST OF FIGURES

		Page No
Figure 1	Stress-Rupture Tests for Stainless Alloy 310 at 900°C in Synthetic Combustion Gas	10
Figure 2	Stress-Rupture Tests for Cast Alloy HK40 at 900°C in Synthetic Combustion Gas	11
Figure 3	Stress-Rupture Tests for Incoloy 800H at 900°C in Synthetic Combustion Gas	12
Figure 4	Stress-Rupture Tests for Stainless Alloy 347H at 900°C in Synthetic Combustion Gas	13
Figure 5	Stress-Rupture Tests for Incoloy 800H at 800°C in Synthetic Combustion Gas	15
Figure 6	Stress-Rupture Tests for Cast Alloy HK40 at 800°C in Synthetic Combustion Gas	16
Figure 7	Appearance of Ruptured 310 and HK40 Specimens After 900°C Tests in Synthetic Combustion Gas and Simulated Deposit	17
Figure 8	Appearance of Ruptured 800H and 347H Specimens After 900°C Tests in Snnthetic Combustion Gas and Simulated Deposit	18
Figure 9	Appearance of Ruptured HK40 and 800H Specimens After 800°C Tests in Synthetic Combustion Gas and Simulated Deposit	19
Figure 10	Sulphidation Observed in 310 Specimens After Life to Rupture of 5.6 and 822.4 h at 900°C	20
Figure 11	Effect of Hot Corrosion on 347H and HK40 After Targeted 1000 h Tests at 900°C	21
Figure 12	Microprobe Analyses of 800H After 93.8 h Life at 900°C	23
Figure 13	Microprobe Analyses of 310 After 247 h Life at 900°C	24
Figure 14	Effect of Hot Corrosion on 310 Furnace Retort Liner After Fourteen Repetitive Tests Totalling 2000 h at 900°C in Synthetic Combustion Gas	25
Figure 15	Microprobe Analyses of 310 Furnace Retort Liner	27

SUMMARY

Phase 3, Parts 1 and 2 of the contract were successfully completed according to the statement of work.

Stress-Rupture tests were carried out on two alloys at 800°C and four alloys at 900°C in a synthetic coal combustor atmosphere. The alloys tested at 900°C were stainless 310 and 347H, cast alloy HK40 and Incoloy 800H. These alloys were tested in contact with a simulated combustor deposit and in a synthetic combustion gas which contained 2% SO_2.

For the 800°C tests, cast alloy HK40 and Incoloy 800H were tested in contact with the simulated combustor deposit but the synthetic combustion gas atmosphere contained 0.2% (2000 ppm) SO_2.

Results showed in general that specimen contact with the simulated combustor deposit had little effect on the rupture lives of the alloys compared to the rupture lives when tested without the deposit. As in Phase 1 and 2, Incoloy 800H was the least suited for use in the simulated combustor environment while HK40 and 347H were the least affected.

1.0 INTRODUCTION

This progress report covers the work conducted during the period April 1, 1984 to June 1, 1985 under revised Phase 3, Parts 1 and 2. In the previous reports for Phase 1, stress-rupture data were presented which compared the stress-rupture properties of the four test alloys when tested at 800 and 900°C in 2000 ppm SO_2 synthetic combustion gas to the properties when tested in air. The Phase 1 data for the 900°C tests showed little difference compared to the expected results when testing the alloys in air. Results for the 800°C Phase 1 tests indicated slightly shorter lives at lower stress levels than comparable tests in air. These findings were attributed to the synthetic combustion gas having an oxidizing potential at 900°C and a sulphidizing potential at 800°C. During Phase 2, stress-rupture data were obtained for the four alloys when tested in contact with a simulated combustor deposit and in the 2000 ppm SO_2 combustion gas. Results for these tests showed that the rupture lives were similar to those of Phase 1. Testing the alloys at 900°C during Phase 2 in 2.0% SO_2 synthetic combustion gas also showed similar rupture lives when compared to results obtained when testing in 2000 ppm SO_2 gas and in air.

The objective for Phase 3, Part 1 was to determine the effect of the 2% SO_2 combustion gas, together with the simulated deposit, on the stress-rupture lives of the alloys when tested at 900°C. Part 2 of Phase 3 was undertaken to augment the data for the 800°C tests of Phase 2, Part 1.

2.0 EXPERIMENTAL

2.1 Materials

2.1.1 Alloys

The alloys used for the stress-rupture tests at 800 and 900°C were from the same heats as those used in Phase 1 and 2. The chemical and room temperature physical properties of the alloys are shown in Tables 1 and 2, respectively. Specimen preparation techniques conformed to the ASTM E8-81 designation, sections 6.1 and 6.4.

2.1.2 Synthetic Combustion Gas

The synthetic combustion gas for Phase 3 was purchased from Matheson of Canada. For the 800°C tests the nominal gas composition was the same as used for Phase 1 and 2, namely 200 ppm CO, 2000 ppm SO_2, 20% CO_2, $\leq$10 ppm O_2, and balance N_2. The gas composition contained in each cylinder was certified by Matheson to be within the preparation tolerance.

Synthetic combustion gas for the 900°C tests had a nominal composition of 540 ppm CO, 2.0% SO_2, 18% CO_2, $\leq$30 ppm O_2 and balance N_2. A certificate of analysis was provided for the gas contained in each cylinder.

2.2 Apparatus and Procedure

Stress-rupture evaluations for Phase 3 were carried out using the apparatus as described in the Phase 1 and 2 interim reports. As pointed out in the Phase 2 report, although the useful life of the stainless 310 clevises and pull rods showed improvement over 713C, (a nickel base alloy), considerable corrosive attack was evident after repeated use. Diffusion coating of aluminum appeared to retard hot corrosion in static tests but the coating was not satisfactory in protecting against hot corrosion under conditions of stress-rupture testing. The problem appeared to be exacerbated by temperature fluctuations encountered during heating and cooling. Hot corrosion of the 310 liner, pull rods and clevises was characterized by whiskers growing from each. During Phase 3, Part 1 testing, companion 1000 h tests on HK40 and 347H were terminated after sustained stress for approximately 1500 h failed to result in specimen rupture. Inspection of both stress-rupture units showed that products of hot corrosion had formed between the clevises

Table 1 Chemical Analyses of Test Alloys

	Analyses (%)											
	Incoloy 800H			310			HK40			347H		
	Min	Max	Actual	Min	Max	Actual	Min	Max	Actual	Min	Max	Actual
Al	0.15	0.6	0.31	n.s.	n.s.	-	n.s.	n.s.	-	n.s.	n.s.	-
C	0.05	0.10	0.08	-	0.15	0.12	0.35	0.45	0.45	0.04	0.10	0.07
Cb+Ta	n.s.	n.s.	-	n.s.	n.s.	-	n.s.	n.s.	-	8xC	1.0	0.90
Cr	19.0	23.0	20.17	24.0	26.0	24.37	23.0	27.0	24.81	17.0	19.0	18.2
Cu		0.75	0.61	n.s.	n.s.	-	n.s.	n.s.	-	n.s.	n.s.	-
Mn		1.50	0.94	-	2.00	1.69	-	1.50	0.73	-	2.00	1.83
Mo	n.s.	n.s.	-	n.s.	n.s.	-	-	0.50	0.052	n.s.	n.s.	-
Ni	30.0	35.0	32.9	19.0	22.0	19.01	19.0	22.0	20.69	9.0	13.0	10.77
P	n.s.	n.s.	-	-	0.040	0.031	-	0.040	0.019	-	0.040	0.030
S		0.015	0.001	-	0.030	0.006	-	0.040	0.012	-	0.030	0.007
Si		1.0	0.60	-	0.75	0.66	0.50	2.00	1.11	-	1.00	0.48
Fe	39.5	n.s.	43.95	n.s.	n.s.	-	n.s.	n.s.	-	n.s.	n.s.	-
Ti	0.15	0.60	0.45	n.s.	n.s.	-	n.s.	n.s.	-	n.s.	n.s.	-
ASTM:	B-408-77			A249-80			A608-79			A479-80a		
UNS:	N08810			S31000			J94224			S34709		
Supplier	Inco Alloys Canada Ltd			Specialty Steels			Fahramet			Atlas Alloys		
Heat No:	(4) HH0898A M1989			40477			75016			A11330		

n.s. Not specified

Table 2 Physical Properties of Test Alloys*

Alloy	Supplier	Heat No	Reference ASTM	Short Term Tensile			Hardness R_B	Grain Size ASTM
				YS(MPa)	UTS(MPa)	Elongation(%)		
310 Stainless	Specialty Steels	40477	A249-80	282(205)	642(515)	44(35)	80(90max)	8-9
347H	Atlas Alloys	A11330**	A479-80a	482(205)	662(515)	46(35)	99(n.s.)	9-10
HK40	Fahramet	75016	A608-79	n.s.***	n.s.			
800H	Inco Alloys Canada Ltd	HH0898A M1989	B408-77	179(170)	568(450)	56(30)	78(n.s.)	4.5

* Bracketed numbers represent minimum values, except as noted, from reference data

** Alloy heated to 1066°C min for sufficient time to dissolve carbides then quenched in water

*** As outlined in ASTM A608 Section 8 "tensile tests at room temperature are not recommended as acceptance criteria"

n.s. Not specified

and interior liner walls bonding the two together. Considerable force was required to fracture the bond. This problem was corrected by reducing the diameter of the 310 clevises. Additionally, both the pull rods and clevises were pack diffusion coated with chromium. The chromized supports appeared to offer improved protection against the hostile test environment, especially for the long term tests. However, repetitive usage for short term tests resulted in a break down of the coating leading to hot corrosion of the underlying alloy matrix. As a result the useful life of the specimen supports was shortened.

Synthetic combustion gas flow rates for the 800 and 900°C stress-rupture tests were the same as those used during Phase 1 and 2.

The initial stress levels chosen for each alloy were based on previous Phase 1 and 2 stress-rupture tests. As the number of Phase 3 tests progressed, the stress levels were based on previous data together with a least squares analysis of the Phase 3 test results.

The application of the simulated fluidized bed combustor deposit to the test specimen was conducted using the procedure described in the Phase 1 report. Briefly, a blend of six parts calcium sulphate and one part calcium oxide (both chemically pure substances) was loosely packed into an amorphous refractory silicon dioxide cloth (refrasil) bag which surrounded the specimen gauge length. Platinum-rhodium thermocouple wire was used to secure the bag to the test sample. In all cases the deposit containment bag was found to be intact upon completion of the stress-rupture test.

3.0 RESULTS AND DISCUSSION

Stress-rupture data for Phase 3, Part 1 900°C tests are tabulated in Tables 3 to 6. Least squares computer analyses of the data showed correlation coefficients of $\geq$0.94 for each alloy. These data are compared to previous Phase 1 and 2 test results in Figures 1 to 4 and as illustrated in the Figures, little difference is apparent. (The dashed lines in the Figures represent the minimum and maximum expected results for comparable tests conducted in air without the deposit.)

Stress-rupture data for the 800°C tests are shown in Tables 7 and 8. Targeted rupture lives for the tests conducted during Phase 3 were 300 and 1000 h for the 800H and HK40 specimens respectively. The actual rupture life of 788.8 h for 800H was unexpected and when added to previous Phase 2 data yielded a correlation coefficient of only 0.89. These data are compared to Phase 1 test results in Figures 5 and 6. For alloy 800H the comparison indicates that the simulated deposit in the synthetic combustion gas did not adversely affect the stress to rupture behavior of the alloy. In the case of HK40, the sharp discontinuity in the stress-rupture curve implied by the 56.8 MPa test was not supported by the longer term Phase 3 test. The anomalous former result may have been due to a casting defect in the alloy.

The appearance of the test specimens after stress-rupture testing is shown in the photographs of Figures 7, 8 and 9. (The 800H low stress specimen has an Araldite coating to maintain adherence of the corrosion products.) The relative degree of attack exhibited by the test specimens indicated that 800H was affected the most followed by 310, 347H and HK40. This pattern held for both the 800 and 900°C tests and was the same as that observed for Phase 1 and 2. Metallographic examination of the ruptured test pieces showed that sulphidation had occurred in all specimens. The observed sulphidation appeared to correlate with areas of the specimens that showed high deformation and with time of exposure in the gas atmosphere. Figure 10 for example shows the fracture and filet areas of 310 specimens which had rupture lives at 900°C of 5.6 and 822.4 h respectively. The corrosion deposit near the fracture of the 822.4 h specimen appeared heavier than on the fracture area of the 5.6 h specimen. In the filet area however both specimens showed the same amount of hot corrosive attack.

As indicated in Tables 4 and 6, elongations of the HK40 and 347H ruptured specimens differed markedly. Figure 11 shows the hot corrosion which occurred during targeted 1000 h tests at 900°C for each alloy. As illustrated in the Figure, attack was associated with areas of high deformation in each specimen.

Table 3 Stress-Rupture Data for Stainless Alloy 310 Tested at 900°C in Synthetic Combustion Gas and Simulated Fluidized Bed Deposit

Test Stress (MPa)	Time to Rupture (h)	Elongation (%)
55.0	5.6	52
34.3	121.1	27
27.6	247.0	28
22.7	244.8	25
18.8	822.4	36

Correlation coefficient: $r^2 = 0.94$

Table 4 Stress-Rupture Data for Cast Alloy HK40 Tested at 900°C in Synthetic Combustion Gas and Simulated Fluidized Bed Deposit

Test Stress (MPa)	Time to Rupture (h)	Elongation (%)
92.0	10.7	6
62.9	45.2	4
54.0	139.7	4
44.0	170.4	3
30.8	984.5	7
30.0	n.d.	n.d.*

Correlation coefficient: $r^2 = 0.98$

n.d.* Not determined, test discontinued after 1432.0 h because specimen supports and interior wall of furnace retort were bonded together by corrosion products

Table 5 Stress-Rupture Data for Incoloy 800H Tested at 900°C in Synthetic Combustion Gas and Simulated Fluidized Bed Deposit

Test Stress (MPa)	Time to Rupture (h)	Elongation (%)
52.0	12.9	32
40.5	51.2	25
36.0	93.8	13
30.0	403.7	10
24.8	650.2	20

Correlation coefficient: $r^2 = 0.98$

Table 6 Stress-Rupture Data for Stainless Alloy 347H Tested at 900°C in Synthetic Combustion Gas and Simulated Fluidized Bed Deposit

Test Stress (MPa)	Time to Rupture (h)	Elongation (%)
50.0	16.7	78
34.5	52.4	80
28.3	92.2	90
18.6	420.1	105
14.3	680.3	92
14.0	n.d.	n.d.*

Correlation coefficient: $r^2 = 0.99$

n.d.* Not determined, test discontinued after 1596.5 h because specimen supports and interior wall of furnace retort were bonded together by corrosion products

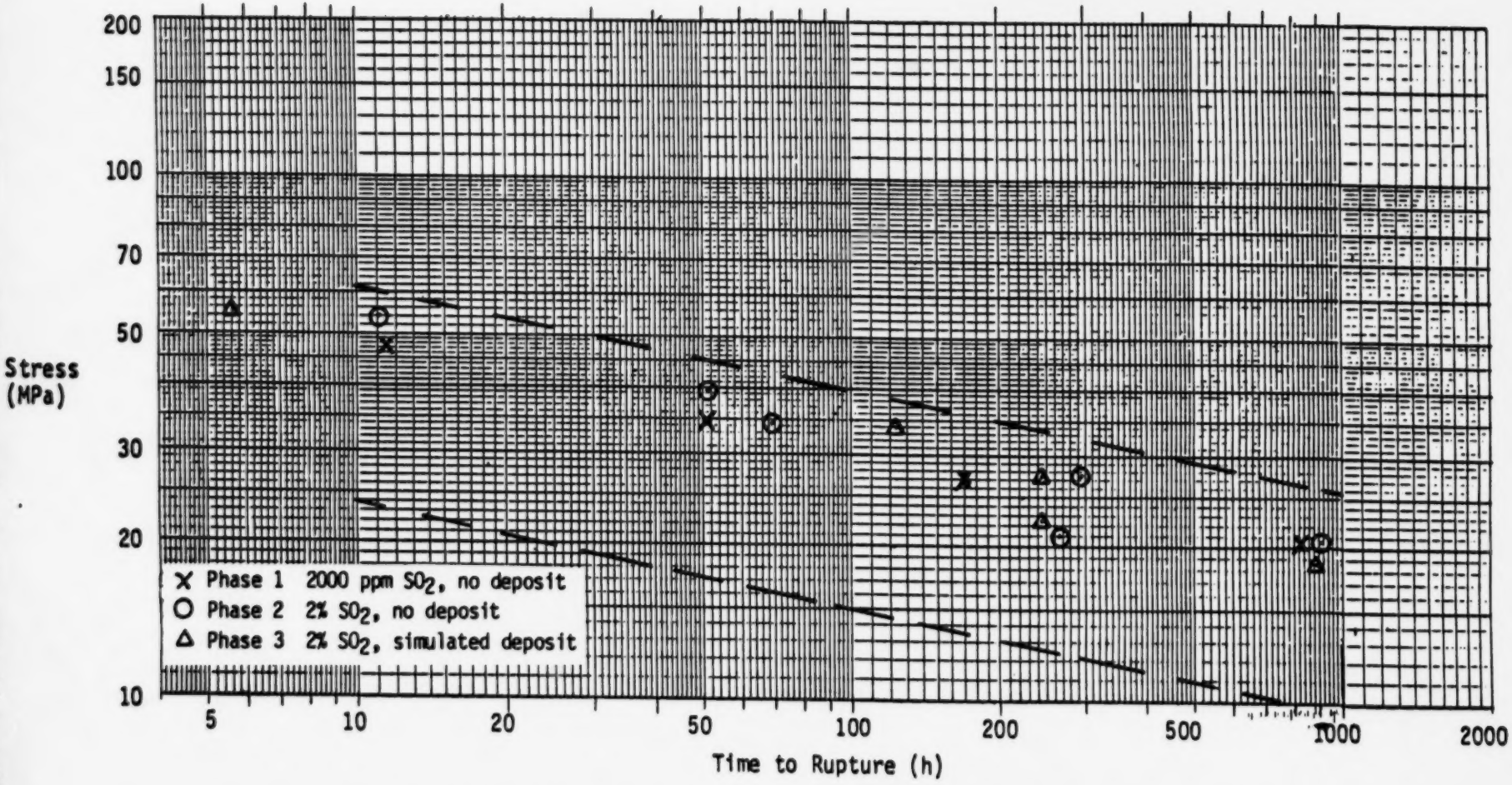

Figure 1 Stress-Rupture Tests for Stainless Alloy 310 at 900°C in Synthetic Combustion Gas

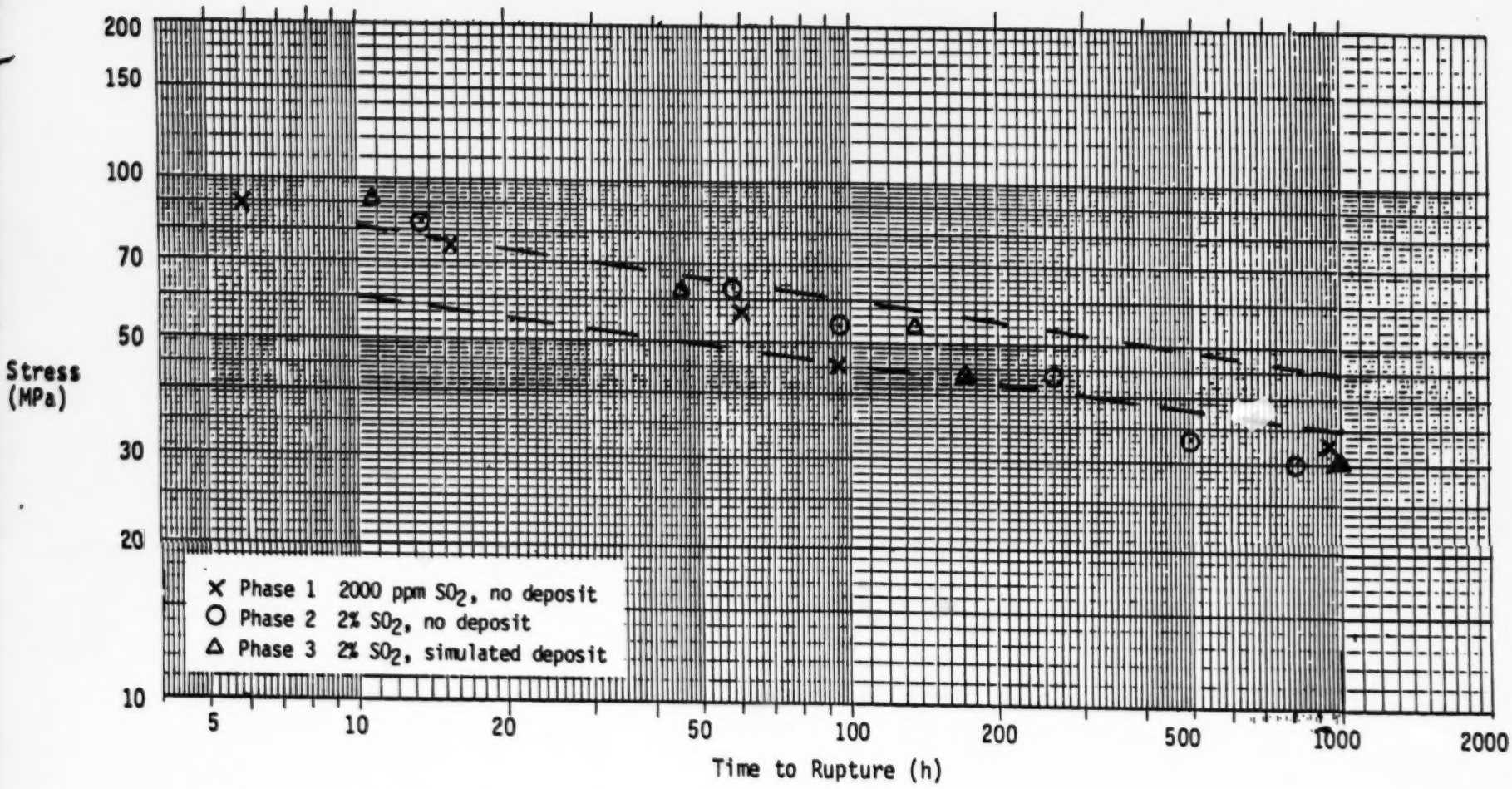

Figure 2 Stress-Rupture Tests for Cast Alloy HK40 at 900°C in Synthetic Combustion Gas

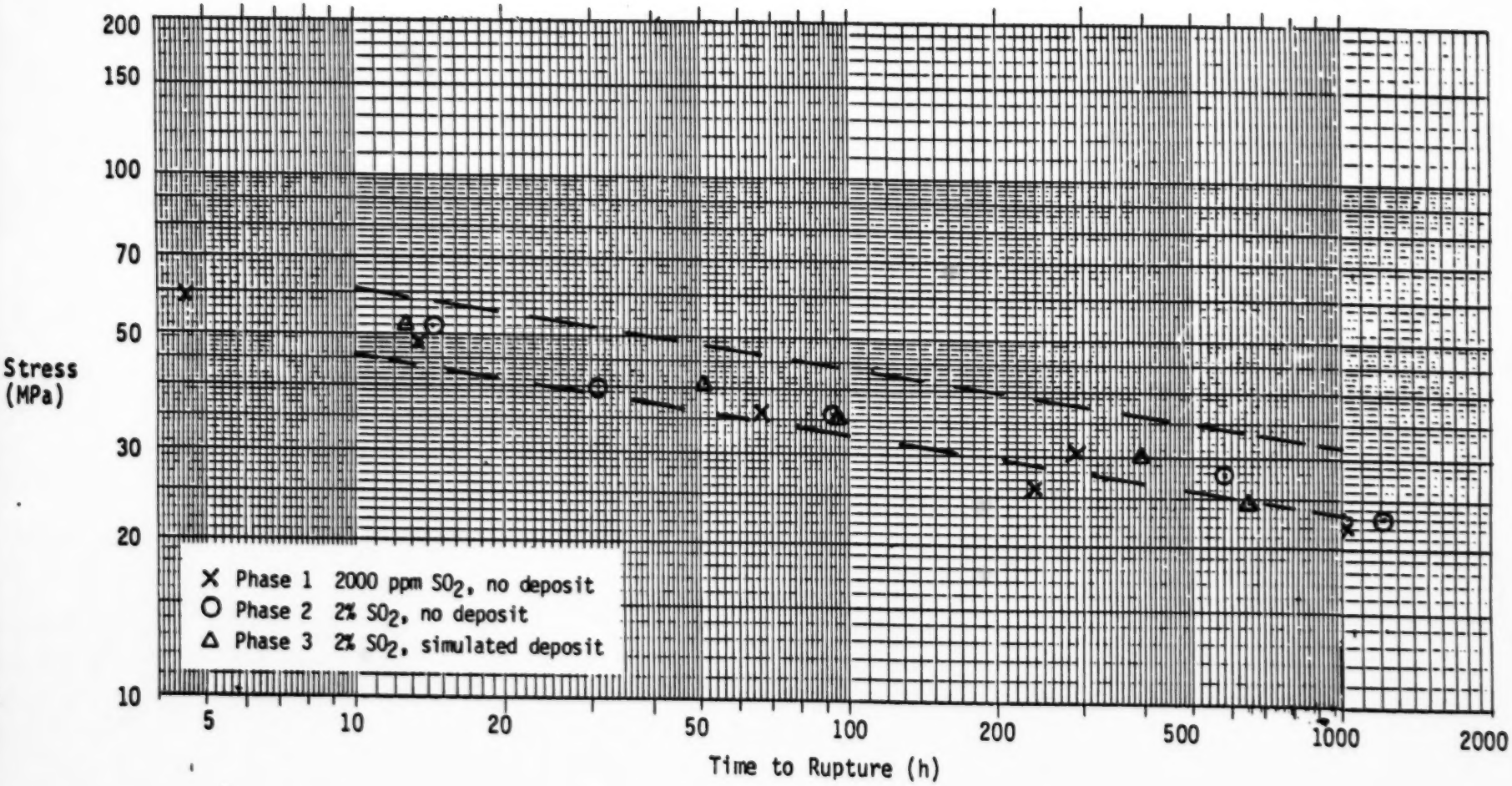

Figure 3 Stress-Rupture Tests for Incoloy 800H at 900°C in Synthetic Combustion Gas

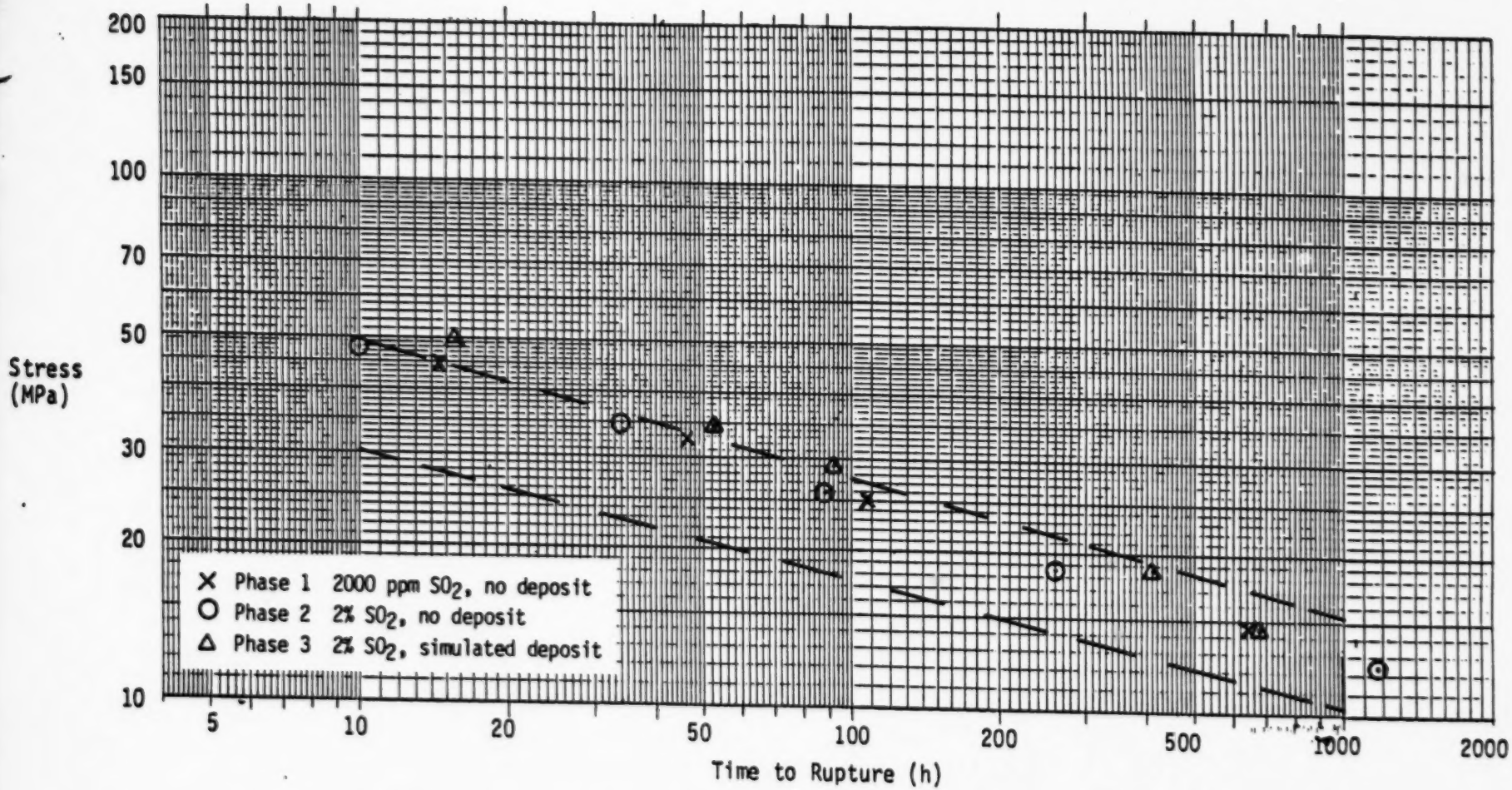

Figure 4 Stress-Rupture Tests for Stainless Alloy 347H at 900°C in Synthetic Combustion Gas

Table 7 Stress-Rupture Data for Incoloy 800H Tested at 800°C in Synthetic Combustion Gas and Simulated Fluidized Bed Deposit

Test Stress (MPa)	Time to Rupture (h)	Elongation (%)
103.4	12.4	63
89.6	17.7	59
76.5	96.3	n.d.
56.5	83.0	40
51.5*	788.8	25
37.2	1445.1	n.d.

n.d. Not determined, heavy corrosion obliterated gauge marks
* Test conducted during Phase 3
Correlation coefficient: $r^2 = 0.89$

Table 8 Stress-Rupture Data for Cast Alloy HK40 Tested at 800°C in Synthetic Combustion Gas and Simulated Fluidized Bed Deposit

Test Stress (MPa)	Time to Rupture (h)	Elongation (%)
133.8	19.0	13
108.3	51.8	6
96.5	78.1	6
70.3	367.3	3
56.8	423.8	4
51.5*	1192.7	4

* Test conducted during Phase 3
Correlation coefficient: $r^2 = 0.97$

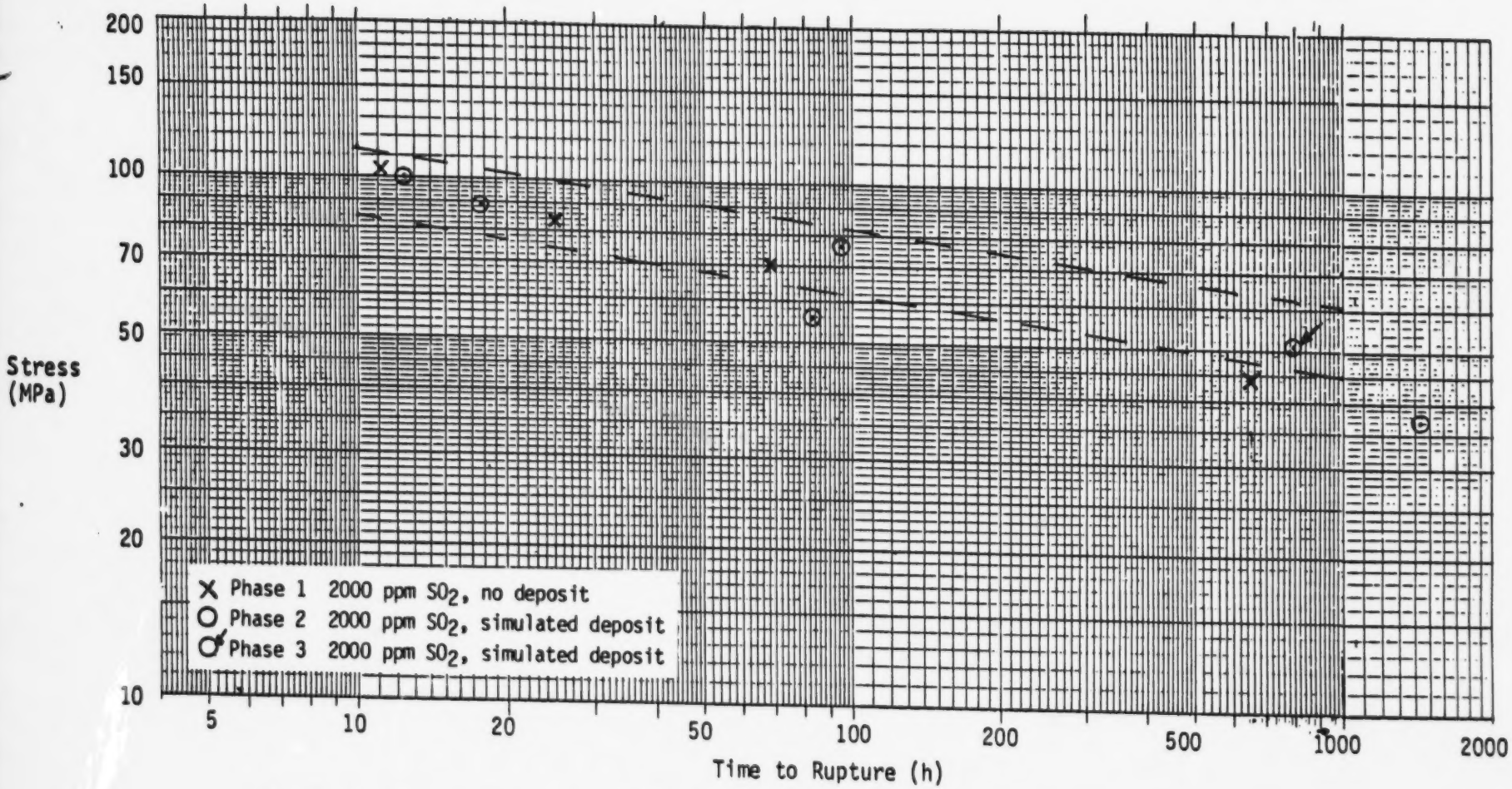

Figure 5 Stress-Rupture Tests for Incoloy 800H at 800°C in Synthetic Combustion Gas

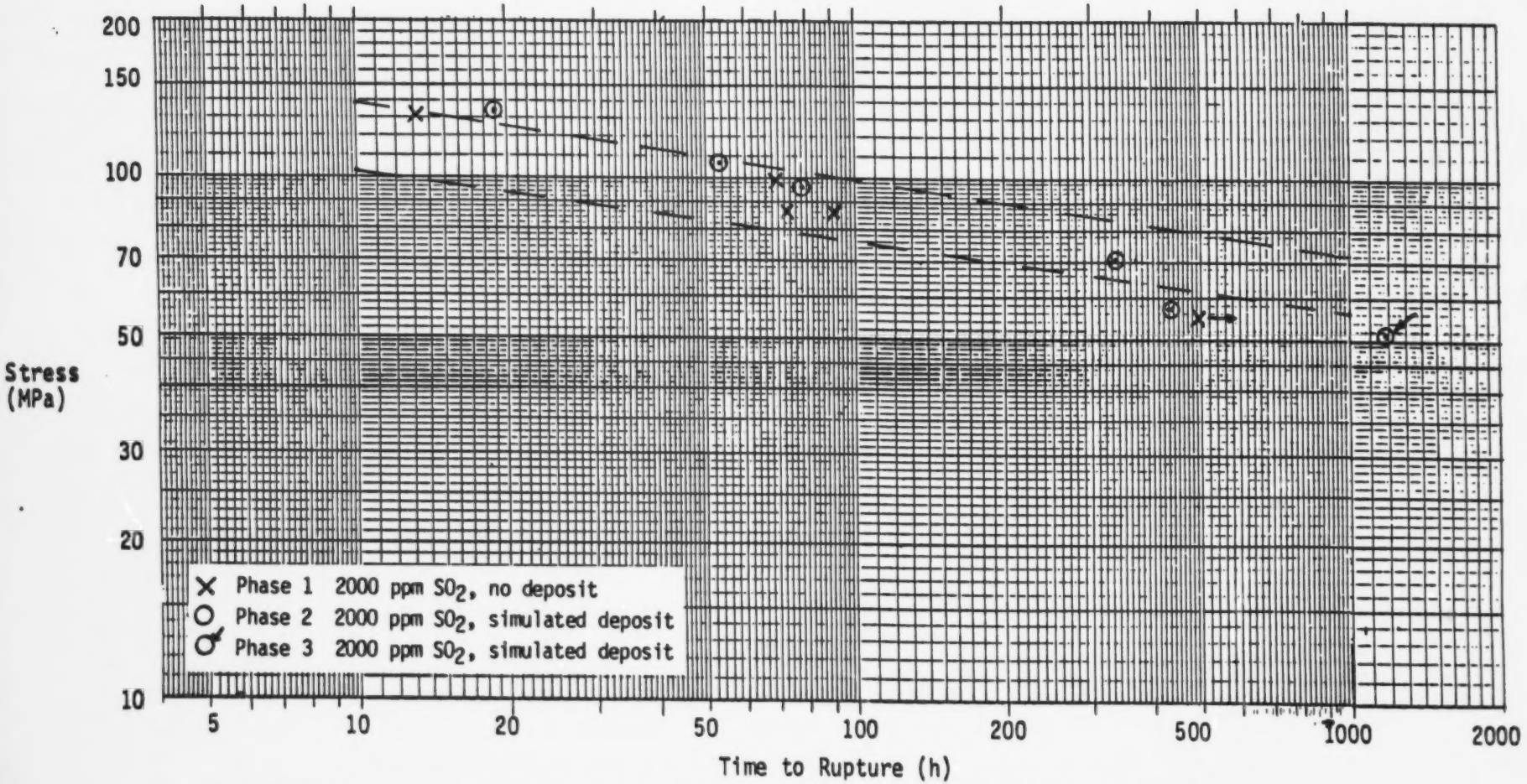

Figure 6 Stress-Rupture Tests for Cast Alloy HK40 at 800°C in Synthetic Combustion Gas

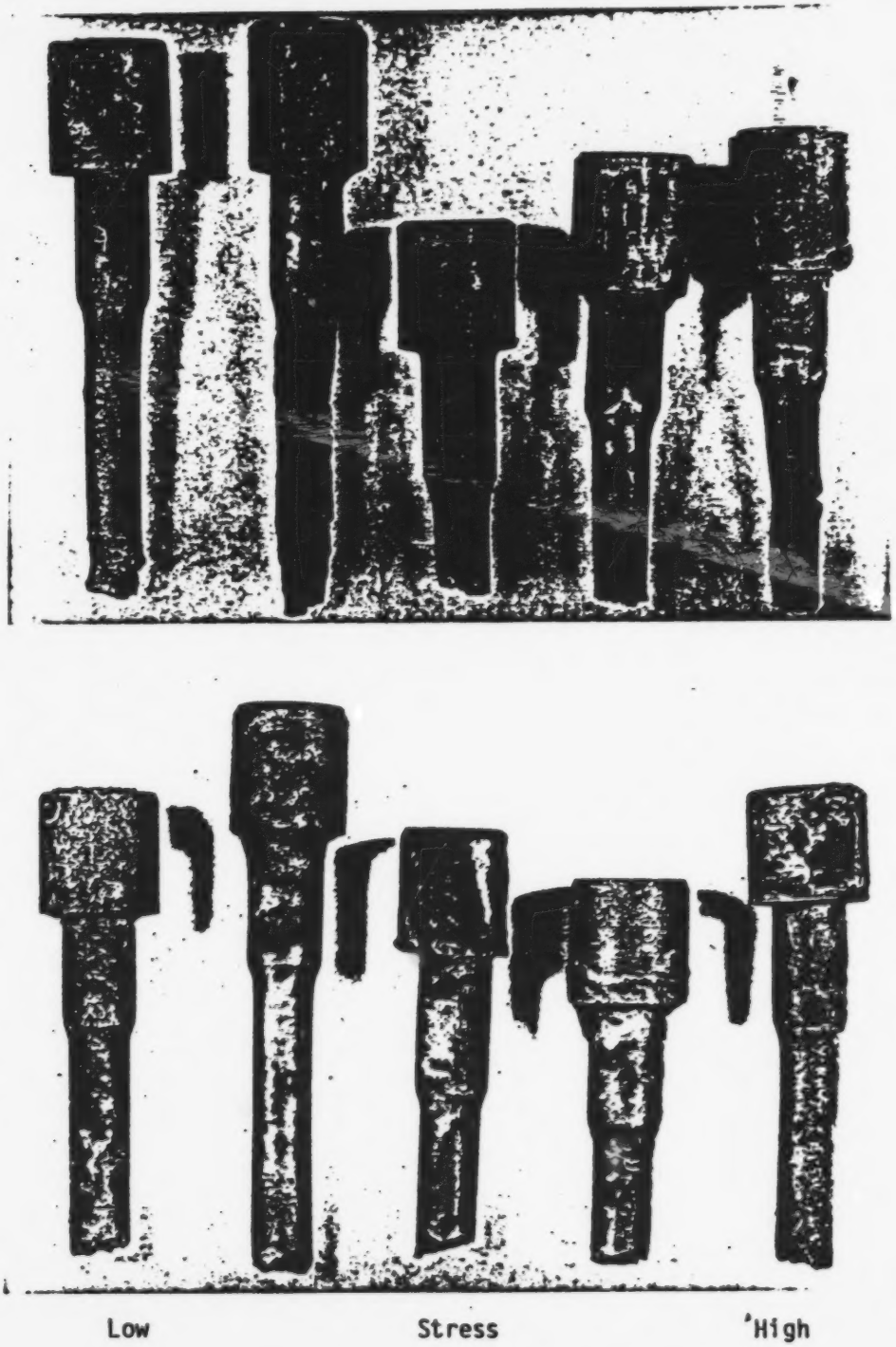

Figure 7 Appearance of Ruptured 310 and HK40 Specimens After 900°C Tests in Synthetic Combustion Gas and Simulated Deposit

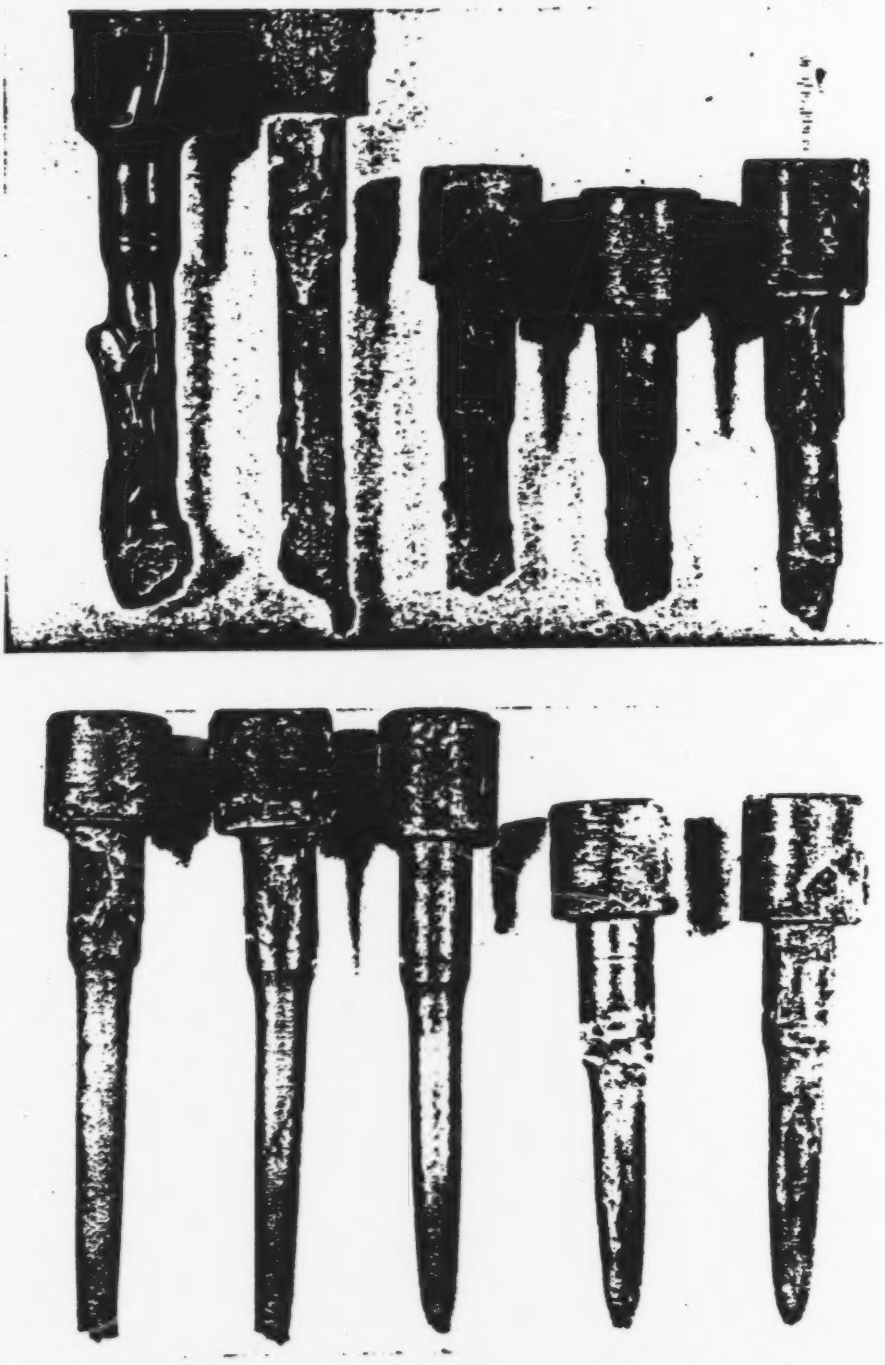

Figure 8 Appearance of Ruptured 800H and 347H Specimens After 900°C Tests in Synthetic Combustion Gas and Simulated Deposit

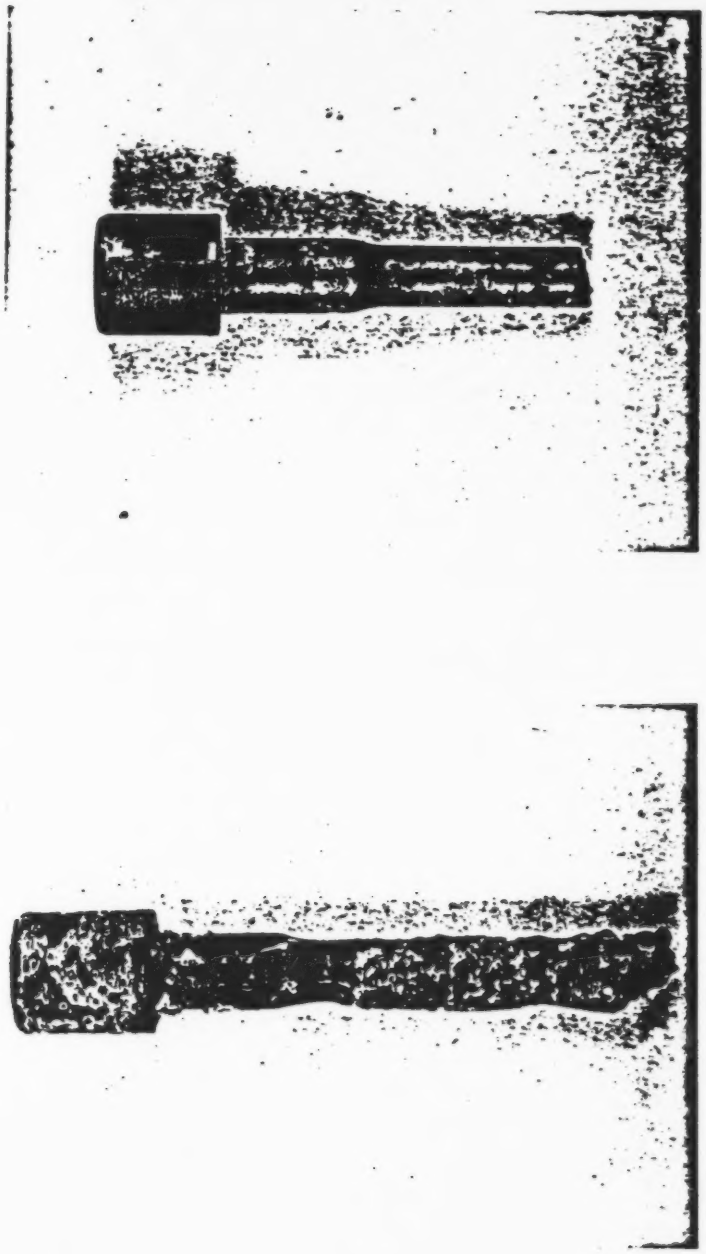

Figure 9 Appearance of Ruptured HK40 and 800H Specimens After 800°C Tests in Synthetic Combustion Gas and Simulated Deposit

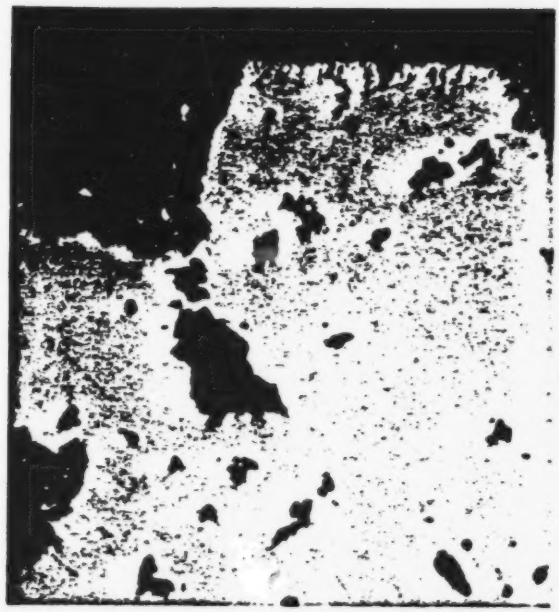

(a) Fracture Area 5.6 h Specimen

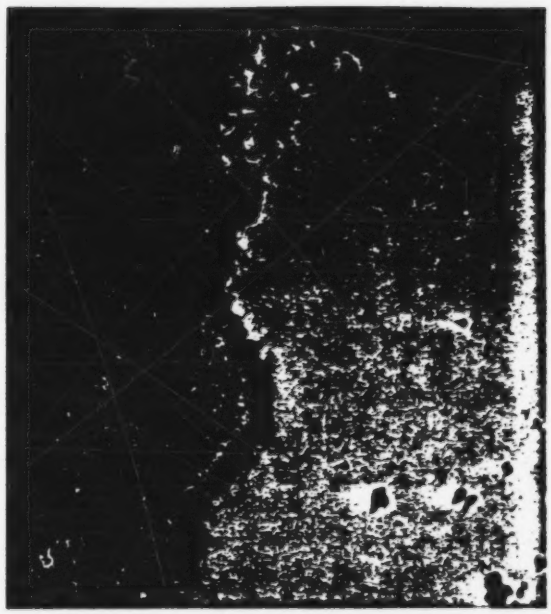

(b) Fracture Area 822.4 h Specimen

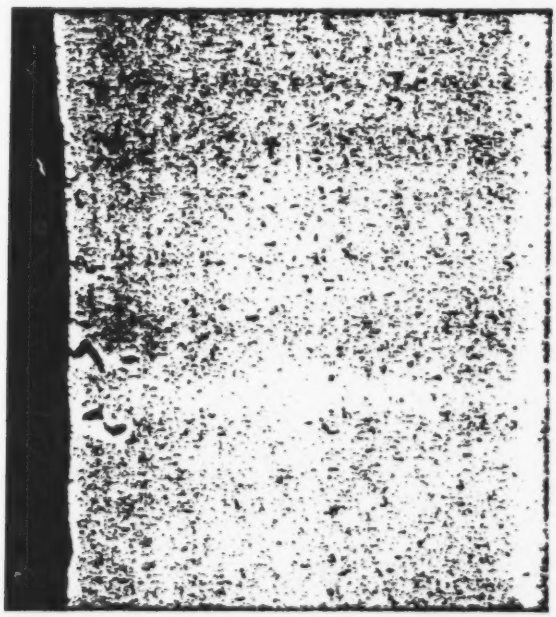

(c) Filet Area 5.6 h Specimen

(d) Filet Area 822.4 h Specimen

Figure 10 Sulphidation Observed in 310 Specimens After Life to Rupture of 5.6 and 822.4 h at 900°C

X100

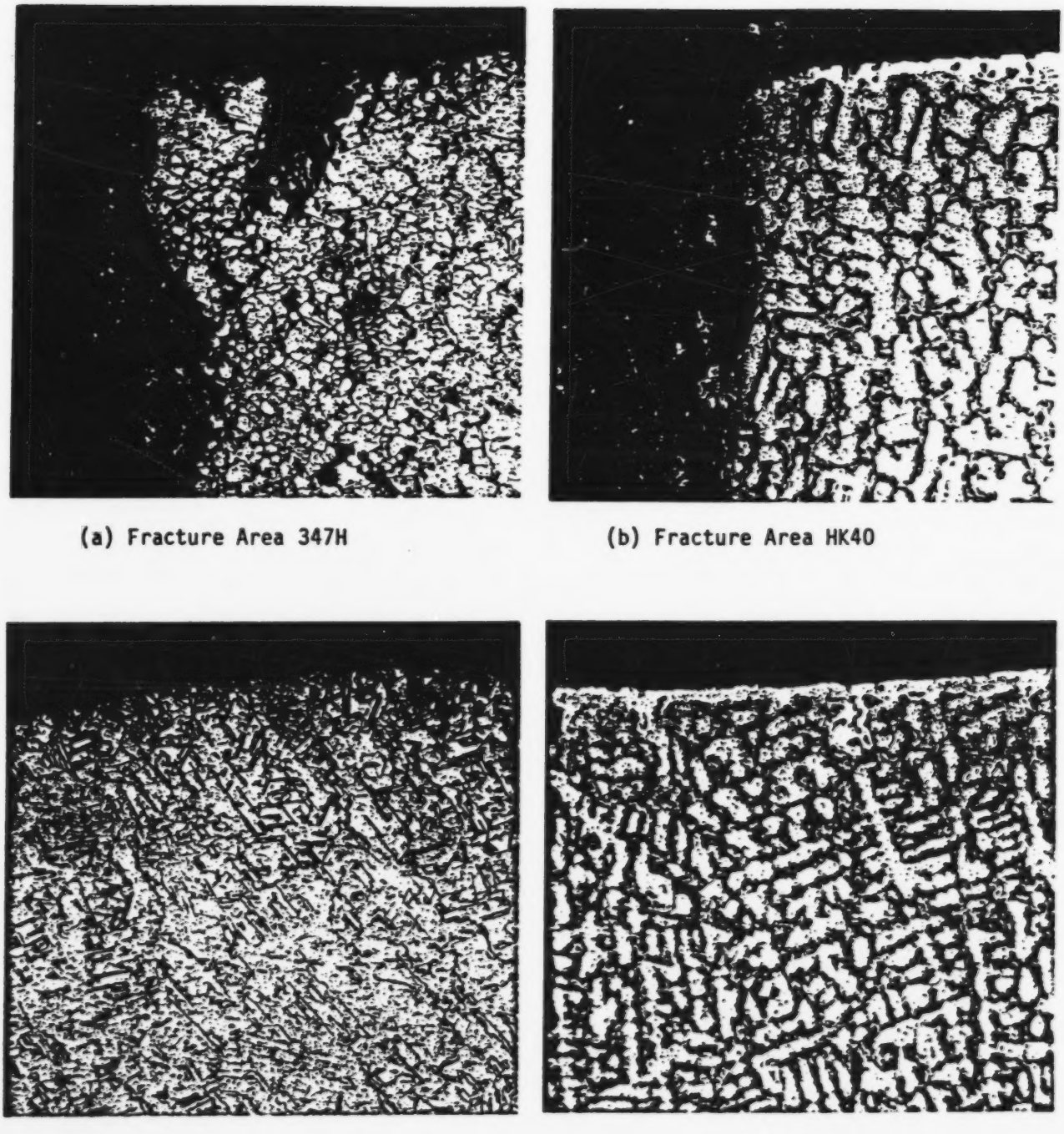

(a) Fracture Area 347H

(b) Fracture Area HK40

(c) Filet Area 347H

(d) Filet Area HK40

Figure 11 Effect of Hot Corrosion on 347H and HK40 After Targeted 1000 h Tests at 900°C

X100

Microprobe analyses of several ruptured specimens were conducted. Figure 12 shows the distribution of nickel, chromium, sulphur and iron in Incoloy 800H which had a rupture life of 93.8 h. The area over which the electron beam was scanned was located just below the exposed outer alloy surface. The sulphur X-ray image shows inward penetration of sulphur along the grain boundaries while the X-ray image for chromium shows the concentration in the grain boundaries and the depletion of chromium in the adjacent regions. These analyses illustrate the classical deterioration of the alloy due to hot corrosion prior to catastrophic attack.

A similar outward movement of chromium was observed in 310, as shown in Figure 13. The rupture life for this specimen was 247 h. The scan area for the microprobe analyses included the outer specimen surface which can be seen in the electron image. High concentrations of chromium in this case however appeared to be associated with stress cracks. A "protective" chromium layer on the specimen surface was also apparent and sulphur penetration was lower compared to the 800H sample.

The metallographic and microprobe analyses suggested that the stress to rupture properties of the test alloys were not adversely affected by the simulated coal combustor test environment because the chromium content provided sufficient protection. Although the applied stress caused alloy deformation, it appeared that chromium diffused rapidly through the deformed areas and thereby continued to form the protective layer inhibiting hot corrosion.

In the case of 347H which showed high elongation and thus high deformation, it is probable that most of the deformation occurred during tertiary creep shortly before rupture of the specimen. This would account for the lack of catastrophic hot corrosion of the alloy.

The present tests and those of Phase 1 and 2 were conducted at temperatures which deviated no more than ~3°C from the 800 or 900°C set point. It is possible that larger temperature fluctuations would affect the integrity of the protective chromium "coating". For example, Figure 14 shows the effect of cyclic heating and cooling on one of the 310 stress-rupture furnace retort liners. This liner, schedule 80 pipe, was used for the 900°C Phase 3, Part 1 stress-rupture tests. The liner was in service for only 2000 h but fourteen tests were conducted and included both short (10 h) and long (1000 h) term tests. It is important to note that the liner is supported in the furnace and thus subject to minimal stress. In spite of the low stress, however,

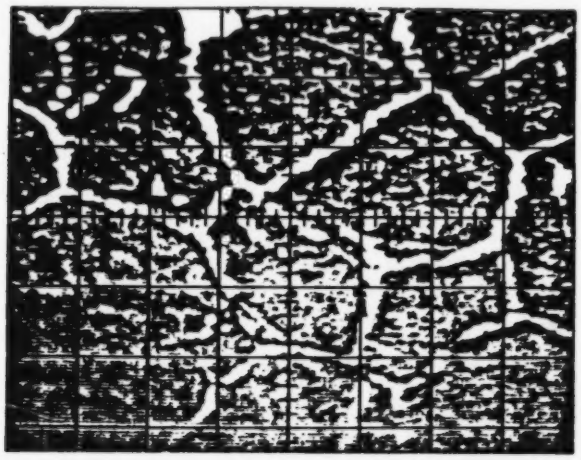

(a) Absorbed Electron Image

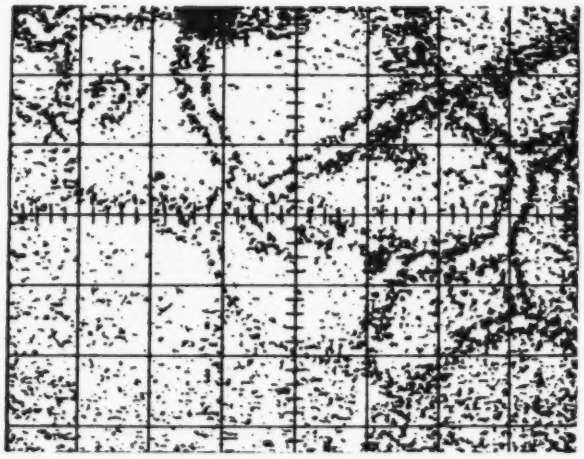

(b) Chromium X-Ray Image

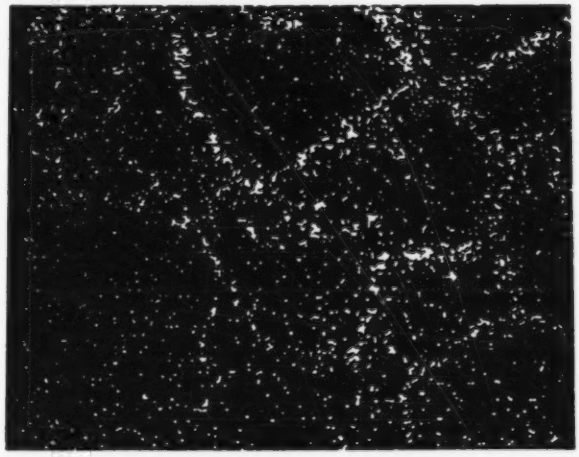

(c) Sulphur X-Ray Image

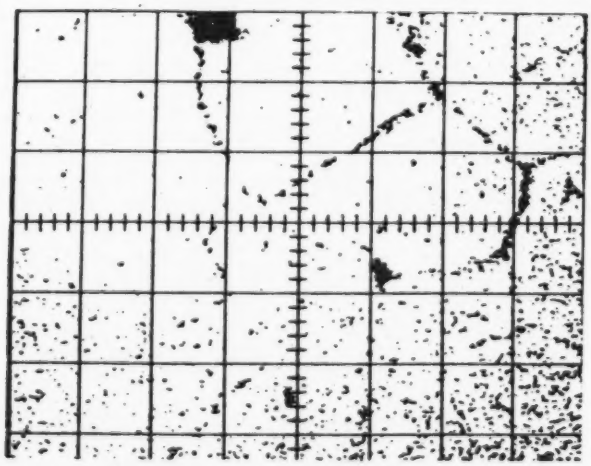

(d) Iron X-Ray Image

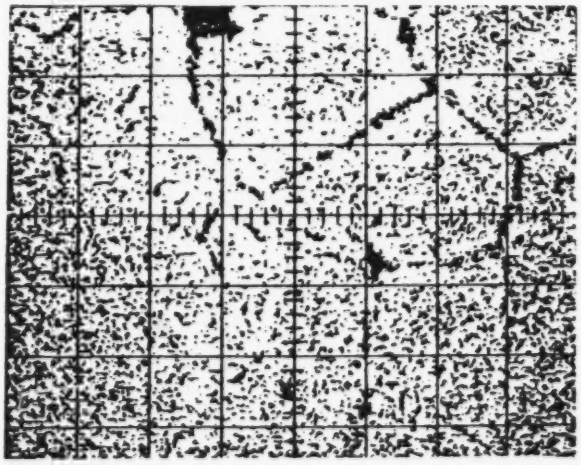

(d) Nickel X-Ray Image

Figure 12 Microprobe Analyses of 800H After 93.8 h Life at 900°C
X400

(a) Absorbed Electron Image

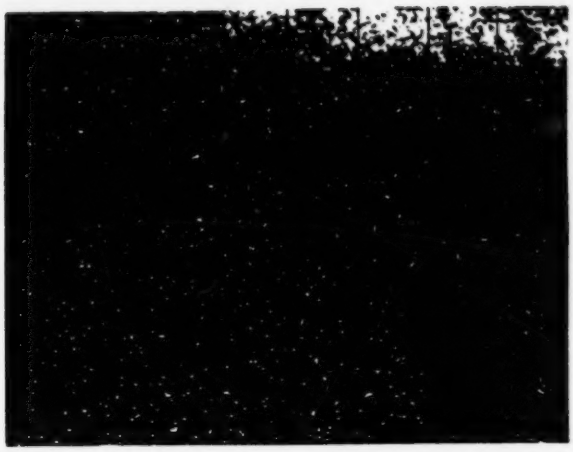

(b) Calcium X-Ray Image

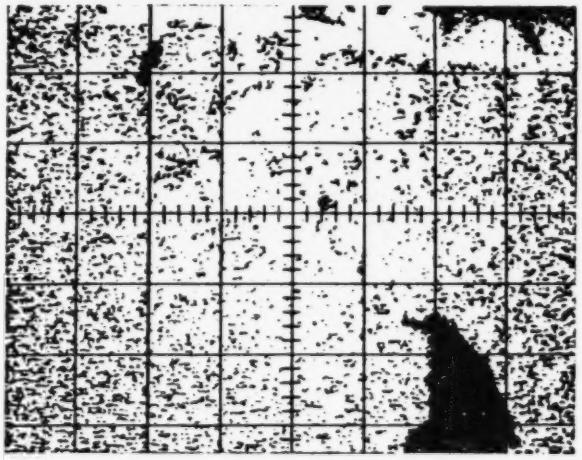

(c) Chromium X-Ray Image

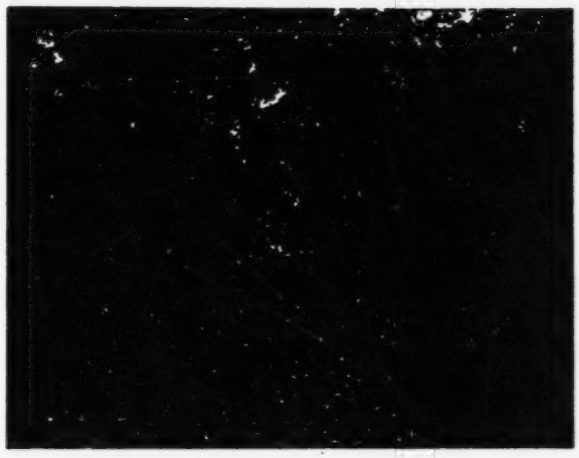

(d) Sulphur X-Ray Image

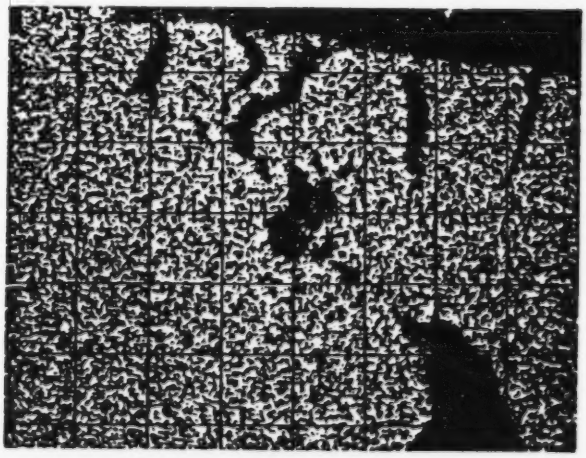

(e) Nickel X-Ray Image

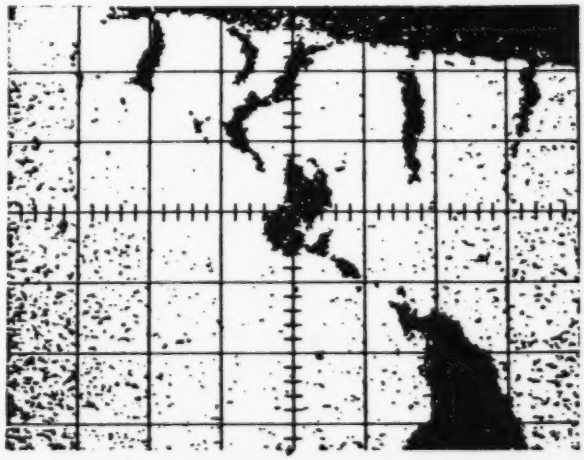

(f) Iron X-Ray Image

Figure 13 Microprobe Analyses of 310 After 247 h Life at 900°C
X400

(a) Bottom of Furnace Retort Liner

(b) Hot Zone Area of Retort Liner

Figure 14 Effect of Hot Corrosion on 310 Furnace Retort Liner After Fourteen Repetitive Tests Totalling 2000 h at 900°C in Synthetic Combustion Gas

Figure 14 shows that massive hot corrosion had occurred in the hot zone area of the liner. The layered structure of the corrosion products suggested repetitive hot corrosive attack. The microprobe analyses of the 310 liner in Figure 15 show severe depletion of chromium from within the grains and high chromium concentrations at the grain boundaries indicative of the advanced state of hot corrosion.

The interesting finding was that hot corrosion had occurred over the entire hot zone liner area, quite unlike the localized attack of the stress-rupture test specimens. As discussed above, hot corrosion of the stress-rupture test specimens appeared to be associated primarily with areas of high deformation.

Cyclic heating and cooling also appeared to have a strong influence on the useful life of the 310 pull rods and clevises. Pack chromized unused supports showed only minor hot corrosive attack when used for targeted 1000 h tests. When used repetitively for short term tests however, massive hot corrosion occurred.

Collectively these test results and observations suggest that temperature fluctuations have a more deleterious effect on the passivating influence of chromium on hot corrosion than does sustained stress at fixed temperature.

Although beyond the scope of the present stress-rupture test program it would be informative to conduct stress-rupture tests under the conditions of an imposed but controlled heating and cooling cycle that is relevant to conditions experienced in a commercial coal combustor.

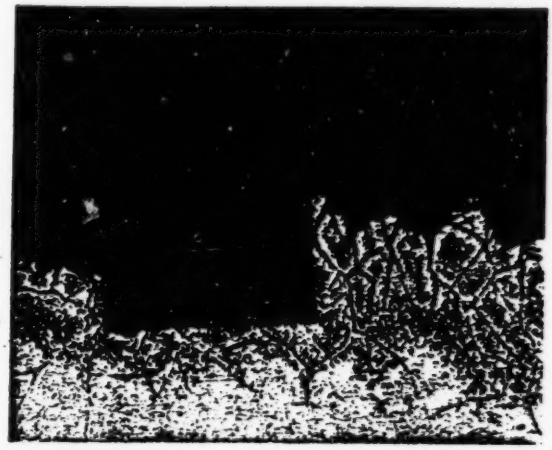

(a) Rectangular Analyses Area (X100)

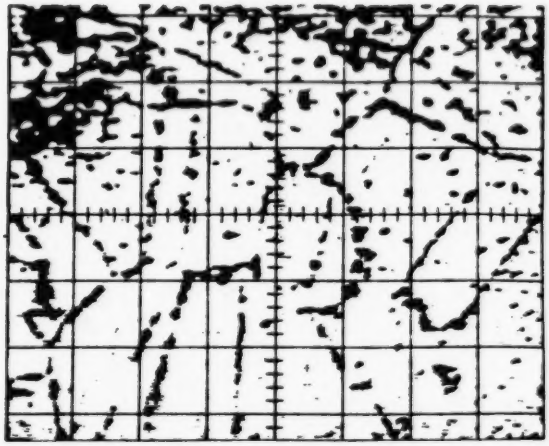

(b) Absorbed Electron Image

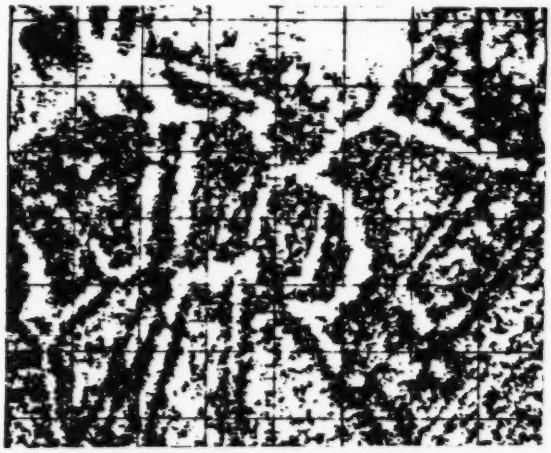

(c) Chromium X-Ray Image

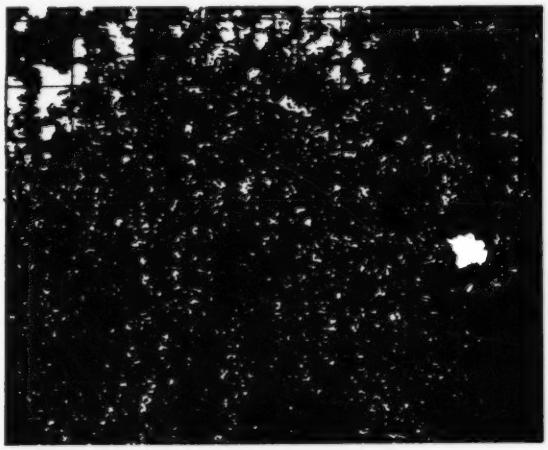

(d) Sulphur X-Ray Image

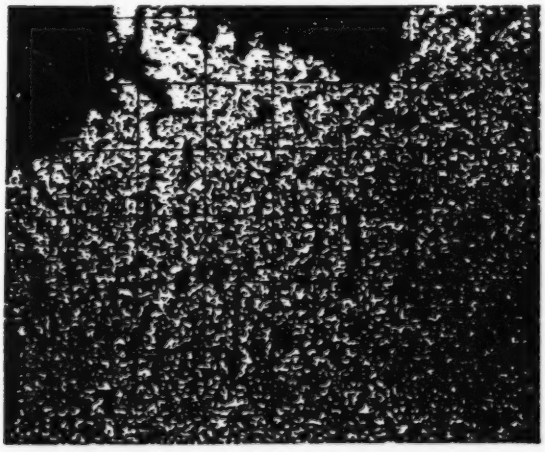

(e) Nickel X-Ray Image

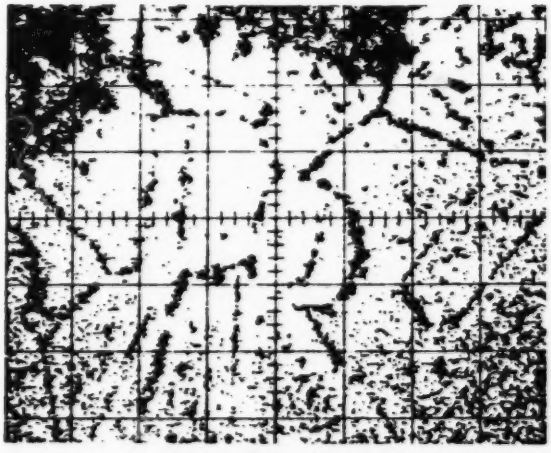

(f) Iron X-Ray Image

Figure 15 Microprobe Analyses of 310 Furnace Retort Liner
X400